Dottorato di Ricerca in Ingegneria Civile
Graduate School in Civil Engineering
Sede: Facoltà di Ingegneria - Università di Pavia - Via Ferrata, 1 - 27100 Pavia - Italy
- Dipartimento di Meccanica Strutturale - Tel. 0382 - 985450 - Fax. 0382 - 528422
- Dipartimento di Ingegenria Idraulica ed Ambientale - Tel. 0382 - 985300 - Fax. 0382 - 985589

Structural Control of Cable-stayed and Suspended Bridges

Marco Domaneschi

Ph.D. Thesis

Advisors:

Prof. Fabio Casciati

Prof. Agnessa Kovaleva

Revisor:

Prof. Aldo Cauvin

Description of the Ph.D. course

Settore: **Field**:	Ingegneria Engineering
Sede amministrativa non consortile: **Administrative location**	Università degli Studi di Pavia University of Pavia
Durata del dottorato in anni: **Duration** in years	3 3
Periodo formativo estero in mesi: **Period in external organization** in months	come previsto dal regolamento del Dottorato di Ricerca as required by the Doctorate regulation
Numero minimo di corsi: **Minimum number of courses**:	6 6

Il dottorato di ricerca in Ingegneria Civile presso la Facoltá di Ingegneria dell'Universitá degli Studi di Pavia é stato istituito nellanno accademico 1994/95 (X ciclo). Il corso consente al dottorando di scegliere tra quattro curricula: Idraulico, Sanitario, Sismico e Strutturale. Egli svolge la propria attivitá di ricerca rispettivamente presso il Dipartimento di Ingegneria Idraulica e Ambientale o quello di Meccanica Strutturale. Durante i primi due anni sono previsti almeno sei corsi. Il Collegio dei Docenti, composto da professori dei due Dipartimenti, organizza i corsi con lo scopo di fornire allo studente di dottorato opportunità di approfondimento su alcune delle discipline di base. Corsi e seminari vengono tenuti da docenti di Università nazionali ed estere. Il Collegio dei Docenti, cui spetta la pianificazione della didattica, si é orientato ad attivare ad anni alterni corsi sui seguenti temi:

- Meccanica dei solidi e dei fluidi.
- Metodi numerici per la meccanica dei solidi e dei fluidi.
- Rischio strutturale e ambientale.
- Metodi sperimentali per la meccanica dei solidi e dei fluidi.
- Intelligenza artificiale.

più corsi specifici di indirizzo. Al termine dei corsi del primo anno il Collegio dei Docenti assegna al dottorando un tema di ricerca da sviluppare sotto forma di tesina entro la fine del secondo anno; il tema, non necessariamente legato all'argomento della tesi finale, é di norma coerente con il curriculum, scelto dal dottorando. All'inizio del secondo anno il dottorando discute con il Coordinatore l'argomento della tesi di dottorato, la cui assegnazione definitiva viene deliberata dal Collegio dei Docenti. Alla fine di ogni anno

i dottorandi devono presentare una relazione particolareggiata sull'attivitá svolta. Sulla base di tale relazione il Collegio dei Docenti, "previa valutazione della assiduità e dell'operositá dimostrata dall'iscritto", ne propone al Rettore l'esclusione dal corso o il passaggio all'anno successivo. Il dottorando puó svolgere attivitá di ricerca sia di tipo teorico che sperimentale, grazie ai laboratori di cui entrambi i Dipartimenti dispongono, nonché al Laboratorio Numerico di Ingegneria delle Infrastrutture. Il "Laboratorio didattico sperimentale" del Dipartimento di Meccanica Strutturale dispone di:

- una tavola vibrante che consente di effettuare prove dinamiche su prototipi strutturali;
- opportuni sensori e un sistema di acquisizione dati per la misura della risposta strutturale;
- strumentazione per la progettazione di sistemi di controllo attivo e loro verifica sperimentale;
- strumentazione per la caratterizzazione dei materiali, attraverso prove statiche e dinamiche.

Il laboratorio del Dipartimento di Ingegneria Idraulica e Ambientale dispone di:

- un circuito in pressione che consente di effettuare simulazioni di moto vario;
- un tunnel idrodinamico per lo studio di problemi di cavitazione;
- canalette per lo studio delle correnti a pelo libero.

The Graduate School of Civil Engineering at the Faculty of Enginnering at the University of Pavia was established in the Academic Year of 1994/95 (X cycle). The School allows the student to select one of the four offered curricula: Hidraulics, Environment, Seismics and Structure. Each student develops his research activity either at the Departement of Hidraulics and Environmental Engineering or at the Departement of Structural Mechanics. During the first two years, a minimum of six courses must be selected and their examinations successfully passed. The Faculty, represented by Professors of the two Departements or by internationally recognized scientists, organizes courses so as to provide the student with opportunities to deepen his basic knowledge. Courses and seminars are held by University Professors from all over the country and abroad. The Faculty starts up courses, in alternate years, on the following subjects:

- solid and fluid mechanics,
- numerical methods for solid and fluid mechanics,
- structural and environmental risk,
- experimental methods for solid and fluid mechanics,
- artificial intelligence

and other, more specific courses.
At the end of each course, for the first year the Faculty assigns the student a research argument to develop, in the form of report, by the end of the second year; the topic, not necessarily on the final doctorate thesis, should be consistent with the curriculum selected by the student. At the beginning

of the second year the student discusses with his Coordinator the subject of the thesis and eventually, the Faculty assigns it. At the end of every year, the student has to present a complete report on his research activity, on the basis of which the Faculty proposes his term for the successive year or his admission to the final examination to the Rector. The student is supposed to develop either theoretical or experimental research activities, and therefore has access to the Department Experimental Laboratories, even to the Numerical Laboratory of Infrastructure Engineering. The Experimental Teaching Laboratory of the Department of Structural Mechanics offers:

- a shaking table which permits one to conduct dynamic tests on structural prototypes;
- sensors and acquiring data system for the structural response measurements;
- instrumentation for the design of active control system and their experimental checks;
- an universal testing machine for material characterization through static and dynamic tests.

The Department of Hidraulics and Environmental Engineering offers:

- a pression circuit simulating various movements;
- a hydrodynamic tunnel studing cavitation problems;
- micro-channels studing free currents.

Recapiti - Addresses

Dipartimento di Meccanica Strutturale
Via Ferrata, 1 - 27100 Pavia - Italy
Tel. +39.0382.985450 - Fax. +39.0382.528422

Dipartimento di Ingegneria Idraulica ed Ambientale
Via Ferrata, 1 - 27100 Pavia - Italy
Tel. +39.0382.985300 - Fax. +39.0382.985589

Coordinatore - Coordinator

CASCIATI Fabio - Professore Ordinario - ICAR/08
Dipartimento di Meccanica Strutturale
Via Ferrata, 1 - 27100 Pavia - Italy
Tel. +39.0382.985458 - Fax. +39.0382.528422
Email. fabio@dipmec.unipv.it

Collegio dei Docenti - Teaching Staff

CAPODAGLIO Andrea Giuseppe Professore Associato - ICAR/03

CASCIATI Fabio Professore Ordinario - ICAR/08 - (Coordinatore)

CAUVIN Aldo Professore Ordinario - ICAR/09

CIAPONI Carlo Professore Straordinario - ICAR/01

FARAVELLI Lucia Professore Ordinario - ICAR/08

FUGAZZA Mario Professore Associato - ICAR/02

GOBETTI Armando Professore Associato - ICAR/08

MOISELLO Ugo Professore Ordinario - ICAR/02

PAPIRI Sergio Professore Associato - ICAR/02

SALA Roberto Professore Associato - ING - IND/08

MARCELLINI Alberto Dirigente di Ricerca, CNR - Milano. Docente di Sismologia, Università Statale di Milano

Previous Ph.D. Theses

Marco Battaini (X Ciclo)	Sistemi strutturali controllati: progettazione ed affidabilitá
Claudia Mariani (X Ciclo)	Problemi di ottimizzazione per strutture bidimensionali anisotrope
Antonella Negri (X Ciclo)	Stima delle perdite idrologiche nei bacini di drenaggio urbani
Aurora Angela Pisano (XI Ciclo)	Structural System Identification: Advanced Approaches and Applications
Carla Saltalippi (XI Ciclo)	Preannuncio delle piene in tempo reale nei corsi d'acqua naturali
Eugenio Barbieri (XI Ciclo)	Thermofluid Dynamics and Topology: Optimization of an active Thermal Insulation Structure
Massimiliano Barbolini (XII Ciclo)	Dense Snow Avalanches: Computational Models, Hazard Mapping and Related Uncertanties
Paolo Espa (XII Ciclo)	Moti atmosferici generati da forze di galleggiamento: simulazioni numeriche e studio su modello fisico
Lorenza Petrini (XII Ciclo)	Shape Memory Alloys: Modelling the Martensitic Phase Behaviour for Structural Engineering Exploitation
Stefano Podestà (XIII Ciclo)	Risposta sismica di antichi edifici religiosi: una nuova proposta per un modello di vulnerabilità
Daniele Sturla (XIII Ciclo)	Simulazioni lagrangiane di flussi rapidamente variati nell'approssimazione di acque poco profonde
Marazzi Francesco (XV Ciclo)	Semi-active control of civil structures: implementation aspects
Nascimbene Roberto (XV Ciclo)	Sail Modelling for Maximal Speed Optimum Design

Giudici Massimo (XVI Ciclo)	Progettazione in regime non lineare di strutture in CAP a cavi aderenti e non aderenti
Mutti Matteo (XVI Ciclo)	Stability analysis of stratified three-phase flows in pipes
Petaccia Gabriella (XVI Ciclo)	Propagazione di onde a fronte ripido per rottura di sbarramenti in alvei naturali
Casciati Sara (XVII Ciclo)	Damage Detection and Localization in the Space of the Oserved Variables
D'Amico Tiziana (XVI Ciclo)	Ricerca e Sviluppo di Metodologie Diagnostiche per il Recupero di Edifici Monumentali: Prove Vibroacustiche sul Tufo

Contents

List of Figures

List of Tables

Chapter 1

Introduction

1.1 Introduction

The world today is faced with a growing need to control the great and still increasing number of large structures. Structural control solutions are supposed to meet the high standards of performance, feasibility and safety [1] [2] [3].

1.1.1 Motivation

The modern design of complex structures must be in line with the definition and evaluation of performance, while safety must be assessed under different conditions. The norm imposed by the structural codes can not be considered sufficient when the structures in question are complicated due to their geometry or materials used. Therefore, the performance based design is the answer to complex structures, such as long span bridges [4]. Structural control solutions can give an important contribution so as to satisfy certain performance standards.

The globalization of scientific research has brought to our knowledge an

approach to structural control based on developing control devices as structural elements [5] rather than something apart from the structure [6].
Numerical methods are commonly used to simulate the structural response under external excitations. Structural control solutions can also be modelled to evaluate their efficiency in the mitigation of unwanted dynamic effects. An international benchmark control case for a cable-stayed bridge was recently introduced to the attention of the control community. It is herein considered as a reference and several control schemes are suggested with the common sense to research the best control solution, mantaining the simplicity and the feasibility.
The work finally implements a numerical model for a suspended bridge and evaluates the control strategies, previously performed for the cable-stayed bridge benchmark.

1.1.2 Planning

In order to deal with problems of structural control in the dynamic field, some definitions and governing relations must be introduced. Chapter 2, 3 and 4 are dedicated to this topic. Chapter 2 and 4 presents the main features of linear and non-linear mechanic systems. Chapter 3 describes some different device typologies for vibration protection.
Chapter 5, 6 and 7 develops numerical control solutions applied on the bridge benchmark control issue. Passive devices are first applied in Chapter 5, which closes with an open-loop semi-active strategy. Further on, the semi-active scheme is improved, with the aim of getting as close as possible to the target of an active control solution.
Chapter 8 introduces the suspended bridge model and reports the results

of several control simulations.

Appendices A, B and C synthesize some background topics.

Bibliography

[1] Proc. of the Third World Conference on Structural Control, F. Casciati ed., April 7-11, 2002, Como, Italy, Vol. 1-2-3, ISBN 0-471-48980-8.

[2] Proc. of the US-Europe Workshop on Sensors and Smart Structures Technology, L. Faravelli and Billie F. Spencer Jr. eds., April 12-13, 2002, Como and Somma Lombardo, Italy, ISBN 0-471-48980-8.

[3] Proc. of the Third European Conference on Structural Control, R. Flesch, H. Irschik and M. Krommer eds., July 12-15, 2004, Vienna, Austria, ISBN 3-901167-90-0.

[4] Bontempi F., 2004
Approccio sistemico alla manutenzione strutturale (in Italian),
Bridge and Viaduct: control, analysis, maintenance, rehabilitation. Politecnico di Milano, Milan, June, 22-25, 2004.

[5] Kolovsky M.Z., 1999
Nonlinear Dynamics of Active and Passive Systems of Vibration Protection,
Foundations of Engineering Mechanics, Springer-Verlag, ISBN 3-540-65661-8.

[6] Meirovitch L., 1990
Dynamics and Control of Structures,
John Wiley and Sons, ISBN 0-471-62858-1.

Chapter 2

Linear dynamics modelling of vibration protection systems

2.1 Introduction

According to [1], for an arbitrary mechanical system subjected to dynamic forces and kinematic excitations, the following definitions are possible.

Definition 1: *Force excitations are time-varying forces applied at different points of the system body.*

Definition 2: *Kinematic excitations are assigned, time-dependent displacements of some points of the system body.*

A vibration field of displacement can be observed in the system under the application of dynamic excitations. Vibration fields of velocity, acceleration, force, strain etc. are observed in the system. Several branches of construction technology require a reduction in the intensity of the vibration fields.

Definition 3: *The facilities aimed at decreasing the intensity of the vibration fields in the system are referred to as vibration protection systems.*

Basically, two main different methods of vibration protection exist.

Definition 4: *Considered some secondary mechanical systems in addition to the object to be protected, the parameters of the added system are chosen in such a way that a decrease in the vibration of the object is ensured. This method of vibration protection is called vibration absorption and the added systems are called dynamic vibration absorbers.*

The absorbers have the main role of dissipating the input energy in the system to be protected by reducing the applied external excitations.

Definition 5: *Sectioning the original system into two subsystems connected by additional mechanical systems, the connection devices are often called vibration isolators and this method is called vibration isolation.*

The isolators devices have their reasons in changing or shifting the main natural frequency of the system part to be protected.

Usually, one of the separated subsystems turns out to be a free body disconnected from the other mechanical systems. This part is the *object to be protected* whereas the second part is referred to as the *base* or the *support structure*. When the dynamic excitations are applied to the base, the aim of vibration isolation is to protect the object. When the excitations act directly up on the object, the vibration isolators must ensure vibration protection to the base.

The following definition is then introduced:

Definition 6: *The control forces are the forces which act on the object to be protected and change its vibration field.*

It is easy to see that the actions of any vibration protection facility may be considered as creating additional dynamic excitations which provide the required change in the vibration field.

This allows the approach of the theory of control for the analysis and the

synthesis of the vibration protection systems.

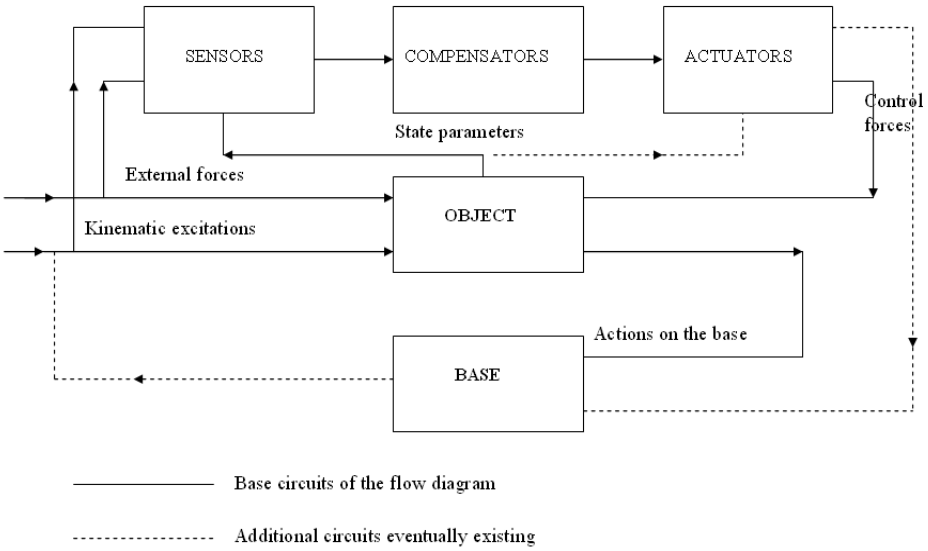

Figure 2.1: Flow diagram of an active vibration protection system

2.2 Transfer function based schemes

As mentioned in the previous paragraph, the purpose of any vibration protection system is to produce control forces.

Definition 7: *Systems generating a single control force are referred to as one-dimensional, while systems generating more than one control forces are called multidimensional.*

Figure 2.1 shows the block diagram of a classical multidimensional active vibration protection system. The path of the scheme is known:

- the parameters of the vibration fields, (absolute and relative displacements, velocities, accelerations at some points, forces and strain in the

structural elements etc.), external forces and/or kinematic excitations are inputs to the *controller*.

- The input variables are measured by the *sensors*.
- The information coming from the sensors is transformed and the result acts as input to the *compensator* (see Appendix C).
- The output of the compensator is first amplified by an amplifier and then acts as input for the *actuator*, with the latter producing the control force.

The vibration field parameters can directly influence the actuator, whereas the control forces may depend on the motion of the object. In addition to this, the actuators which isolate the object act not only on the object but also on the base, changing the kinematics excitations. These branches are displayed as additional lines in Figure 2.1.
If the system is linear each of its elements can be described by a transfer function. Figure 2.2 shows the block diagram of a linear multidimensional system, in which:

- $\mathbf{F}(t)$ and $\delta(t)$ are the vectors of the forces and kinematics excitations, respectively, and $\mathbf{y}(t)$ denotes the vector of the vibration field parameters which is measured.
- The transfer function matrices $W_{sF}(s)$, $W_{s\delta}(s)$ and $W_{sy}(s)$ characterise the properties of the corresponding linear sensors. These matrices are diagonal provided that each component of the vectors $\mathbf{F}(t)$, $\delta(t)$ and $\mathbf{y}(t)$ is measured independently. If a measure is reconstructed

in terms of measured displacements of particular points (for example the rotation angle), these matrices can have a more complicated structure.

- The outputs of the sensors are signals which form a vector ψ. These signals are summed, integrated or differentiated and amplified within a compensator. All these linear transformations are described by the matrix $W_c(s)$.

- The vector $\mathbf{c_{out}}$ is the compensator output: it acts as the input to the actuator. Furthermore, vector $\mathbf{y}(t)$ acts directly as an additional input to the actuator.

- The transfer function $W_a(s)$ relates the input variables of the actuator to the control forces $\mathbf{u}(t)$ acting on the object (or base) with the transfer function $W_0(s)$ and forces $\mathbf{R}(t)$ applied to the base (or object).

- Transfer function $W_1(s)$ relates the excitation, acting on the base to the kinematics excitations.

Figure 2.3 displays a block diagram of a one-dimensional system (see Definition 7) whose control force $u(t)$ is formed by a single output $y(t)$ and the base is assumed to be rigid. The governing equation of motion for the object is given by

$$y(s) = \sum_{i=1}^{k} w_{0i}^{(F)}(s) F_i(s) + \sum_{j=1}^{s} w_{0j}^{(\delta)}(s) \delta_j(s) + w_0^{(u)}(s) u(s) \qquad (2.1)$$

where F_i and δ_j are components of the dynamic excitations, and $w_{0i}^{(F)}$, $w_{0j}^{(\delta)}$ and $w_0^{(u)}$ are the rows of the transfer functions of the object $W_0(s)$. The

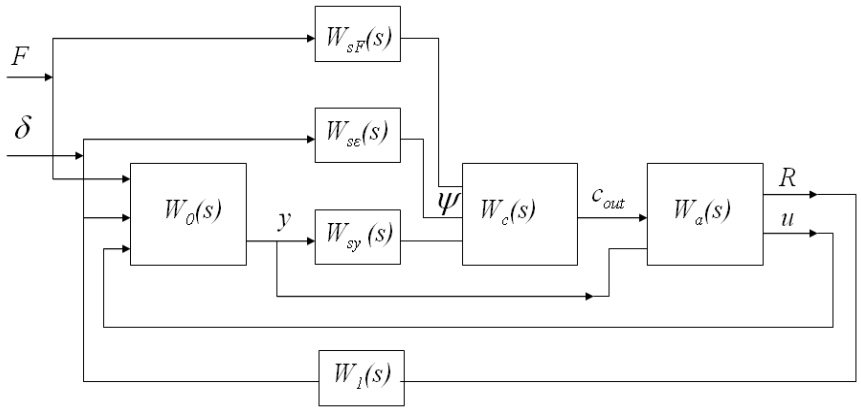

Figure 2.2: Flow diagram of a linear multidimensional system

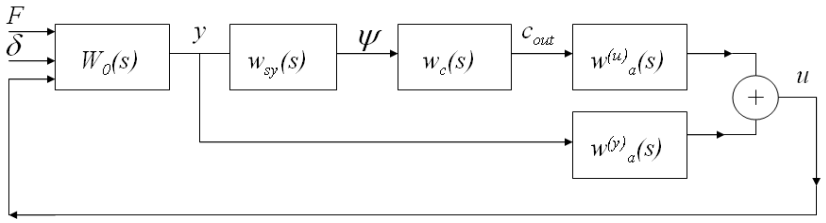

Figure 2.3: Flow diagram of a one-dimensional system with rigid base

system is one-dimensional, so only one control force is processed; it does not imply that the d.o.f. of the object could not be more than one. Eq. 2.1 is written in terms of Laplace transforms of the functions involved and s is the *Laplace variable*, see Appendix A.

The transfer function relating u and y is

$$\begin{aligned} u(s) &= w_a^{(u)}(s)c_{out}(s) + w_a^{(y)}(s)y(s) = \\ &= [w_a^{(u)}(s)w_c(s)w_{sy}(s) + w_a^{(y)}(s)]y(s) \end{aligned} \tag{2.2}$$

and finally

$$u(s) = -w_y(s)y(s) \tag{2.3}$$

In what follows, $w_y(s)$ is the $feedback\ transfer\ function$, with the meaning graphically shown in Figure 2.3: the transfer function of the three blocks connected in the series ($w_a^{(u)}(s)w_c(s)w_{sy}(s)$) is the product of their elementary transfer functions. The resulting additive block is connected in parallel with $w_a^{(y)}(s)$, so the whole transfer function of this feedback is a sum [3] [4]. A minus sign appears in eq. 2.2 since feedbacks are usually negative.

Inserting eq. 2.2 into 2.1 yields

$$y(s) = \sum_{i=1}^{k} w_{0i}^{(F)}(s)F_i(s) + \sum_{j=1}^{o} w_{0j}^{(\delta)}(s)\delta_j(s) - w_0^{(u)}(s)w_y(s)y(s) \tag{2.4}$$

The function

$$\Phi(s) = w_0^{(u)}(s)w_y(s) \tag{2.5}$$

is treated as the transfer function of an open-loop system. The transfer function of an open circuit with elements connected in a series is the product of the transfer functions of the single elements [3] [4].

It follows from eq. 2.4 that

$$y(s) = [1 + \Phi(s)]^{-1}[\sum_{i=1}^{k} w_{0i}^{(F)}(s)F_i + \sum_{j=1}^{o} w_{0j}^{(\delta)}(s)\delta_j] \tag{2.6}$$

The function

$$k_y(s) = [1 + \Phi(s)]^{-1} \tag{2.7}$$

is the transfer function of a closed-loop system (see the end of this Chapter for the main definitions of an open and closed-loop system).

The functions

$$w_i^{(F)}(s) = k_y(s)w_{0i}^{(F)}(s), \qquad w_j^{(\delta)}(s) = k_y(s)w_{0j}^{(\delta)}(s) \tag{2.8}$$

are the transfer functions of the object for the dynamic excitations which also include the feedback influence of the control system.

If there were no active facilities in the system, the following expression for the variable y would hold

$$y(s) = \sum_{i=1}^{k} w_{0i}^{(F)}(s) F_i(s) + \sum_{j=1}^{s} w_{0j}^{(\delta)}(s) \delta_j(s) \tag{2.9}$$

which could be obtained from eq. 2.1 by letting $u = 0$. In this case y could be considered as uncontrolled. Comparing eqs. 2.9 and 2.6, one finds that the operator $k_y(s)$ characterises the active facility efficiency with respect to the variable y [1].

The transfer function approach for the analysis of this linear systems is also treated in [5] in addition to several methods of system analysis in the dynamic field like the modal one with the eigenvalues problem. It is worth underlining that in [1] the attention is focused on the devices of vibration protection so the transfer function method is introduced and developed in order to analise the vibration protection devices and their characteristics. The control devices are considered like elements of the whole structure not as something to be added and thought separately.

2.2.1 Transfer function of a feedback connection

Figure 2.4 presents a general system composed by two elements and a feedback connection. It is possible to evaluate the transfer function of the whole system through each single element one:

$$y(s) = w_1(s)(u(s) + F(s)) \tag{2.10}$$

$$u(s) = w_2(s) y(s) \tag{2.11}$$

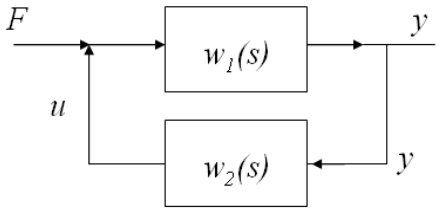

Figure 2.4: Closed-loop system

substituting last equation in the previous one

$$y(s) = w_1(s)w_2(s)y(s) + w_1(s)F(s) \tag{2.12}$$

so it results

$$y(s) = \frac{w_1(s)}{1 - w_1(s)w_2(s)}F(s) \tag{2.13}$$

Considering $w_1(s) = 1$ the transfer function of the feedback is

$$y(s) = \frac{1}{1 - w_2(s)}F(s) \tag{2.14}$$

Note that it is the same expression of eq. 2.7 with $w_2(s) = \Phi(s)$.

2.3 Efficiency of one-dimensional active systems

Attention is now focused on the efficiency of one-dimensional active systems, with a more general approach, like the one depicted in Figure 2.5, under the assumption that the system to be protected is linear and possesses weak dissipation. The transfer function of the closed-loop system is represented by

$$k_y(s) = [1 + e_{AB}(s)w_y(s)]^{-1} \tag{2.15}$$

where e_{AB} is the *dynamic compliance operator* relating a force applied to a system point and acting in a prescribed direction to the projection of the

displacement of another point on some different direction. The system is one-dimensional for the control force (see Definition 7) but presents multi d.o.f. It can be also defined as SIMO system (single input $F(t)$ and multi output y).

Comparing eq. 2.7 and eq. 2.15 the operators e_{AB} here introduced in a more general approach is the same $w_0^{(u)}$ with the assumption that the two one-dimensional systems considered are the same.

From Figure 2.5 and eq. 2.15 one derives

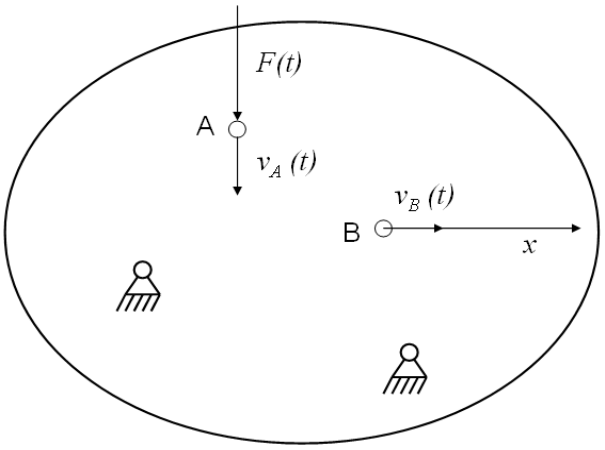

Figure 2.5: Definition of the dynamic compliance operator

$$v_B(t) = e_{AB}(s)F(t) = e_{BA}(s)F(t) \tag{2.16}$$

Let e_A be the compliance relating $F(t)$ at point A and $v_A(t)$ the displacement of the same point in the direction of $F(t)$ (see Figure 2.5), so $v_A(s) = e_A F(s)$, one obtains

$$y_A(s) = [1 + e_A(s)w_y(s)]^{-1}\zeta_A(s) \tag{2.17}$$

or

$$y_A(t) = k_y(s)\zeta_A(t) \tag{2.18}$$

Eq. 2.18 expresses that the controlled displacement is function of the uncontrolled one by the term $k_y(s)$ (it follows also from eqs. 2.6 and 2.9). This implies that the efficiency condition of the one-dimensional vibration protection system is $|k_y(s)| < 1$. The efficiency of the system of vibration protection aims at decreasing the intensity of the vibration field. The efficiency condition can also be expressed (see eqs. 2.5, 2.7 and 2.15)

$$|1 + \Phi(s)| > 1 \tag{2.19}$$

Since a complex quantity can be written as

$$\Phi(s) = |\Phi(s)|(cos\varphi + isin\varphi) \tag{2.20}$$

where $\varphi = arg\Phi(s)$, the system efficiency can be investigated analitically. From 2.19 and 2.20

$$|1 + |\Phi(s)|(cos\varphi + isin\varphi)| > 1 \tag{2.21}$$

$$(1 + |\Phi(s)|cos\varphi)^2 + (|\Phi(s)|sin\varphi)^2 > 1 \tag{2.22}$$

$$1 + |\Phi(s)|^2 cos^2\varphi + 2|\Phi(s)|cos\varphi + |\Phi(s)|^2 sen^2\varphi > 1 \tag{2.23}$$

$$|\Phi(s)|cos^2\varphi + |\Phi(s)|sin^2\varphi > -2cos\varphi \tag{2.24}$$

$$|\Phi(s)| > -2cos\varphi \tag{2.25}$$

Plotting the resulting expression, Figure 2.6, for the nature not negative of the function $|\Phi(s)|$, one can underline the following sufficent conditions of efficiency

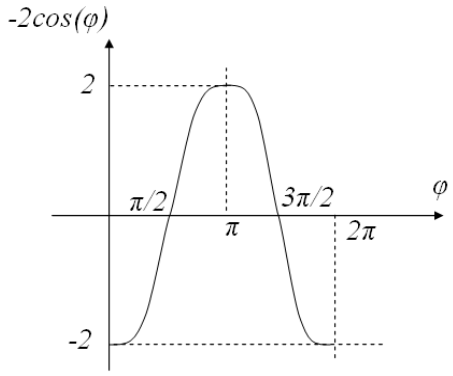

Figure 2.6: Curve $1/cos(\varphi)$ between the argument values $[0, 2\pi]$

- $|\Phi(s)| > 2$
- $|\Phi(s)| > 0$ and φ not in the bandwidth $[\pi/2, 3\pi/2]$
- $|\Phi(s)| > 0$, φ in the bandwidth $[\pi/2, 3\pi/2]$ and eq. 2.25 verified

Another graphic solution for the efficiency condition is the polar plot in the complex plane $(Re\Phi(s), Im\Phi(s))$. Considering a general form for the function $\Phi(s)$, the domain where it is not possible to verify eq. 2.25 is represented by the circle of radius 1 with centre in $-1 + j0$. From Figures 2.6 and 2.7 one can recognize:

- when the argument φ is between $[0, \pi/2[$ and $]3\pi/2, 2\pi]$ there are not efficiency limitations.
- When φ is in $[\pi/2, 3\pi/2]$ the circle limits the inefficiency domain for $\Phi(s)$.

The efficiency problem of an one-dimensional system of vibration protection is here developed following reference [1].

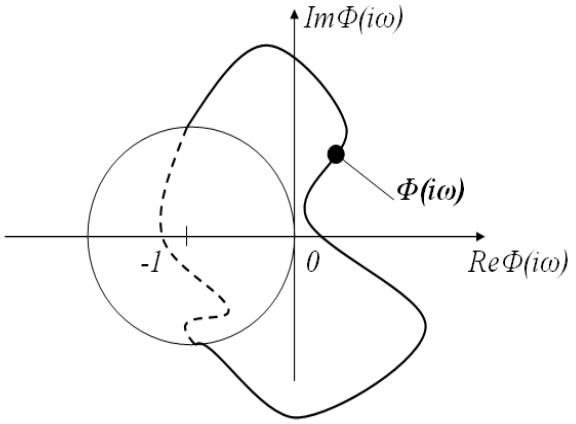

Figure 2.7: Part of the complex plane where the efficiency condition is verified.

The efficiency for a system of vibration protection can be also considered like an index of performance: if $|\Phi(s)| \gg 1$ (see eq. 2.18 and 2.19) the controlled displacement ζ_A is strongly reduced.

In [5] the problem of performance for a system of vibration protection is reported. A transfer function approach is developed and it is addressed on the evaluation of the error of the control system, the difference between the realization and the command. Finally this approach concludes defining some evaluation criteria. This methodology is frequently used by the control community, different evaluation criteria can be defined to estimate the system performance where one want to focus his attention. The evaluation criteria approach reveals to be very effective in order to assess the system efficiency.

2.4 Evaluation of efficiency by graphical methods

It is convenient to carry out the main methods available to investigate the efficiency of active systems of vibration protection by means of graphic-analytical methods. One of these methods it is been presented for a one-dimensional system in the previous section.
Another method of analysis of efficiency is the Bode plot of the transfer function $\Phi(s)$. If the system is *asymptotically stable*, this implies the real part of Laplace variable can be neglected, so let be $s = j\omega$. The meaning of "asymptotically stable" will be clarified in the next section which is devoted to the stability conditions for dynamic systems.
The Bode plot actually consists of two plots, namely, *gain versus frequency* and *phase versus frequency*. The following expression

$$L = 20log|\Phi(j\omega)| \tag{2.26}$$

is introduced to plot the logarithmic frequency characteristics of $\Phi(j\omega)$ as a function of $log\omega$: it is referred to as the *logarithmic amplitude characteristic* (LAC) for the open-loop system $\Phi(j\omega)$. The factor 20 indicates that L is measured in decibels. The relation

$$\varphi = arg\Phi(j\omega) \tag{2.27}$$

on $log\omega$ is referred to as the *logarithmic phase characteristic* (LPC).

2.4.1 Bode plot of a system as sum of simple elements

The transfer function of the system can be represented as the product of the transfer functions of the following simple elements:

- aperiodic element

$$w(s) = \frac{k}{Ts+1} \tag{2.28}$$

- vibratory element

$$w(s) = \frac{k}{T^2s^2 + 2\zeta_d Ts + 1} \tag{2.29}$$

- integrator and differentiator

$$w(s) = \frac{k}{s}, \qquad w(s) = ks \tag{2.30}$$

- first order element (proportional-derivative element) and second order element

$$w(s) = k(Ts+1), \qquad w(s) = k(T^2s^2 + 2\zeta_d Ts + 1) \tag{2.31}$$

where T and ζ_d are respectively the time constant of the system and the damping factor [1].
The product of transfer functions consists in a connection in series of the respective systems [3] [4]. For the linear property the LAC and LPC of the whole system can be determined as sums of LAC and LPC of the simple elements.

2.4.2 Bode analysis of efficiency

Consider the active system of vibration protection having transfer function 2.17. The active feedback in this system forms a control force proportional to the absolute displacement of point A (see eq. 2.3).

$$w_y(s) = k \tag{2.32}$$

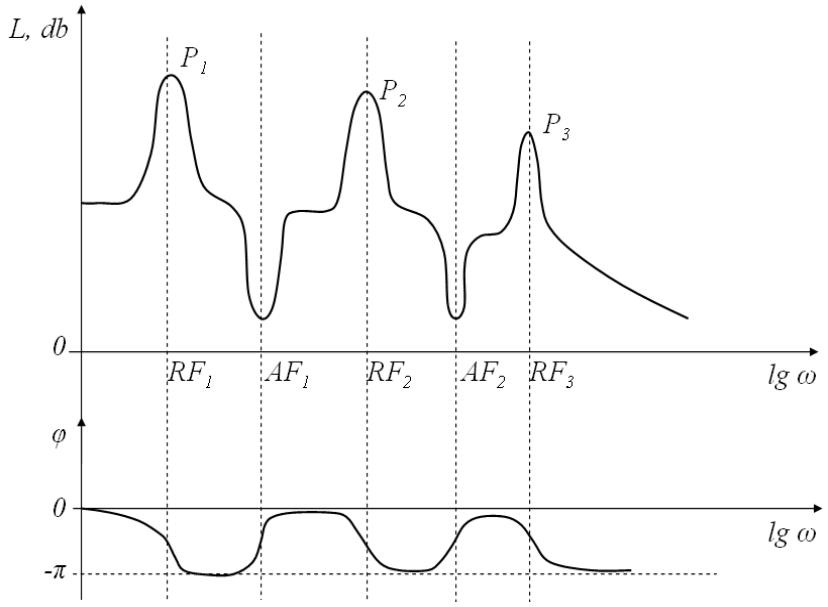

Figure 2.8: Bode plots for proportional active feedback [1]

Accurate informations about the efficiency of active feedback can be obtained by investigating the LAC and LPC of the Bode plot depicted in Figure 2.8 [1].
It is possible to distinguish, according with [5]:

- *peak amplitude* for LPC, the local maximum value of L ($P_{1,2,3}$ in Figure 2.8);
- *resonant frequency*, the frequency corresponding to to the peak amplitude ($RF_{1,2,3}$ in Figure 2.8);
- $anti-resonant\ frequency$, the frequency corresponding to the minimum local value of L ($AF_{1,2}$ in Figure 2.8);
- *crossover frequency*, the frequency value where L is 0 (from eq. 2.26,

also where $|\Phi(j\omega)| = 1$.

In the case of Figure 2.8 the active facility is ineffective at high frequency, when exceeding the crossover frequency.
The LAC curve decreases at anti-resonant frequencies $AF_{1,2}$. It is a reduction of the amplitude or magnitude of the active system of vibration protection, which may lead to inefficiency of the system.
Additional information on the efficiency of active feedback can be also obtained by investigating the LPC of the Bode plot [1].
Between the limits

- $0 \leq lg\omega \leq RF_1$
- $AF_1 < lg\omega \leq RF_2$
- $AF_2 < lg\omega \leq RF_3$

the efficiency condition is satisfied for any value of $|\Phi(j\omega)|$, as it also results from Figures 2.6 and 2.7.
On the other side if

- $RF_1 < lg\omega \leq AF_1$
- $RF_2 < lg\omega \leq AF_2$

for satisfying the efficiency condition it is necessary that the absolute value of $\Phi(j\omega)$ is sufficiently large. Increasing the feedback gain leads to an increase in feedback efficiency (where *gain* means the magnitude of the frequency response $|\Phi(j\omega)|$ [5]).
Bode plots for the evaluation of the system efficiency result to be more effective than the mathematic approach (eqs. 2.19-2.25): the dependence on the

variable ω is clearly expressed as well as the increment and the decrement of efficiency as function of the gain.
The Bode plots for system analysis are reported in both [5] and [1]. In the last book more emphasis is devoted to the control devices.
Finally it is worth noting that the efforts toward an increase of the efficiency of a vibration protection system are closed to an optimization process [3] [4] [6] [7].

2.5 Conditions for stability

In order to properly perform, any active system must be *stable* and posses a certain *stability margin*. The system stability must not be affected by occasional deviations in system parameters. In what follows the stability theory of linear time-invariant systems is detailed [1] [3] [5].
Consider a system of linear homogeneous differential equations with constant coefficients which can be written in a vector form

$$\dot{\mathbf{y}} = A\mathbf{y} \tag{2.33}$$

Here $\mathbf{y}$ is a vector of n dimensions and A is a constant matrix. System 2.33 is said to be stable if, all its solutions $\mathbf{y} = \mathbf{y}(t, \mathbf{y}_0, t_0)$ due to initial conditions $\mathbf{y} = \mathbf{y}(t_0, \mathbf{y}_0, t_0) = \mathbf{y}_0$ are bounded for all $t > t_0$. In this definition, $\mathbf{y}(t)$ is termed to be *bounded* if its components are all bounded. If all solutions of eq. 2.33 are stable in the above sense, and satisfy the following condition

$$\lim_{t \to \infty} \mathbf{y}(t) = 0 \tag{2.34}$$

then system 2.33 is called asymptotically stable.
If system 2.33 is stable it is easy to prove that all solutions of the inhomo-

geneous equation

$$\dot{\mathbf{y}} = A\mathbf{y} + \mathbf{f}(t) \tag{2.35}$$

are bounded for any bounded function $\mathbf{f(t)}$. In other words, the presence of function the $\mathbf{f(t)}$ does not affect stability.

System 2.33 is asymptotically stable (necessary and sufficient condition) if the eigenvalues of $\lambda_1, ...\lambda_n$ of matrix A, the roots of the following characteristic equation

$$det(A - \lambda I_n) = 0 \tag{2.36}$$

have negative real values. For mere (non-asymptotic) stability it is necessary and sufficient that the real parts of all eigenvalues are non-positive, and additionally, the rank of matrix $A - \lambda I_n$ is equal to multiplicity of eigenvalue λ_k.

In designing vibration protection systems one usually deals with conditions of asymptotic stability. Vibration protection systems which are not asymptotically stable are not encountered in practice. Determinant 2.36 can be cast as follows

$$a_0\lambda^n + a_1\lambda^{n-1} + ... + a_{n-1}\lambda + a_n = 0 \tag{2.37}$$

with $a_0 > 0$.

There exist a number of criteria which enable one to judge the stability of system 2.33 in terms of the factors of the characteristic equation 2.37 without solving this equation. In that follows, the *Stodola criterion* and the *Hurwitz criterion* are discussed [1] [3] [5].

According to the Stodola criterion, for asymptotic stability it is *necessary* that alI coefficients are positive (note that $a_0 > 0$, eq. 2.37).

The Hurwitz criterion says that a *necessary and sufficient* condition for asymptotic stability is that all the principal minor determinants of the *Hurwitz matrix*

$$H_w = \begin{bmatrix} a_1 & a_0 & 0 & 0 & ... & 0 \\ a_3 & a_2 & a_1 & a_0 & ... & 0 \\ a_5 & a_4 & a_3 & a_2 & ... & 0 \\ ... & ... & ... & ... & ... & ... \\ a_{2n-1} & a_{2n-2} & a_{2n-3} & a_{2n-4} & ... & a_n \end{bmatrix} \tag{2.38}$$

are positive. The rule for the matrix construction is transparent from formula 2.38, furthermore $a_i = 0$ for $i > n$.

2.5.1 Example

The Hurwitz criterion allows one to investigate the stability conditions for the system with the following parametric transfer function

$$W(s) = \frac{1}{s^3 + as^2 + bs + a(b-1)} \tag{2.39}$$

Only the denominator plays a basic role for the system stability

$$D(s) = s^3 + as^2 + bs + a(b-1) \tag{2.40}$$

If all the coefficients have the same sign a preliminary condition for stability is verified but it is not sufficient. So this last is verified if $a > 0$ and $b > 1$. Only the Hurwitz criterion furnishes the necessary and sufficient condition for asymptotic stability.
So the Hurwitz matrix is the following

$$H_w = \begin{bmatrix} a & 1 & 0 \\ a(b-1) & b & a \\ 0 & 0 & a(b-1) \end{bmatrix} \tag{2.41}$$

The principal minor diagonal determinants are the following

$$\Delta_1 = a \tag{2.42}$$

$$\Delta_2 = ab - a(b-1) \tag{2.43}$$

$$\Delta_3 = a^2 b(b-1) - a^2(b-1)^2 \tag{2.44}$$

for the Hurwitz criterion they have to be positive. It is verified only if $a > 0$ and $b > 1$. So the necessary condition evaluated by the preliminary step is verified to be also sufficient.

2.6 Summary of Chapter 2

In this chapter a theoretical approach to linear active systems of vibration protection is discussed. For this purpose:

- the use of Laplace transforms and system transfer functions is illustrated.
- Polar plots and Bode plots are introduced toward an efficiency evaluation of the system.
- Stability definitions are introduced together with some fundamental criteria.

Finally a synthesis on some basic issues concerning control systems is proposed:

- the passive system of vibration protection can be presented as the simplest typology: the device works without using data collected from other elements as sensors. The passive protection can be considered asymptotically stable.

- Active systems are the most effective in the vibration protection of mechanical systems. They are complicated by a large number of elements which participate in the input data processing and the formation of the control forces. They are sensors, actuator devices and other facilities, acting in the amplification and manipulation of data.

- The semi-active system can be considered as a passive system, able to change its characteristics actively, driven by an external command.

- An open-loop system is a combination in a series of elements, from a starting point to another point in a flow scheme. Its transfer function is the result of the product of each single element transfer function.

- A closed-loop system is a combination of elements with a feedback connection.

Notation

All symbols used in this chapter have been defined chronologically, as they appear in the text.

s	Laplace variable
$\mathbf{F}$	vector of forces excitations
δ	vector of kinematics excitations
$\mathbf{y}$	vector of vibration field measured
W_{sF}	transfer function matrix of forces excitations
$W_{s\delta}$	transfer function matrix of kinematics excitations
W_{sy}	transfer function matrix of vibration field measured
ψ	output signal vector of the sensors
W_c	transfer function matrix of the linear compensators

W_a	transfer function matrix of the linear actuators
$\mathbf{u_{out}}$	vector of the compensator output
$\mathbf{u}$	control forces on the object
W_0	transfer function matrix of the object
$\mathbf{R}$	forces applied on the base
W_1	transfer function matrix relates forces applied on the base to the kinematics excitations
$w_{0i}^{(F)}$	row of $W_0^{(F)}$
$w_{0j}^{(\delta)}$	row of $W_0^{(\delta)}$
$w_0^{(u)}$	row of $W_0^{(u)}$
$w_a^{(u)}$	row of $W_a^{(u)}$
$w_a^{(y)}$	row of $W_a^{(y)}$
w_c	row of W_c
w_{sy}	row of W_{sy}
w_y	feedback transfer function
Φ	transfer function of an open-loop system
k_y	transfer function of an closed-loop system
w_i^F, w_i^δ	rows of W_0 including the feedback influence of the control system
w_1, w_2	generic transfer function
e_{AB}	dynamic compliance operator
ζ	uncontrolled displacement
v	generic displacement
φ	phase function
π	constant, semi-perimeter of circle with radius 1
j	immaginary constant
ω	frequency (rad/sec)
L	logarithmic amplitude of Φ
k	proportionality coefficient
T	time constant of a system
ζ_d	damping factor of a system
P	peak amplitude of LAC
RF	resonant frequency of LAC
AF	anti-resonant frequency of LAC
t	time
A	constant matrix
$\mathbf{f}$	generic bounded function
λ	eigenvalues of A
I_n	identity matrix of n dimension
a_n	generic coefficient
H_w	Hurwitz matrix
a, b	generic coefficients

Bibliography

[1] Kolovsky M.Z., 1999
Nonlinear Dynamics of Active and Passive Systems of Vibration Protection,
Foundations of Engineering Mechanics, Springer-Verlag, ISBN 3-540-65661-8.

[2] Battaini M., 1998
Sistemi strutturali controllati: progettazione ed affidabilitá,
Ph.D. Thesis (in Italian), Structural Mechanics Dept., University of Pavia.

[3] Kovaleva A., 2005
Control Theory with Application to Engineering Systems,
Lectures, January 17-21, 2005, Structural Mechanics Dept., University of Pavia.

[4] Kovaleva A., 1999
Optimal Control of Mechanical Oscillations ,
Foundations of Engineering Mechanics, Springer-Verlag, ISBN 3540654429.

[5] Meirovitch L., 1990
Dynamics and Control of Structures,
John Wiley and Sons, ISBN 0-471-62858-1.

[6] Kwakernaak H., Sivan R., 1972
Linear Optimal Control Systems,
John Wiley and Sons, ISBN 0471511102.

[7] Bryson A.E., 1981
Applied Optimal Control,
Hemisphere Pub. Corp., ISBN 0891162283.

Chapter 3

Actuators for vibration protection systems

3.1 Introduction

The actuators generate the control forces, and, for this reason, they are among the most important elements in systems of vibrations protection. It is the actuator which determines a particular type of vibration protection systems [1]. A governing law for the control forces $u(t)$ for active and semi-active systems depends on the output signal of the compensators u_{out}, but also on the motion of the object (see eq. 2.2).

Control algorithms are developed for driving active and semi-active systems of vibration protection; some details can be found in [2] [3]. Passive control systems are the simplest devices, they do not need to be driven by algorithm because they generate control forces as a function of the structure dynamic configuration.

It is worth mentioning that, in some cases, actuators are nonlinear systems with complex dynamic characteristics. A linearization of these character-

istics is feasible under some simplifying assumptions. The applicability of linear models is bound and dependent on the validity of basic assumptions. The equations for the dynamic characteristics of the most popular actuators are derived further on in this chapter.

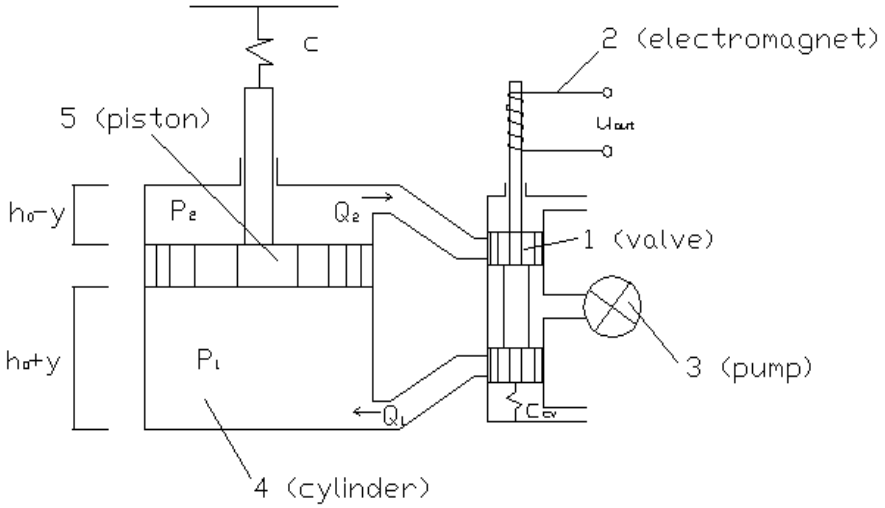

Figure 3.1: Scheme of a simple hydraulic actuator

3.1.1 Hydraulic actuators

One of the simplest hydraulic actuators is schematically displayed in Figure 3.1 where one can find:

- 1 the control valve,
- 2 the electromagnet,
- 3 the pump,
- 4 the cylinder divided in two chambers,

- 5 the piston.

The roles of these elements can be described as follows:

- the displacement of the control valve 1 is due to the electromagnet 2 which is activated by the electric input signal $u_{out}(t)$. This facility is called *electrohydraulic.*
- The displacement of the control valve causes the working fluid to enter into one of the chambers of cylinder 4, the other chamber being connected via the control valve to an outlet discharge pipe.
- The pressure in the working fluid is provided by pump 3.
- The pressure difference in the chambers produces a force $u^*(t)$ which acts on piston 5 and the object connected to it.

The relationship between the input voltage $u(t)_{out}$ and the control valve displacement $v(t)$ can be cast in the form

$$v = \frac{k_v}{m_{cv}s^2 + b_{cv}s + c_{cv}} u_{out} = \frac{k_v}{c_{cv}} \frac{1}{T_{cv}^2 s^2 + 2\zeta_{cv} T_{cv} s + 1} u_{out} \tag{3.1}$$

where m_{cv}, c_{cv} and b_{cv} are the mass of the control valve, the rigidity of its elastic element (rigidity of the compressive working fluid) and the resistance factor, respectively. k_v denotes the factor relating the electromagnet force to the input voltage, $T_{cv}$the system time constant.
The dependence of v on u_{out} may deviate from that given by eq. 3.1. It is suggested that a control valve facility consists of an ideal delay circuit, non-inertial linear amplifier (see Appendix C) and an element implementing the limitation of valve movement in a series.

The piston dynamic characteristic can be now derived; it relates the force acting on the piston to the piston displacement. To this aim, one considers a dynamic model of the system which takes into account the compresibility of the working fluid and the leakage via the clearance between the piston and the cylinder wall.
One assumes that the working fluid enters the lower cylinder chamber whereas the upper chamber is connected to the outlet discharge pipe. By looking at the Figure 3.1 it is possible to notice that:

- the pressures in the lower and upper chambers are denoted by p_1 and p_2, respectively,
- S is the piston area,
- h_0 is the length of each chamber in the middle position of the piston,
- y is the piston displacement, with $y = 0$ denoting the middle position, of the piston,
- V_1 and V_2 are chambers volumes,
- Q_1 is the volume flow rate of fluid entering the lower chamber, and Q_2 is the volume flow rate of fluid leaving the upper chamber.

One writes

$$V_1 = S(h_0 + y), \qquad V_2 = S(h_0 - y) \tag{3.2}$$

and hence

$$\dot{V}_1 = -\dot{V}_2 = S\dot{y} \tag{3.3}$$

A relative decrease in volume for a compressive fluid may be considered to be proportional to an increase in pressure

$$\Delta V = \mu V \Delta p \tag{3.4}$$

where μ designates the compressibility factor.

If pressure and volume are time-dependent, it follows from eq. 3.4 that

$$\dot{V} = -\mu V \dot{p} \tag{3.5}$$

Let us assume that the fluid leakage is proportional to the difference in pressure in the cylinder chambers

$$Q_l = \chi(p_1 - p_2) \tag{3.6}$$

where Q_l denotes the volume flow rate through clearance and χ is the leakage factor.

From eqs. 3.5 and 3.6 one has

$$\begin{aligned} \dot{V}_1 &= Q_1 - \mu V_1 \dot{p}_1 - \chi(p_1 - p_2) \\ \dot{V}_2 &= -Q_2 - \mu V_2 \dot{p}_2 + \chi(p_1 - p_2) \end{aligned} \tag{3.7}$$

Substituting eqs. 3.2 and 3.3 into 3.7, one obtains the following expressions for the volume flow rates

$$\begin{aligned} Q_1 &= S\dot{y} + \mu S(h_0 + y)\dot{p}_1 + \chi(p_1 - p_2) \\ Q_2 &= S\dot{y} - \mu S(h_0 - y)\dot{p}_2 + \chi(p_1 - p_2) \end{aligned} \tag{3.8}$$

On the other hand, the value of volume flow rate through the control valve depends on the piston displacement and on the difference of the input and output pressures. Since considerable pressure differences are typical for hydraulic actuators it is common practice to assume that the volume flow rates Q_1 and Q_2 depend only on the control valve position v, so the following

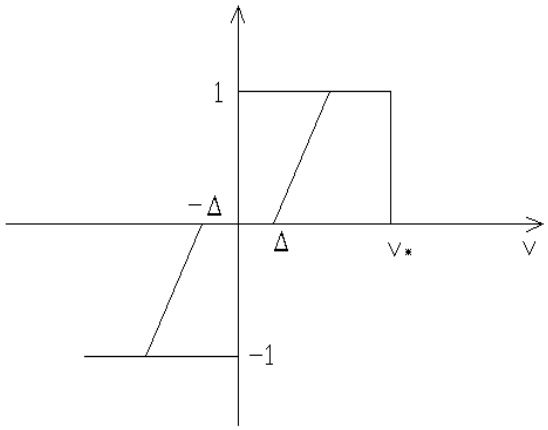

Figure 3.2: Non linear law of the fluid flow rate

relation is deduced

$$Q_i = f(v)Q_{max}(i = 1, 2) \tag{3.9}$$

Here $f(v)$ is a nonlinear function schematically shown in Figure 3.2 where 2Δ denotes the value of the control valve overlap which is equal to the difference between the sizes of the control valve port and the port of the cylinder in which the control valve slides. The maximum volume flow rates corresponding to the fully open port is denoted in eq. 3.9 as Q_{max}.
Provided that the control valve overlap is sufficiently small and v_{max} does not exceed v_*, which corresponds to *saturation* in Figure 3.2, the dependence 3.9 can be treated as linear

$$Q_i = k_v v Q_{max}(i = 1, 2) \tag{3.10}$$

Inserting eq. 3.9 into 3.8 one obtains a system of nonlinear equations relating pressures p_1 and p_2 to the piston displacement $y(t)$ and the control

valve displacement $v(t)$

$$\begin{aligned} Q_{max} f(v) &= S\dot{y} + \mu S(h_0 + y)\dot{p}_1 + \chi(p_1 - p_2) \\ Q_{max} f(v) &= S\dot{y} - \mu S(h_0 - y)\dot{p}_2 + \chi(p_1 - p_2) \end{aligned} \tag{3.11}$$

These equations can be simplified if it is adopted that in the regime under consideration the piston exhibits small displacements about the middle position ($|y| \ll h_0$). Summing the equations in 3.11 yields

$$\frac{\mu h_0}{2}\dot{u}_* + \frac{\chi}{S}u_* = Q_{max} f(v) - S\dot{y} \tag{3.12}$$

where $u_* = S(p_1 - p_2)$ is the force acting on the piston. If function $f(v)$ can be linearized one obtains from eq. 3.12 the following linearised dynamic characteristic for the working cylinder

$$\frac{\mu h_0}{2}\dot{U}_* + \frac{\chi}{S}U_* = Q_{max} k_v v - S\dot{y} \tag{3.13}$$

When the control valve is at rest in the middle position, i.e. $v = 0$, and no leakage is observed, $\chi = 0$, it follows from eq. 3.13 that

$$U_* = -\frac{2S}{\mu h_0} y \tag{3.14}$$

Thus, the working fluid produces a restoring force and, in a certain sense, is equivalent to an elastic element with the following rigidity

$$c_f = \frac{2S}{\mu h_0} \tag{3.15}$$

The dynamic characteristic of the working cylinder is simplified if the fluid compressibility and the leakage through the piston clearance are neglected. Indeed, in this case $\mu = 0$ and $\chi = 0$, and eqs. 3.12 and 3.13 yield

$$\dot{y} = \frac{Q_{max}}{S} f(v) \tag{3.16}$$

$$\dot{y} = \frac{Q_{max}}{S} k_v v \tag{3.17}$$

In this case, the actuator provides a law of the piston motion rather than a control force. The actuator motion is therefore independent of the properties of the control object and depends only on the control valve motion.
Two points have to be highlighted [1]:

- using simplified dynamic characteristics 3.16 and 3.17 is allowed in the case of an approximate investigation of low frequency processes and the respective displacement of the piston is given by

$$y_p = \frac{Q_{max}}{Ss} k_v v \tag{3.18}$$

- In case of high frequency vibrations of the control valve, the amplitude of the respective vibration of the piston becomes small and the hydraulic facility acts as a rigid element, connecting the object and the base. Accordingly, the properties of the vibration protection system at high frequencies turn out to be insufficient. In order to improve these properties, an elastic element is usually installed between the piston and the object. Denoting the rigidity of this element as c and the relative displacement of the object as y_o, one obtains the following equation for the control force

$$u(t) = -c(y_o - y_p) = -cy_o + \frac{cQ_{max}k_v}{Ss} v \tag{3.19}$$

Equation 3.13 determines the force acting on the piston. In order to obtain the control force $u(t)$, one accounts for the piston inertia force and the resistance force, to get

$$u(t) = u_*(t) - m_p \ddot{x}_p - b_p \dot{y} \tag{3.20}$$

Here m_p denotes the equivalent mass of the piston and of the possible elements attached to the piston, $\ddot{x}_p$ is the absolute acceleration of the piston, and b_p is a factor taking into account the resistance force. As mentioned above, a hydraulic device produces not only a control force $u(t)$ applied to the object to be protected, but also a force acting on the base. Clearly, the latter force is equal to $-u(t)$ when the cylinder housing is attached to the base.

In the above investigation, the possible disturbances of the hydraulic facilities (for example air in the working fluid) have not been taken into account.

3.1.2 Pneumatic actuators

A gas pneumatic working chamber bound by a piston of area S, Figure 3.3, is considered. Let y denote the piston displacement relative to the initial position h_0. The input throttle has cross-sectional area f which is controlled by the flap displacement $u_f(t)$. p' is the pressure external to the chamber.

In line with the conventional practice in the design of pneumatic systems,

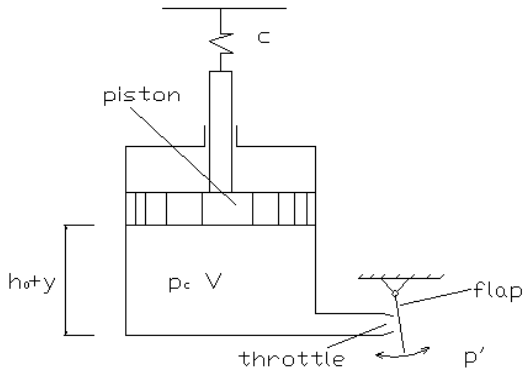

Figure 3.3: Scheme of a single throttle pneumatic working chamber

the following assumptions are made:

- the influence of the working body mass density on the flow rate is negligible for small pressure differences.
- Flow rate variations through the throttle are not influenced by gas inertia but only by pressure variations.
- The pressure is equal in any point of the chamber, at any instant of time.

Under these assumptions, the mass flow rate of the gas via the throttle depends on the position of the flap and on the input and output pressures

$$G = G(p', p_c, u) \tag{3.21}$$

where p_c stands for the chamber pressure. The mass flow rate characteristics depend on the pressure ratio p_c/p'. If this ratio is larger than some critical value (which is 0.53 for air), the outflow is called under-critical; otherwise it is called over-critical. With these introductions one can distinguish:

- In the case of an under-critical outflow, the mass flow rate is determined by the following formula

$$G = \zeta f(u_f) g \sqrt{2\rho' p' [\frac{k}{k-1} (\frac{p_c}{p'})^{2/k} - (\frac{p_c}{p'})^{(k+1)/k}]} \tag{3.22}$$

  Here ζ is a flow rate factor which varies between 0.75 and 0.9, depending upon the throttle design, $f(u_f)$ is the cross-sectional area of the throttle, ρ' is the mass density of the gas before the throttle, k is the ratio of the specific heat at constant pressure to the specific heat at constant volume ($k = 1.4$ for air), g the gravity acceleration.

- In the case of an over-critical outflow, the mass flow rate does not depend upon the pressure ratio and is given by

$$G = \zeta f(u_f) g \sqrt{2\rho' p' \frac{k}{k+1} (\frac{2}{k+1})^{2/(k-1)}} \tag{3.23}$$

Equations 3.22 and 3.23 correspond to an adiabatic outflow which is normally observed for throttles of pneumatic systems. As a rule, the process of filling the working chamber is accompanied by intensive heat exchange and may be deemed as being isothermal. In this case, the gas equation

$$p_c V = \frac{M}{\mu_m} R\Theta \tag{3.24}$$

where M is mass of the gas in the chamber, μ_m the molecular mass, Θ is the absolute temperature and R is the gas constant, yields

$$\frac{d}{dt}(p_c V) = \frac{R\Theta}{\mu_m} \frac{dM}{dt} = \frac{R\Theta}{\mu_m g} G(p', p_c, u_f) \tag{3.25}$$

Taking into account that

$$V = S(h_0 + y), \qquad \dot{V} = S\dot{y} \tag{3.26}$$

one obtains

$$\dot{p}_c S(h_0 + y) + p_c S\dot{y} = \frac{R\Theta}{\mu_m g} G(p', p_c, u_f) \tag{3.27}$$

Provided that $p'(t)$ and $u_f(t)$ are prescribed, one can determine p_c from this equation. The linearization of this equation is feasible if small displacements about some stationary position are considered, y and $\dot{y}$ are small and p is close to a constant value p_0. In this case, eq. 3.27 can be written as follows

$$Sh_0\dot{p}_c + Sp_0\dot{y} = \frac{R\Theta}{\mu_m g}[G(p', p_c, 0) + (\frac{\partial G}{\partial u_f})_0 + (\frac{\partial G}{\partial p})_0 (p_c - p_0)] \tag{3.28}$$

Assuming that in the stationary state $p' = p_c$, and, thus, $G = 0$, eq. 3.28 yields

$$h_0\dot{u}_* + u_0\dot{y} = \frac{R\Theta}{\mu_m g S}(\frac{\partial G}{\partial p_c})_0(u_* - u_0) + \frac{R\Theta}{\mu_m g}(\frac{\partial G}{\partial u_f})_0 u_f \tag{3.29}$$

Here $u_* = Sp_c$ is the pressure force acting on the piston, and $u_0 = Sp_0$. Introducing the time constant

$$T_a = \frac{h_0\mu_m g S}{R\Theta(\frac{\partial G}{\partial p_c})_0} \tag{3.30}$$

the final result is

$$T_a\Delta\dot{u} + \Delta u = \frac{S(\frac{\partial G}{\partial u_f})_0}{(\frac{\partial G}{\partial p_c})_0}u_f - \frac{U_0\mu_m g S}{R\Theta(\frac{\partial G}{\partial p_c})_0}\dot{y} \tag{3.31}$$

where $u = u_* - u_0$. Equation 3.31 must be solved together with the equation of motion for the object to be protected.

Pneumatic actuators can have design solutions which differ from those afore shown (for example a connection of several chambers), but the approach presented can be generalized [1].

3.1.3 Electromechanical actuators

Direct current (DC) and alternate current (AC) motors are actuators of an electromechanical nature. The rotor movement is ordinarily transmitted to the object so that the velocity of the object $\dot{y}$ related to the motor housing is proportional to the rotor angular velocity Ω, see Figure 3.4, while the control force $u(t)$ is proportional to the load torque moment M_l, i.e.

$$\dot{y} = r\Omega, \qquad M_l = rU \tag{3.32}$$

Here r is a proportionality factor depending on the gear parameters.

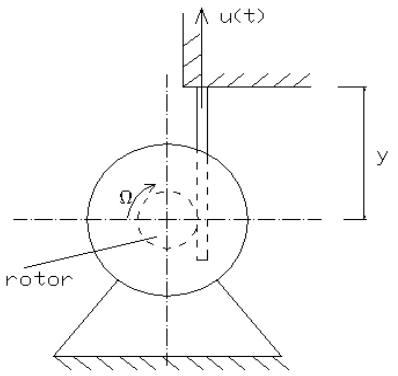

Figure 3.4: Scheme of an electromechanical actuator

From a general point of view, considering the relation between the torque M_t applied by a motor on a rotating mass and the angular velocity Ω of this mass, it is known that

$$M_t = \dot{\Omega} J + \beta \Omega \tag{3.33}$$

where J is the moment of inertia of the mass, β is the coefficient of viscous friction resistance .

So the general governing equation for the rotor adds with M_l, as follows

$$M_t = \beta \Omega + J \dot{\Omega} + M_l \tag{3.34}$$

where J is the equivalent moment of inertia of all masses connected to the rotor, β is the coefficient of viscous resistance and M_t is the motor torque. The relationship between torque and angular velocity is given by the so called working characteristic of the motor. The dynamic characteristic of a DC-motor is given by

$$(T_e s + 1) M_t = M_0 - \eta \Omega \tag{3.35}$$

Here T_e is the electric time constant of the motor which is equal to the ratio of the armature inductance L_a to the resistance of the armature R_a. M_0 and η, denote the starting torque and the characteristic slope for which the following relationships hold

$$M_0 = k_1 \Phi_f u_a, \qquad \eta = k_2 \Phi_f^2 \tag{3.36}$$

where Φ_f denotes the flux, u_a is the armature voltage, and k_1 and k_2 are factors whose values are dependent on the particular type of the motor. The control of the motor can be performed by changing the armature voltage or the flux. Therefore, u_a and Φ_f may be viewed as the input variables of the actuator. Substituting M_t from eq. 3.34 into 3.35 and taking into account eqs. 3.32 and 3.36 yields

$$(T_e s + 1)[(Js + \beta)\frac{sy}{r} + ru] = k_1 \Phi_f u_a - k_2 \Phi_f^2 \frac{sy}{r} \tag{3.37}$$

and, after some algebra

$$u = \frac{k_1 \Phi_f}{r(T_e s + 1)} u_a + \frac{[T_e J s^2 + (J + T_e \beta)s + \beta + k_2 \Phi_f^2]s}{r^2 (T_e s + 1)} y \tag{3.38}$$

This expression relates the control force u with the object displacement y and the input variables. This equation must be supplemented with the equation of motion which relates y and $u(t)$.Characteristic 3.38 is linear provided that $\Phi_f = 0$.

The dynamic characteristic for an AC-motor differs from 3.35 by the presence of a harmonic component. The dynamic characteristic for a two-phase asynchronous motor is

$$(T_e s + 1) M_t = \delta u_{in} - \eta \Omega + k_f \Omega cos 2\nu t \tag{3.39}$$

where δ, ν, and k_f are factors depending on the motor parameters, u_{in} is the input voltage and α is the frequency of the alternating current.

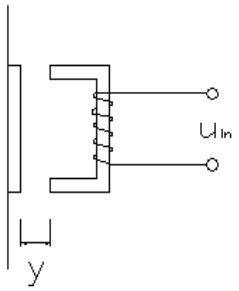

Figure 3.5: Scheme of an electromagnet

3.1.4 Electromagnetic actuators

An electromagnet can be used as a device for providing force. The simplest scheme of an actuator involving an electromagnet is shown in Figure 3.5. The input variable is the voltage $u_{in}(t)$. The electromagnet housing is mounted on the base whereas the armature is attached to the object to be protected from vibration. Relative displacement of the object changes the gap between the core and the armature which in turn changes the electric circuit inductance L, the latter becoming a nonlinear function of the air gap y. The force produced by an electromagnet is proportional to the square of the current and nonlinearly depends on the air gap. In general, the following equation holds

$$u = \mu_0 S(Ni)^2 \varphi(y) \tag{3.40}$$

Here μ_0 is the magnetic permeability, S is the cross-sectional area of the armature, i is the current and N is the number of spires. Further, φ is a nonlinear function, for example $\varphi(y) = (y)^{-2}$ if the magnetic field is homogeneous. The current is governed by the following differential equation

$$\frac{d}{dt}[L(y)i] = u_{in}(t) - r_s i \tag{3.41}$$

where r_s is the resistance. The system of equations 3.40 and 3.41 defines the dynamic characteristic of the device, the dependence of the control force $u(t)$ on $u_{in}(t)$ and $y(t)$ [1].

Figure 3.6: Brushless motor device [4]

Figure 3.7: Device mounted on the universal testing machine

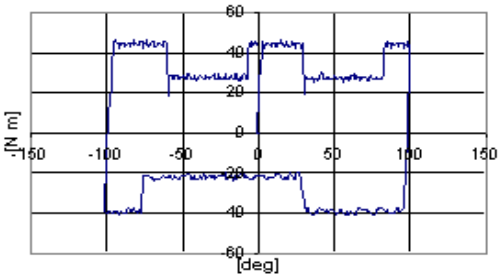

Figure 3.8: Motor operating as semi-active device [4]

3.1.5 Electro-inductive control device

Electro-inductive devices were recently proposed for the passive control of buildings and structures. The feasibility of large size devices for long span bridges was already studied in the occasion of the project of specific bridges: the positive aspect resulting from the adoption of electro-inductive devices is the reduction of the damper size when compared with a hydraulic damper. The way to make an electro-inductive brushless motor device semi-active without loosing its passive control properties was also investigated [4]. The semi-active choice for control applications is given significant attention because it offers adaptability and requires low power supply.

A brushless motor (see Figures 3.6 and 3.7) was tested in the laboratory, for the control of velocity (set equal to zero), with the limit torque constrained to a specific value. The torque value is externally controlled by a board (see Figure 3.8).

The control force $u(t)$ can be realized by adding a device able to transform the rotation of the motor shaft in a linear movement. The semi-active function can be implemented through appropriate mathematic models (for example the Bouc-Wen model [2]). This device typology is applied to a

bridge structural model in Chapter 7.

It is worth noting that the electro-inductive control device has all the practical good points of the brushless motors one usually meets in modern engineering systems.

3.1.6 Electro and magnetorheological dampers

Electrorheological (ER) and magnetorheological (MR) dampers are semi-active control devices that use electrorheological or magnetorheological fluids to produce controllable dampers [6] [3]. They potentially offer highly reliable operation and can be viewed as fail-safe in that they become passive dampers for control hardware malfunction.

This typology of dampers is based on controllable fluids. The essential

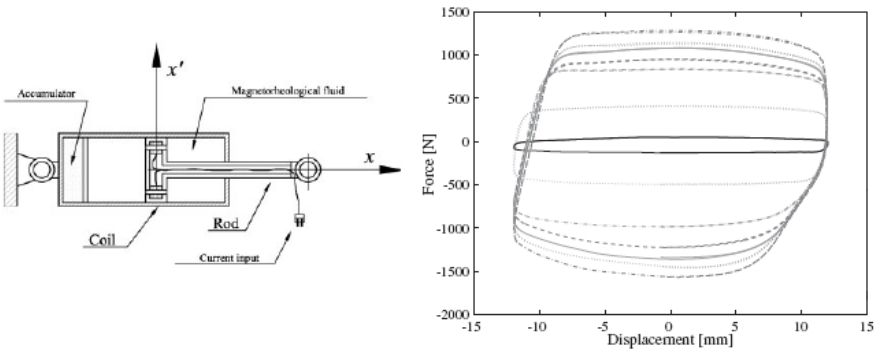

Figure 3.9: MR damper with semi-active behaviour [7]

characteristic of controllable fluids is their ability to reversibly change from a free-flowing, linear viscous fluid to a semisolid one with a controllable yield strength when exposed to an electric or magnetic field.

Figure 3.9 depicts the scheme of an MR damper and its semi-active behav-

iour. The control force $u(t)$ can be modeled with mathematic models as the Bouc-Wen one [2].

3.1.7 Bumpers

Bumpers devices (Figure 3.10) are usually adopted as limiters for the deck displacements in bridge structures. Under external forces or kinematic excitations the deck shows free displacements into a limited region. This region can be differently characterized depending from the structure typology [8].

Figure 3.11 depicts the force-displacement characteristic of bumper devices

Figure 3.10: Bumper [9]

one can adopt for cable-stayed or suspended bridges. The indication $free$ in the picture stands for the free displacement range for the structure; the indication *spring* represents the bumper participation. The elastic force can be designed specifically to prevent undesiderable high frequency vibrations generated after the impact between structure and bumper.

Two situations have to be highlighted:

- Cable-stayed and suspended bridges with great self-centering capacity can be equipped with bumpers between the deck and the piers or between the deck and the bends. The bumpers fix the domain where

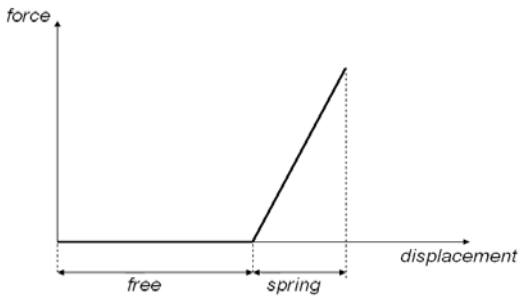

Figure 3.11: Bumpers characteristic

the deck moves freely under external excitations, they work only when the displacement exceeds the limit value of displacement. After the excitation event the structure is able to return into the initial configuration.

- For structures unable to show self-centering characteristics, the bumpers fill the space between the object to be protected and the base. Under external excitations, the structure is able to show large displacements and the centering is reached by the control device.

3.1.8 Elasto-plastic dissipators

The elasto-plastic dissipators are used to reduce structure vulnerability and assure its integrity, by buffering seismic effects. Their main role is to dissipate the input energy in hysteretic cycles and to reduce the applied forces to the object to be protected.
Dissipator devices are usually used between bridge deck and piers. They are coupled with viscous devices able to be stiff for the high velocity induced by strong earthquake and soft for low velocities due to thermal loads [8].

The mechanism of energy dissipation is the elasto plastic flexure of steel

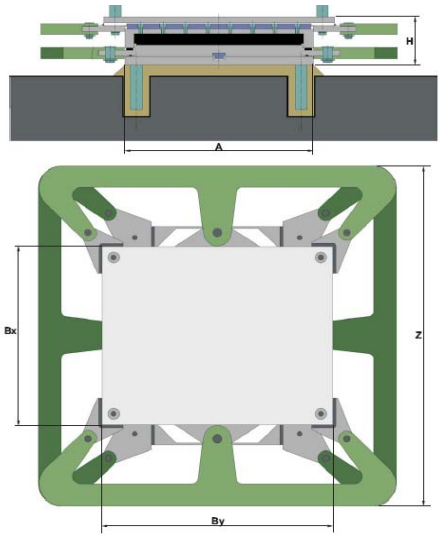

Figure 3.12: Dissipator device [9]

elements. Optimized shape, for example E-shape, see Figure 3.12, allow diffusion of plasticization over most of the volume and by preventing localization and concentration of deformation, provide extended low fatigue cycles. The characteristic force-displacement of these dissipators devices is typically bi-linear, see Figure 3.13. The control force $u(t)$ can be described by means of appropriate mathematic models (like the Bouc-Wen model [2]). This device typology is developed by numerical simulations in Chapter 5. Dissipators devices are very durable, only periodic observations are required in particular after seismic events and the maintenance is needed only in case of ruptures.

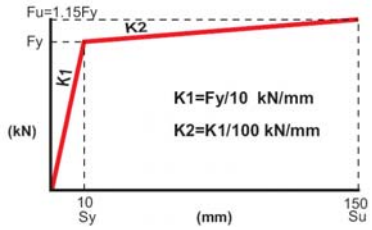

Figure 3.13: Dissipator characteristic force - displacement [9]

3.1.9 Fluido dynamic devices

These devices consist of a steel cylinder filled with a sylicon fluid divided in two chambers by a piston, see Figure 3.14.
The piston incorporates a valve which allows the silicon fluid to move from one chamber to the other, according to the piston movements. The device is usually connected to the structure with two spherical hinges. The force $u(t)$ generated can be described by the law

$$u = \beta \dot{y}^n \tag{3.42}$$

where β is a constant, $\dot{y}$ is the velocity, n is an exponent that may range between 0.2 and 0.1 according to the following typologies:

- 0.1 is normally adopted for viscous dampers. This value maximizes the energy dissipated in the hysteretic cycles [8].
- 0.2 is normally adopted for lock-out devices.

The choice of an exponent 0.2 minimises the reactions of the device for slow movements (creep, temperature effects), and maximises the reaction for dynamic effects (earthquake). The value 0.1 maximizes the energy dissipated in the hysteretic cycles [8].

The life span of these devices is about 35 years. An inspection to the

Figure 3.14: Fluido dynamic device [9]

devices is advised after the first 10 years and subsequently every 5 years. Maintenance consists in verifying the anticorrosion protection of the metal parts and replacing the dust bellows.

3.2 Summary of Chapter 3

Chapter 3 gives the main features of different devices for systems of vibration protection. Table 3.1 provides a brief overview on the control forces produced.

Notation

All symbols used in this chapter have been defined chronologically, as they appear in the text.

Device typology	**Control force**
Hydraulic	$u = \frac{Q_{max} k_v v - S\dot{y}}{\frac{\mu h_0}{2} + \frac{\chi}{S}} - m_p \ddot{x} - b_p \dot{y}$
Pneumatic	$T_a \Delta\dot{u} + \Delta u = \frac{S(\frac{\partial G}{\partial u_f})_0}{(\frac{\partial G}{\partial p_c})_0} u_f - \frac{U_0 \mu_m g S}{R\Theta(\frac{\partial G}{\partial p_c})_0} \dot{y}$
Electromechanical (DC motor)	$u = \frac{k_1 \Phi_f}{r(T_e s+1)} u_a + \frac{[T_e J s^2 + (J + T_e \beta)s + \beta + k_2 \Phi_f^2]s}{r^2(T_e s+1)} y$
Electromagnetic	$u = \mu_0 S (Ni)^2 \varphi(y)$
Electro-inductive	mathematic model (for ex. Bouc-Wen)
Electro and magnetorheological	mathematic model (for ex. Bouc-Wen)
Bumper	elastic linear spring
Elasto-plastic	mathematic model (for ex. Bouc-Wen)
Fluido dynamic	$u = \beta \dot{y}^n$

Table 3.1: Overview of control forces produced by devices

s	Laplace variable
u	control force
u_{out}	compensator output (actuator input)
$u*$	forces acting on the piston
v	displacement of the control valve
m_{cv}, b_{cv}, c_{cv}	mass, resistance and rigidity factor of the control valve
k_v	proportionalyty factor of the control valve
T_{cv}	time constant of the control valve
ζ_{cv}	damping factor of the control valve
p_1, p_2	chamber pressures
S	piston area
h_0	piston initial position
y	piston displacement
V_1, V_2	chamber volumes
Q_1, Q_2	volume flow rate
μ	compressibility factor
χ	leakage factor
f	open port function
Δ	overlap displacement
$v*$	saturation displacement
y_o	displacement of the object
m_p	piston equivalent mass
b_p	piston resistance factor
x_p	piston absolute displacement
u_f	flap displacement
p'	gas external pression
p_c	gas pression in the chamber
ζ	flow rate factor
ρ'	mass density

g	gravity acceleration
k	ratio of the specific heat at constant pressure to the specific heat at constant volume
M	mass of the gas
μ_m	molecular mass
R	gas constant
Θ	absolute temperature
t	time
p_m	pressure constant value for for small piston displacement
Ω	rotor angular velocity
M_l	load torque moment
r	proportionality factor
M_t	torque applied by a motor
J	moment of inertia
β	coefficient of viscous resistance
L_a	armature inductance
R_a	resistance of the armature
M_0	starting torque
η	characteristic slope
Φ_f	flux
u_a	armature voltage
k_1, k_2	factors of motor type
δ, ν, k_f	factors of motor parameters
α	frequency of alternate current
L	circuit inductance
μ_0	magnetic permeability
i	current
N	number of spires
ϕ	non-linear function
r_s	circuit resistance

Bibliography

[1] Kolovsky M.Z., 1999
Nonlinear Dynamics of Active and Passive Systems of Vibration Protection,
Foundations of Engineering Mechanics, Springer-Verlag, ISBN 3-540-65661-8.

[2] Battaini M., 1998
Sistemi strutturali controllati: progettazione ed affidabilitá,
Ph.D. Thesis (in Italian), Structural Mechanics Dept., University of Pavia.

[3] Marazzi F., 2002
Semi-active control of civil structures: implementation aspects,
Ph.D. Thesis, Structural Mechanics Dept., University of Pavia.

[4] Battaini M., Casciati F., Domaneschi M., 2003
Electro-inductive passive and semi-active control devices,
System-based Vision for Strategic and Creative Design (ISEC02), Bontempi (eds.), 23-26, September 2003 Rome, Italy, Kluwer, pp.2085-2090.

[5] Casciati F. and Faravelli L., 1991
Fragility Analysis of Complex Structural Sysytems,
Research Study Press Ltd, Taunton, Somerset, England.

[6] Spencer Jr. B.F. , Dyke S.J. , Sain M.K. , Carlson J.D., 1997
Phenomenological Model for Magnetorheological Dampers,
Journal of Engineering Mechanics, 123(3), pp. 230-238.

[7] Jiménez R., Álvarez-Icaza L., 2005
LuGre friction model for a magnetorheological damper,
Structural Control and Health Monitoring, Vol. 12, Issue 1, pp. 25-45.

[8] Marioni A., 2004
Dispositivi per la Mitigazione dell'Azione Sismica (in Italian),
Bridge and Viaduct: control, analysis, maintenance, rehabilitation. Politecnico di Milano, Milan, June, 22-25, 2004.

[9] Alga S.p.A., Milan, 2005
Products description manuals.

Chapter 4

Non linear control systems

4.1 Introduction

The dynamic characteristics of the elements of vibration protection systems were assumed to be linear in Chapter 2. While analysing actual engineering systems, one has often to use non-linear dynamic models. This Chapter is therefore devoted to nonlinear systems.
The nonlinearities can be found in the whole mechanical system or only in the control system with different influences depending if it is of passive or active nature.
The main reasons for the existence of nonlinearities in vibration protection systems are listed below [1][3].

- Passive elastic elements can be considered as linear only under small deformations. When the deformations are large, one observes the non-linearity of the overall elastic characteristics caused either by material properties (rubber), constructive peculiarities of the element (presence of some initial compressive force, use of a conical spring etc.), or

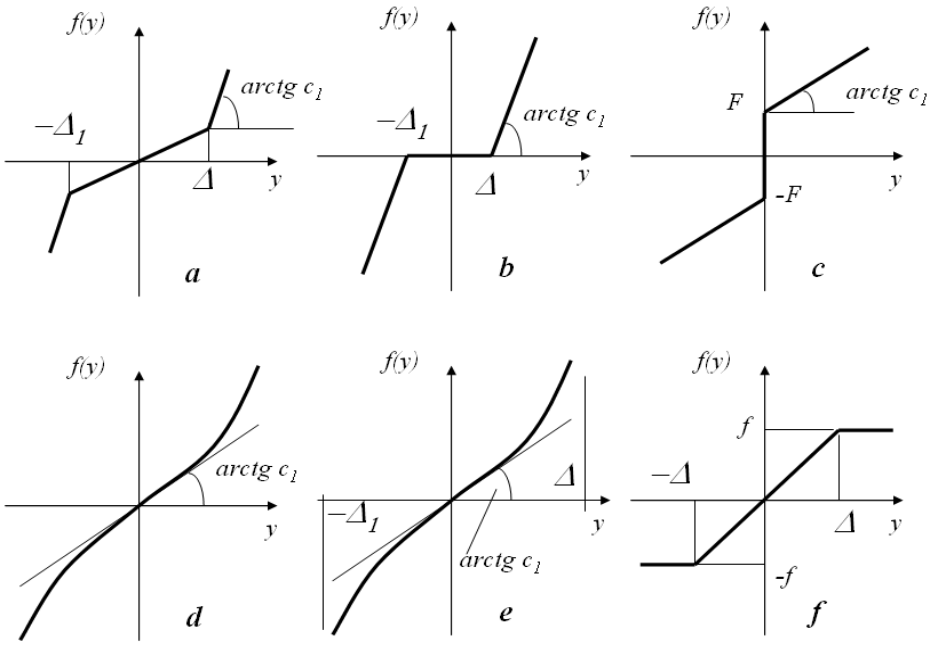

Figure 4.1: Nonlinear characteristics

the presence of barriers. Figure 4.1 displays schematically the most typical nonlinear elastic restoring characteristics. The characteristic shown in Figure 4.1a corresponds to a linear vibration isolator with high stiffness buffers. The governing equation is given by

$$\begin{array}{rcc} f(y) = cy & if & -\Delta_1 \leq y \leq \Delta \\ f(y) = c\Delta + c_1(y-\Delta) & if & y > \Delta \\ f(y) = -c\Delta_1 + c_1(y-\Delta_1) & if & y < \Delta_1 \end{array} \tag{4.1}$$

Using the Heaviside step function

$$H = \{ \begin{array}{ccc} 1 & if & y > 0 \\ 0 & if & y \leq 0 \end{array} \tag{4.2}$$

one can represent eq. 4.1 in the form of a single equation

$$f(y) = c_1 y + (c_1 - c)\Delta_1 + (c - c_1)(y + \Delta_1)\eta(y + \Delta_1) +$$

$$+(c_1 - c)(y - \Delta)\eta(y - \Delta) \tag{4.3}$$

Letting $c = 0$ yields a system representing clearance, see Figure 4.1b. Figure 4.1c shows the characteristics of an elastic element with some initial compressive force F, i.e.

$$f(y) = cy + Fsign(y) \tag{4.4}$$

Some smooth nonlinear restoring forces are displayed in Figures 4.1d and 4.1e. The symmetric characteristic of Figure 4.1d can be approximated by a linear-plus-cubic function of the displacement

$$f(y) = cy + \gamma y^3 \tag{4.5}$$

Figure 4.1e shows the characteristic of a nonlinear elastic element with rigid barriers. This type of the nonlinear restoring force may be conveniently approximated as follows

$$f(y) = \frac{2c\Delta}{\pi} tan \frac{\pi y}{2\Delta} \tag{4.6}$$

- Nonlinear characteristics may also contain some dissipative elements. Elements utilising interface friction are frequently used. As a first approximation, they obey the Coulomb's law

$$f(\dot{y}) = h_0 sign(\dot{y}) \tag{4.7}$$

In some cases, the internal friction in the material of the elastic element should be taken into account.

- Nonlinear elements can be used in active systems of vibration protection. Typically, the nonlinearity has a constrained output

$$\begin{array}{rrl} f(y) = k_y y & if & |y| \leq \Delta \\ f(y) = k_y \Delta sign(y) & if & |y| > \Delta \end{array} \tag{4.8}$$

see Figure 4.1f.

4.2 Analysis of nonlinear systems

In nonlinear systems, harmonic excitations usually excite periodic vibrations, the first harmonic being dominant. In order to investigate these vibrations, use will be made of the method of *harmonic linearization*.
Let there exist a nonlinear element with the following characteristic

$$f = f(y, \dot{y}) \tag{4.9}$$

where y stands for the input while$f(y, \dot{y})$ denotes some nonlinear function. In accordance with the method of harmonic linearization, it is assumed that the function $y(t)$ is approximately the sum of a harmonic process of frequency ω and a constant component

$$y \approx a_0 + acos\omega t, \qquad \dot{y} = -a\omega sin\omega t \tag{4.10}$$

Substituting eq. 4.10 in eq. 4.9 yields a periodic function whose Fourier's series is as follows

$$f(a_0 + acos\omega t, -a\omega sin\omega t) = f_0 + f_{1c}cos\omega t + f_{1s}sin\omega t + ... \tag{4.11}$$

The Fourier coefficients are calculated by the formulae

$$\begin{array}{c} f_0 = \frac{1}{2\pi}\int_0^{2\pi} f(a_0 + acos\phi, -a\omega sin\phi)d\phi = f_0(a_0, a) \\ f_{1c} = \frac{1}{\pi}\int_0^{2\pi} f(a_0 + acos\phi, -a\omega sin\phi)cos\phi d\phi = f_{1c}(a_0, a) \\ f_{1s} = \frac{1}{\pi}\int_0^{2\pi} f(a_0 + acos\phi, -a\omega sin\phi)sin\phi d\phi = f_{1s}(a_0, a) \end{array} \tag{4.12}$$

To apply the method of harmonic linearization means that the higher harmonics of the process 4.11 are ignored since they have little influence on the parameters of approximation 4.10.

Clearly, the nonlinear function 4.9 in the equations of motion may be replaced by any other function $f^*(y, \dot{y})$ provided that the latter has the same three first terms in the Fourier series and eq. 4.10 holds. Now it possible to realize the linearization process considering the following linear function

$$f^*(y, \dot{y}) = qy + r\dot{y} + i \tag{4.13}$$

Comparing eqs. 4.14 and 4.11 it is concluded that the right hand sides of these equations are identical if the factors q, r, and i are defined as follows

$$q = \frac{f_{1c}(a_0, a)}{a}, r = \frac{f_{1s}(a_0, a)}{a\omega}, i = f_0(a_0, a) - qa_0 \tag{4.14}$$

Thus, under the above assumptions, the nonlinear function 4.9 can be replaced by the linear function 4.13 with factors q, r, and i given by eq. 4.14. This replacement is called the *harmonic linearization* of nonlinear functions while factors 4.14 are referred to as the *harmonic linearization factors*. Notice that these factors depend on the parameters a and a_0 of the process $y(t)$. For this reason, the linearization factors are determined only after an approximate solution of the linearised equation of motion has been found.

Let $y^0(t)$ denote the harmonic component in $y(t)$, i.e.

$$y = a_0 + y^0, \qquad \dot{y} = \dot{y}^0 \tag{4.15}$$

then, eq. 4.13 can be written down in the form

$$f^*(y, \dot{y}) = qy^0 + r\dot{y}^0 + f_0 \tag{4.16}$$

One of the linearization factors coincides with the constant term in the Fourier series which makes the linearization more convenient.
In addition to the harmonic linearization method one can also mentioning:

- the method of *linearization based upon the distribution function*;
- the method of *statistical linearization.*

They are based on a probabilistic approach to the linearization problem. Details can be found in [1] [2] [3] [4].

4.3 Non linear passive systems in the frequency domain

The group of passive systems span from typical elements, like beams and columns, to passive control devices with their specific role of vibration mitigation.
Consider a nonlinear single-degree-of-freedom system with the following equation of motion

$$m\ddot{y} + u(y, \dot{y}) = Q(t) \tag{4.17}$$

Here m denotes the mass of the object to be isolated, y denotes the displacement of the elastic vibration isolator relative to the equilibrium point, u denotes the force applied to the vibration isolator in the direction y. $Q(t)$ stands for the vibration action which implies either an active force or the inertia force acting on the object in its relative motion. In the latter case this is simply the product of the object mass and the base acceleration changed of sign [1][3].
One assumes first that the dissipation force is proportional to the relative

velocity in the vibration isolator $\dot{y}$. The force acting on the object to be protected can be represented as

$$u(y, \dot{y}) = u_e(y) + b\dot{y} \tag{4.18}$$

where $u_e(y)$ stands for the elastic restoring force and b is a constant factor. Let us also assume that the vibration action is a single frequency harmonic function of time

$$Q(t) = Fcos\omega t \tag{4.19}$$

Inserting eqs. 4.18 and 4.19 into 4.17 yields

$$m\ddot{y} + b\dot{y} + u_e(y) = Fcos\omega t \tag{4.20}$$

The solution of this equation is sought by means of the harmonic linearization method in the form

$$y = a_0 + y^0(t) = a_0 + acos(\omega t + \phi) \tag{4.21}$$

To this end, one linearizes the nonlinear elastic force

$$u_e \approx u_0(a_0, a) + c_d(a_0, a)y^0 \tag{4.22}$$

where

$$u_0 = \frac{1}{2\pi}\int_0^{2\pi} u_e(a_0 + acos\phi)d\phi \tag{4.23}$$

$$c_d = \frac{1}{\pi a}\int_0^{2\pi} u_e(a_0 + acos\phi)cos\phi d\phi \tag{4.24}$$

Substituting eq. 4.22 in 4.20 one obtains the linearized equation

$$m\ddot{y}^0 + b\dot{y}^0 + u_0 + c_d y^0 = Fcos\omega t \tag{4.25}$$

Considering eq. 4.21, one gets the following equations for the static displacement a_0, the vibration amplitude a and the phase angle φ between the vibration and the excitation

$$u_0(a_0, a) = 0 \tag{4.26}$$

$$a = \frac{F_1}{\sqrt{(\lambda^2 - \omega^2)^2 + 4n^2\omega^2}} \tag{4.27}$$

$$tan\varphi = \frac{2n\omega}{\omega^2 - \lambda^2} \tag{4.28}$$

where

$$\lambda^2 = \frac{c_d(a_0, a)}{m}, n = \frac{b}{2m}, F_1 = \frac{F}{m} \tag{4.29}$$

The relationship between the static displacement a_0 and the vibration amplitude a due to eq. 4.26 is the same holding for free vibration. Comparing eqs. 4.24 and 4.29 it is easy to see that $\lambda(a_0, a)$ defines the frequency of free vibration of amplitude a relative to static displacement a_0. By expressing a_0 in terms of a with the help of eq. 4.26 one can obtain the following explicit formula

$$\lambda^2 = \frac{c_d}{m} = \frac{1}{\pi a m} \int_0^{2\pi} u_e[(a_0(a) + acos\phi]cos\phi d\phi \tag{4.30}$$

The dependence $\lambda(a)$ is referred to as the *backbone curve*. Inserting $\lambda(a)$ in eq. 4.27 one can determine the vibration amplitude a. The most convenient way of solving this equation is graphical. So it is possible to plot the graph $\lambda(a)$ considering λ in eq. 4.27 as an independent variable. If n is small, which is normally the case, this graph takes the form shown in Figure 4.2. The backbone curve $\lambda(a)$ is also plotted in this figure. The points of the curves's intersection determine the solutions of eq. 4.27.

Figure 4.2 shows that eq. 4.27 may have a number of solutions in the case

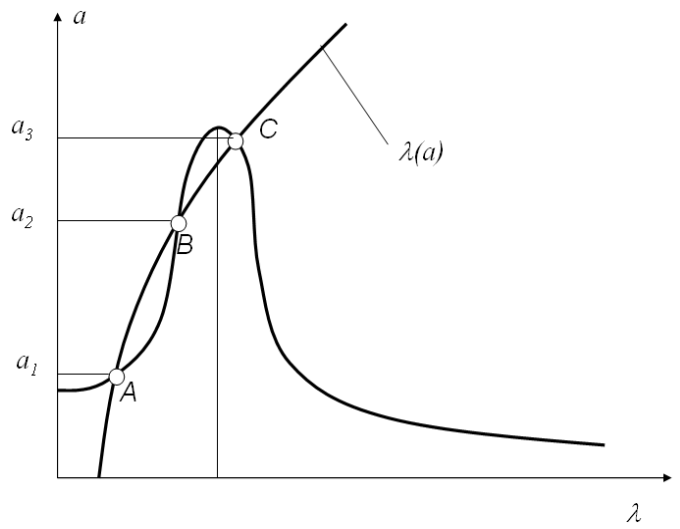

Figure 4.2: Backbone curve and resonance curve

of the nonlinear elastic restoring force. This implies that a number of different oscillatory regimes with different amplitudes and phases may occur, all the solutions being close to harmonic. The initial conditions are of crucial importance for establishing a particular regime. In practice however, the initial conditions are not strictly determined as they depend upon many random factors. For this reason one has to face the possibility of any of the above regimes. Multiplicity of the steady-state solutions is one of the typical features of the non-autonomous nonlinear systems which one deals with.

The *amplitude-frequency characteristic* a can be obtained by computing the vibration amplitude from eq. 4.27 for any frequency ω of the input sinusoidal force from $\omega = 0$ to the maximum limit value in the range of interest. The graph of this curve is called the *response curve* or the *resonance curve*

Figure 4.2 [1] [3].

Before one proceeds to analyse the form of the resonance curves let us note that the amplitude of the driving force F is usually a frequency-dependent function. For this reason, the general form of the equation for the amplitude-frequency characteristic is given by

$$a = \frac{F_1(\omega)}{\sqrt{[\lambda^2(a) - \omega^2]^2 + 4n^2\omega^2}} \tag{4.31}$$

Let us determine the intersection points of the resonance (eq. 4.31) and backbone (eq. 4.30) curves. At the intersection pionts it is verified $\lambda = \omega$, so from eq. 4.31 the following dependence of the amplitude on frequency results

$$a = \frac{F_1(\omega)}{2n\omega} \tag{4.32}$$

This equation determines the locus of the points of intersection of the res-

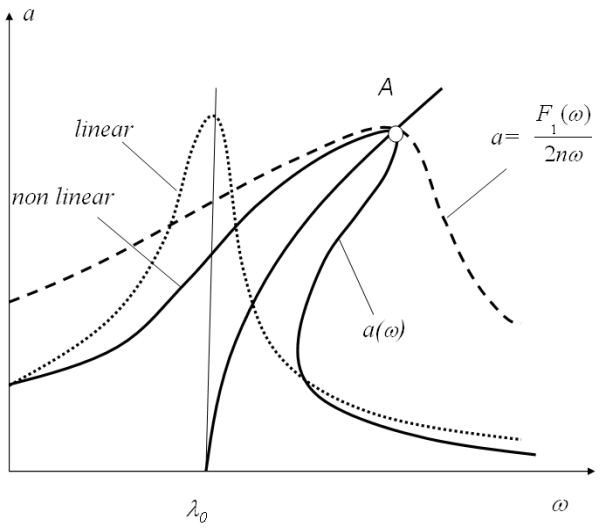

Figure 4.3: Linear and non linear resonance curve with respective backbones curves (eq. 4.32)

onance with the backbone curve. This curve intersects the backbone curve at the same points at which the resonance curve intersects the backbone curve, point A in Figure 4.3. In the same figure it is also depicted the linear elastic resonance curve with natural frequency λ_0.

Since $F_1 > 0$ and the denominator of eq. 4.31 is larger than $2n\omega$ for any λ and ω, the resonance curve lies under the curve 4.32 for the same values of ω.

The behaviour of the resonance curves far from these points essentially depends on the particular form of the backbone curve and function $F_1(\omega)$. Let us consider for example

$$F_1(\omega) = F_1 = const \tag{4.33}$$

then curve 4.32 is a hyperbola. This hyperbola intersects a *hard* backbone curve only once, see Figure 4.4, while it intersects a $soft$ backbone curve either twice, Figure 4.5, or never, Figure 4.6 (see also 4.8). Assume that the driving frequency is so slowly varied that the free vibration response is neglected and only the steady-state vibration is considered. Determining the vibration amplitude a for any frequency it is possible to plot the resonance curve. Increasing frequency ω, see Figure 4.4, one can determine the points of the resonance curve corresponding to the AM portion of the curve. A further increase in ω requires a jump from point M to point M' with an accompanying decrease in the amplitude. Starting at point B and decreasing ω the amplitude follows the BN portion of the curve and then jumps to the point N' .It is not possible to get the MN portion of the curve because the regimes corresponding to this portion are unstable. It is possible to demonstrate that the region between the two jumps ($NN'MM'$)

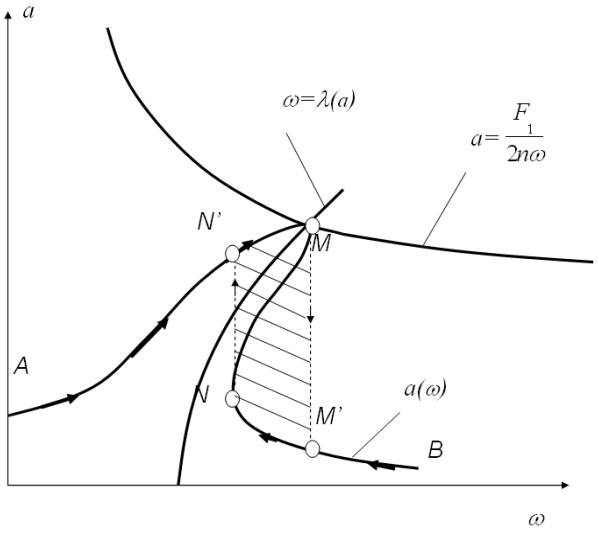

Figure 4.4: Hard backbone curve, points of intersection

represents the instability domain. Jump phenomena are typical for nonlinear systems and often manifest themselves in practice.

Let us assume now that the amplitude of the driving force is proportional to the square of the frequency

$$F_1(\omega) = \xi_0 \omega^2 \tag{4.34}$$

where ξ_0 is a constant coefficient.

Substituting eq. 4.34 into 4.32 one obtains the line equation

$$a = \frac{\xi_0}{2n}\omega \tag{4.35}$$

This line intersects a soft backbone curve at one point only (for $n \neq 0$) and a hard backbone curve at several points. The form of the resonance curve for the system with a hard backbone curve depends upon the number of the

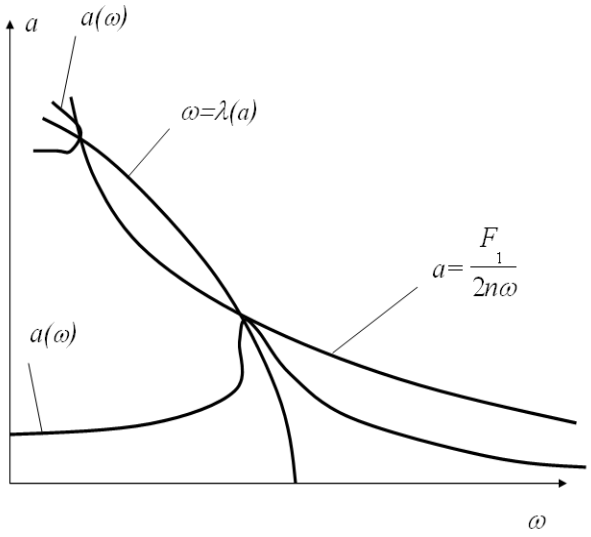

Figure 4.5: Soft backbone curve, points of intersection

points of intersection. One of the most typical forms is indicated in Figure 4.8 [1] [3].

4.3.1 Example

An example of the bifurcation of the dynamic equilibrium can be processed by a numerical model usually used to implement non linear behaviour in mechanic system. The Bouc-Wen model is implemented in Matlab environment to simulate a one degree of freedom elasto-plastic non linear oscillator with the following characteristics [2] [7]:

- mass $m = 1Kg$, damping $c = 0.38Nsec/m$, stiffness $k = 15N/m$;
- Bouc-Wen parameters: $A = n = 1$, $\alpha = 0.5$, $\beta = \gamma = 0.57$.

In order to find the region of bifurcation of the equilibrium, that is the two branches on the left and on the right of the jump of the transfer function,

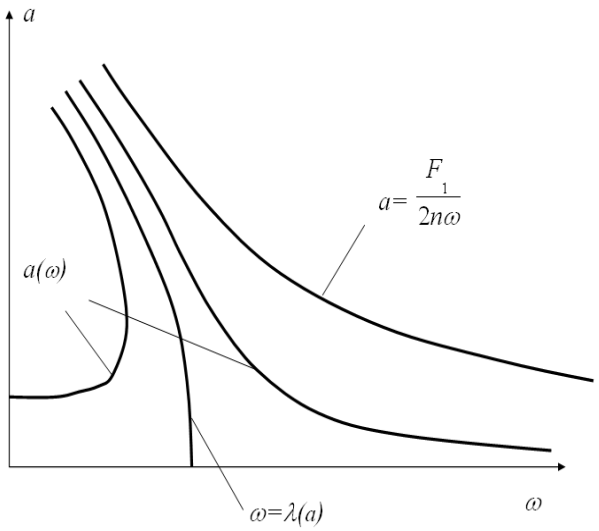

Figure 4.6: Soft backbone curve, no point of intersection

it is necessary to conduct two different tests characterized by a sinusoidal displacement excitation of the type $Asin(\omega t)$ with constant amplitude $A = \pm 1m$ and variable frequency $\omega/2\pi$ from 0 to 10 Hz. Increasing ω first and then decreasing in a second step the resulting curves are reported by Figure 4.9. The non coincidence of the two branches of the transfer functions outside the instability region, on the left of the two peaks, depends on the time step of calculation and the result is therefore an approximation. The mechanical system appears like an hard system. Similar results are reported in [7] for a passive control system tested in laboratory.

Figure 4.10 depicts few hysteretic cycles around an input displacement near 1 Hz. It is worth underling that the bifurcation is not evident with a lower elastic limit and with a perfectly plastic behaviour of the oscillator.

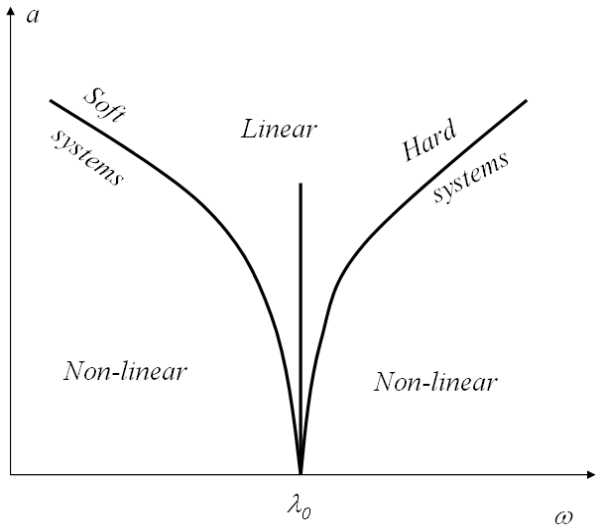

Figure 4.7: Space suddivision for hard and soft systems behaviour

4.4 Active systems

4.4.1 Vibration amplification in nonlinear systems

In this section the influence of nonlinearities in actively protected systems is discussed. The active feedback on the resonance phenomena is approached with the method of harmonic linearization. In addition, an investigation of the global system efficiency is reported [1] [3].

Consider a simple one-dimensional active system (Figure 4.11) composed by

- a linear object with applied forces $F1, ..., F_k$. Without systems of vibration protection those forces result in the uncontrolled displacement $\zeta(t)$ of point A,
- a vibration isolator element with the total reaction $R(t)$ and the dy-

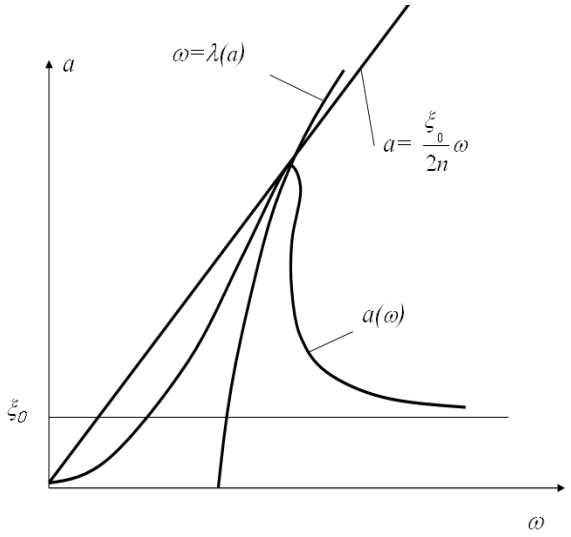

Figure 4.8: Typical form of resonance curve for excitation proportional to the square of frequency (eq. 4.34)

namic compliance operator $e_A(s)$ at point A as introduced in Chapter 2.

The controlled displacement has the following form

$$y(s) = \zeta(s) + e_A(s)R(s) \tag{4.36}$$

The total reaction $R(t)$ results from different contributions

- the elastic reaction force $R_e = cy + f(y)$, with $f(y)$ being some non linear characteristic,
- the linear dissipative reaction force $R_d = b\dot{y}$;
- the control force $u = w(s)y$ produced by a linear feedback of the absolute displacement of point A.

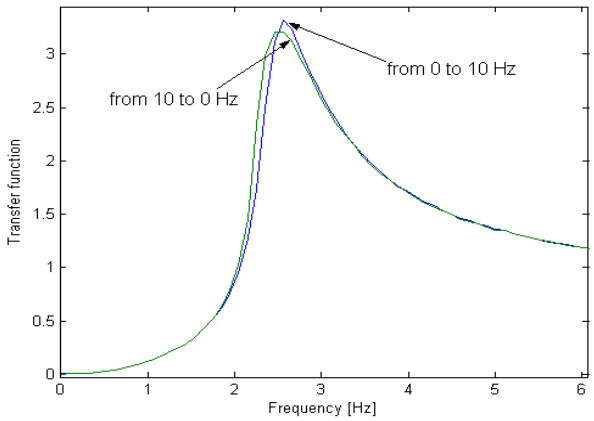

Figure 4.9: Bifurcation of dynamic equilibrium for Bouc-Wen numerical model; detail in the range 0-6 Hz

So the dynamic equation of the global system results from eq. 4.36

$$[d(s) + bs + c + w(s)]y + f(y) = d(s)\zeta(s) \tag{4.37}$$

Here $d(s) = e_A^{-1}(s)$ denotes the dynamic *rigidity operator* at point A. Provided that all dynamic excitation are harmonic with frequency ω, the process $\zeta(t)$ is harmonic, too. In this case the method of harmonic linearization can be applied to find an approximate solution. Assuming that the solution in the form

$$y(t) = a_0 + acos(\omega t + \varphi) = a_0 + y^0(t) \tag{4.38}$$

and replacing the nonlinear function $f(y)$ by the linear one

$$f^*(y) = f_0(a_0, a) + q(a_0, a)y^0 \tag{4.39}$$

leads to the linearised equation

$$[d(s) + bs + c + w(s)](a_0 + y^0(s)) + f_0(a_0, a) + q(a_0, a)y^0 = d(s)\zeta(s) \tag{4.40}$$

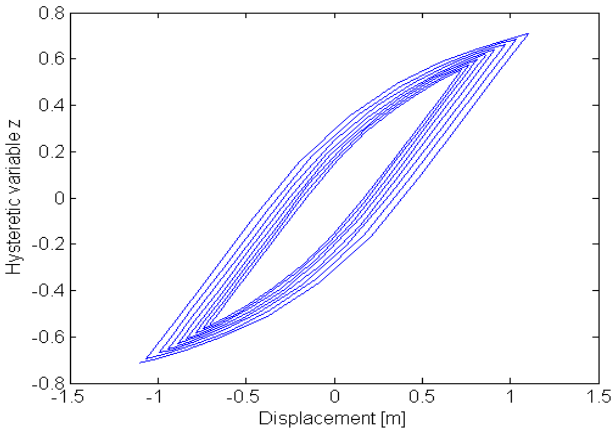

Figure 4.10: Hysteretic cycles of the Bouc-Wen numerical model near to the input excitation of 1 Hz

Separating the constant and harmonic terms yields

$$[d(s) + bs + c + w(s) + q]y^0 = d(s)(\zeta_0 cos\omega t) \tag{4.41}$$

$$[d(0) + c + w(0) + q]a_0 + f_0(a_0, a) = 0 \tag{4.42}$$

Using eq. 4.42 to express a_0 in terms of a and substituting the result into the linearization factor $q(a_0, a)$ one obtains $q(a)$ which is only function of a. Eq. 4.41 renders the following expressions for the vibration amplitude a and the phase φ

$$a = \zeta_0 |d(s)|(|d(s) + bs + c + q(a) + w(s)|)^{-1} \tag{4.43}$$

$$\varphi = argd(s)[d(s) + bs + c + q(a) + w(s)]^{-1} \tag{4.44}$$

An evaluation on the efficiency of the system can be done considering the condition $a > \zeta_0$ in a plot of the resonance curve $a(\omega)$ of eq. 4.43. This can be done assuming the system asymptotically stable, so $S = j\omega$. For a good

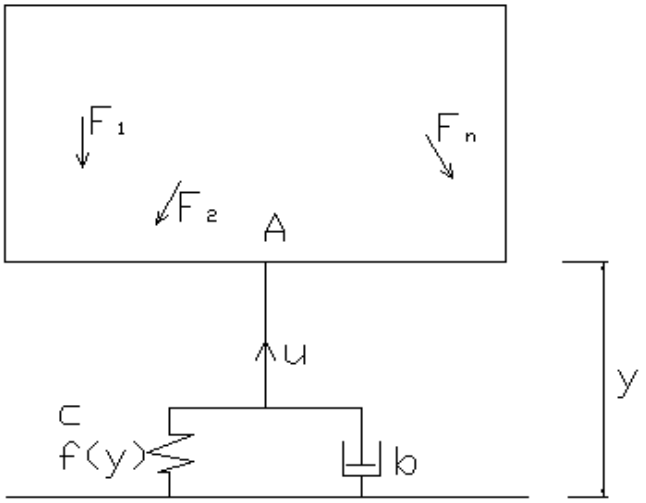

Figure 4.11: Linear object with non linear vibrations isolator

performance of the system it is necessary to remain sufficiently far from the critic value of $a = \zeta_0$.

4.4.2 Nonlinearities in feedback

Sensors, compensators and actuators may have nonlinear characteristics. If the active feedback of the vibration protection system contains a nonlinear element, the analysis of the efficiency and stability of the system cannot be carried out by the methods shown for linear active systems of vibration protection [1] [3].

Assume one of the elements of the control has the nonlinear characteristic shown in Figure 4.12. This characteristic consists of a dead zone ($|y| < \Delta$), a linear part with gain k and a saturation zone ($|y| > d$). For instance, this characteristic is representative of a hydraulic system (see Figure 3.2).

Making use of the method of equivalent linearization one can replace the

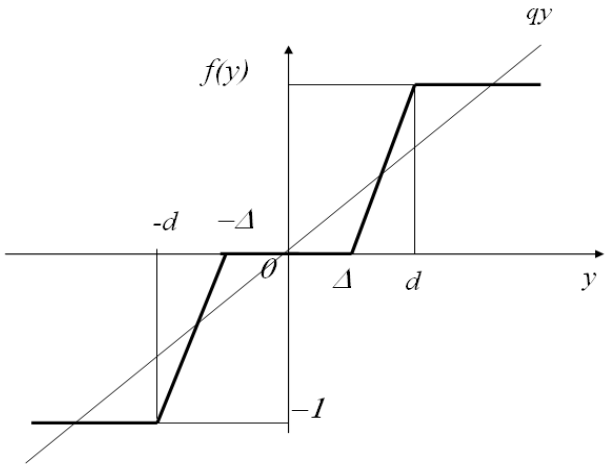

Figure 4.12: Nonlinear characteristic and equivalent linearization

nonlinear characteristic $f(y)$ by a linear element (see Figure 4.12)

$$f_l(y) = qy + f_0 \tag{4.45}$$

whose parameters q and f_0 depend on the input parameters. The characteristic can be casted in the form

$$f(y) = -k(d-\Delta) + k(y+d)H(y+d) - k(y+\Delta)H(y+\Delta) + \\ +k(y-\Delta)H(y-\Delta) - k(y-d)H(y-d) \tag{4.46}$$

Let the input of the nonlinear element be

$$y_* = a cos\omega t \tag{4.47}$$

Through the harmonic linearization method it is possible to evaluate an analytical form for the amplitude. It is worth evidencing from the solution that the equivalent gain is equal to zero if $a < \Delta$ which implies that vibrations within the dead zone are not controlled by the feedback. An increase

in the vibration amplitude increases the gain which approaches k and then when $a > d$ decreases up to zero. Thus, the feedback turns out to be ineffective both for very small and very large amplitudes.

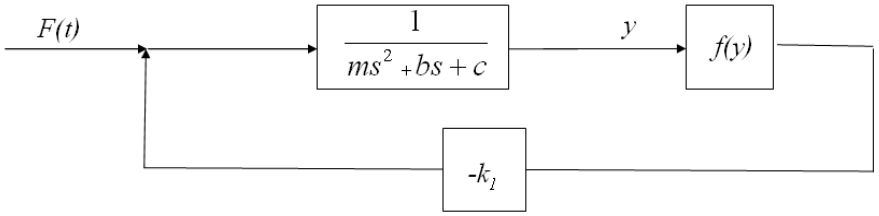

Figure 4.13: Non linear active system; $f(x)$ is the non linear element of characteristic in Figure 4.12

The amplitudes of the higher harmonics can be estimated by means of the expressions for the Fourier coefficients of the periodic process $f(asin\omega t)$. As an example it is considered the system shown in the block diagram in Figure 4.13. This system consists of the mass m mounted on the elastic element and the damper and involves the feedback with the nonlinear element $f(y)$ whose characteristic is depicted in Figure 4.12. In the system under consideration

$$e(s) = (ms^2 + bs + c)^{-1}, w(s) = -k_1 \tag{4.48}$$

The variable $y(t)$ is governed by the following equation

$$y = (ms^2 + bs + c)^{-1}F(t) - k_1(ms^2 + bs + c)^{-1}f(y) \tag{4.49}$$

One determines now the amplitude of the approximate harmonic solution assuming $F(t) = F_0 cos\omega t$. Applying the method of harmonic linearization

one forms the linearized equation

$$y = (ms^2 + bs + c)^{-1}[F_0 cos\omega t - k_1 q(a)y] \tag{4.50}$$

Solving eq. 4.50 one obtains

$$y = acos(\omega t + \varphi) \tag{4.51}$$

where a is determined by the equation

$$a = F_0[(c + k_1 q(a) - m\omega^2)^2 + b^2\omega^2]^{-1/2} \tag{4.52}$$

Equation 4.52 can be solved by a graphical method. It allows to describe the resonance curve which represents the approximate solution of eq. 4.49 [1].

4.5 Summary of Chapter 4

Chapter 4 is devoted to report the main characteristics of non linear systems where the nonlinearities can be found in the object to be protected or in the vibration protection system. The harmonic linearization is presented like a method of analysis of nonlinear systems.
Considerations on the evaluation of efficiency of non linear systems are also reported. Passive and active systems of vibration protection are considered.

Notation

All symbols used in this chapter have been defined chronologically, as they appear in the text.

$f(y)$	nonlinear characteristic
y	input of function f
Δ, Δ_1	fixed values for y
c, c_1	constant coefficients
H	Heavy side step function
F	force fixed value
γ	cubic coefficient
π	constant, semi-perimeter of circle with radius 1
h_0	coefficient
k_y	coefficient
ω	frequency
t	time
a, a_0	coefficients
f_0, f_{1c}, f_{1s}	Fourier coefficients
ϕ	angle
f^*	linear function
q, r, i	coefficients
$y^0(t)$	harmonic component in $y(t)$
u	control force
m	mass of the object
Q	input vibration action
u_e	elastic restoring force
b	constant coefficient
φ	phase angle
u_0	coefficient
c_d	coefficient
λ	system natural frequency
F_1	frequency dependent force
ξ_0	constant coefficient
ζ	uncontrolled displacement
R	reaction force
R_e	elastic reaction force
R_d	linear dissipative reaction force
s	Laplace variable

$w(s)$	transfer function
$e(s)$	dynamic compliance
$d(s)$	dynamic rigidity
f_0	coefficient
k_1	proportional coefficient

Bibliography

[1] Kolovsky M.Z., 1999
Nonlinear Dynamics of Active and Passive Systems of Vibration Protection,
Foundations of Engineering Mechanics, Springer-Verlag, ISBN 3-540-65661-8.

[2] Casciati F. and Faravelli L., 1991
Fragility Analysis of Complex Structural Sysytems,
Research Study Press Ltd, Taunton, Somerset, England.

[3] Kovaleva A., 2005
Control Theory with Application to Engineering Systems,
Lectures, January 17-21, 2005, Structural Mechanics Dept., University of Pavia.

[4] Kovaleva A., 1999
Optimal Control of Mechanical Oscillations ,
Foundations of Engineering Mechanics, Springer-Verlag, ISBN 3540654429.

[5] Meirovitch L., 1990
Dynamics and Control of Structures,
John Wiley and Sons, ISBN 0-471-62858-1.

[6] *Matlab and Simulink*, 2002
The Mathworks Inc., Natick, MA.

[7] L. Faravelli, 2001
Modelling the Response of an Elastomeric Base Isolator,
Journal of Structural Control, Vol. 8, Nr. 1.

Chapter 5

Passive control of cable-stayed bridges toward semi-active control

5.1 Introduction

The benchmark problem introduced in Appendix B accounts for the bi-directional nature of the seismic excitation.
The balance of control devices in the two directions and the introduction of semi-active control concepts are the main points in this chapter. The study has only been developed at a numerical level, using the bridge modelling of the benchmark problem. Nevertheless, the device force-displacement relationship fits the results of laboratory tests conducted for the characterization of the reference electroinductive device [1].
A comparative study of the results with the control strategies suggested by the benchmark organizer is the starting goal [2].

Different typologies of elasto-plastic passive devices can be located be-

tween deck and piers. They differ for the shape and the dimension of the hysteretic cycles. Active cables, able to reduce the vibrations, could be simulated by a scheme which uses the first natural mode shapes of the structure. Analyzing just the first four moe shapes it is possible to meet both bending and torsion vibrations [2] [1].
When compared with previous studies [5], the present structural problem is complicated by the bi-directional nature of the seismic excitation and by its coupling with the snow action: they represent the environment excitation to be contrasted. The confinement of the vibration requires a balance between the devices along the bridge and the devices transversal to it, in the horizontal plane.
Furthermore, semi-active structural control schemes are pursued both following the remarks discussed in [1] and by tuning the devices to the actual value of the external loads.

5.2 Control scheme implementation

5.2.1 Structural idealization

The bridge is first equipped with a series of passive elasto-plastic devices located in the eight positions shown in Figure 5.1. Indeed, the passive devices are located symmetrically with respect to the deck longitudinal axis under the bridge deck: two devices between the ground and Bent 1 (see Figure 5.1), two devices between Pier 2 and the deck, two devices between Pier 3 and the deck, two devices between Pier 4 and the deck. These devices are able to guarantee energy dissipation in two orthogonal directions, the

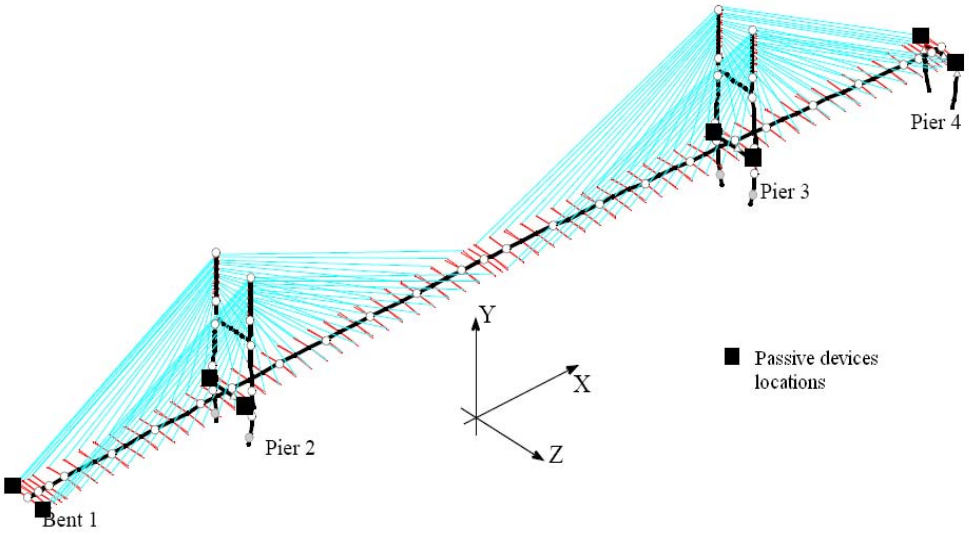

Figure 5.1: Passive devices location along the bridge span

one along the deck and the direction transversal to it. The idea is to sustain the deck on an ideal dissipative surface, not just by the cable linear elastic behaviour. The flow scheme of Figure 5.2 [7] [8] presents the benchmark model and the control system design developed: the implemented passive devices show potentially different characteristics in the longitudinal and transversal directions.

5.2.2 Passive devices simulation

The passive device idealization is pursued by the Bouc-Wen endochronic hysteretic model in the form

$$\dot{z} = A\dot{y} - \beta\dot{y}|z|^n - \gamma|\dot{y}|z|z|^{n-1} \tag{5.1}$$

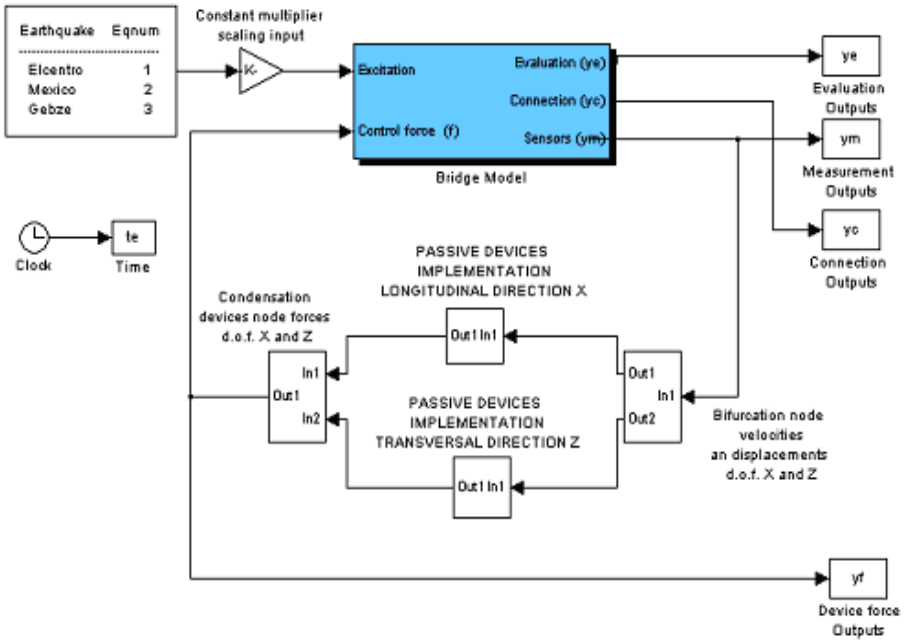

Figure 5.2: Simulink flow diagram developed in this study

$$u = (1-\alpha)kz + \alpha ky \tag{5.2}$$

where z is the auxiliary variable controlling the hysteretic behaviour, u is the processed force, and A, β, α, γ, n are parameters defining the amplitude and the shape of the cycles [12].

The Bouc-Wen parameters for the different devices considered throughout this chapter are summarized in Table 5.1.

5.3 Phase I vs. Phase II

Tables 5.2 and 5.3 present a series of results collected toward a comparison of Benchmark Phase I with Phase II. The devices parameters originally

	A	**N**	α	$\beta = \gamma$	**K**$[KN/m]$
Type 1	1	1	0.02	40 ($V_y = 1000KN$)	80000
Type 2	1	1	0.02	20 ($V_y = 2000KN$)	80000
Type 3	1	1	0.02	8 ($V_y = 5000KN$)	80000
Type 4	1	1	0.00001	8 ($V_y = 5000KN$)	80000
Type 5	1	1	0.02	160 ($V_y = 250KN$)	80000
Type 6	1	1	0.02	40000 ($V_y = 1KN$)	80000
Type 7	1	1	0.00001	40000 ($V_y = 1KN$)	80000
Type 8	1	1	0.02	80 ($V_y = 500KN$)	80000
Type 9	1	1	0.02	10 ($V_y = 4000KN$)	80000

Table 5.1: Device parameters

selected for Phase I [5] are also adopted for Phase II, but together in the longitudinal and transversal directions.

In Phase II a greater number of design situations are investigated, see Appendix B for more details on the differences between Phase I and Phase II. Both seismic incidence directions of 15° and 45° are considered in Tables 5.2 and 5.3. The 15° incidence angle will be the only considered in the successive analyses.

The cable-stayed bridge benchmark in Phase II introduces 18 criteria for the evaluation of the performances of the control solutions, they express ratios to the uncontrolled case. The uncontrolled case includes rigid-links (i.e., shock transmission devices) where the devices are located. Appendix B reports the definitions of the criteria, but they can briefly reassumed as following

- the first six criteria consider the ability of the controller to reduce peak responses,
- the second five criteria consider normed responses over the entire time

B-Wen parameters			Phase I			Phase II Type 1					
Snow			K_1=80000 K_2=10 KN/m			yes			yes		
Incidence angle			V_y=1000 KN			15°			45°		
Accelerogram			EIC	Mex	Geb	EIC	Mex	Geb	EIC	Mex	Geb
Peak responses	Base shear	J_{1x}	0.346	0.538	0.365	0.3	0.382	0.379	0.368	0.407	0.38
		J_{1z}	-	-	-	1.015	1.122	1.039	0.994	1.04	0.997
	Deck shear	J_{2x}	1.08	1.1	1.13	0.966	1.192	1.6	0.858	1.16	1.636
		J_{2z}	-	-	-	0.963	1.006	0.992	0.987	0.983	0.991
	Base mom.	J_{3x}	0.269	0.58	0.389	0.27	0.407	0.742	0.375	0.421	0.85
		J_{3z}	-	-	-	1.095	1.082	1.052	0.981	1.037	0.993
	Deck mom.	J_{4x}	0.664	0.36	0.949	0.642	0.892	2.693	0.746	0.795	2.669
		J_{4z}	-	-	-	1.009	0.993	1.001	0.997	1.001	1.002
	Cable tens.	J_5	0.216	0.0479	0.13	0.271	0.149	0.346	0.276	0.15	0.321
	Deck displ.	J_6	1.35	1.61	2.48	1.364	2.587	10.195	2.193	2.961	12.799
Normed responses	Base shear	J_{7x}	0.493	1.07	0.677	0.248	0.289	0.357	0.25	0.322	0.402
		J_{7z}	-	-	-	1.013	1.054	1.05	0.979	1.004	1.026
	Deck shear	J_{8x}	1.97	1.81	3.21	1.155	1.207	1.904	1.136	1.274	2.122
		J_{8z}	-	-	-	0.978	0.998	0.993	0.993	0.973	1.003
	Base mom.	J_{9x}	0.522	1.14	0.99	0.299	0.392	0.886	0.319	0.447	1.084
		J_{9z}	-	-	-	1.005	1.051	1.038	0.983	0.998	1.023
	Deck mom.	J_{10x}	1.31	1	4.3	0.83	1.007	2.961	0.926	1.091	3.56
		J_{10z}	-	-	-	1.002	1.004	1.003	1.003	1.003	1.005
	Cable tens.	J_{11}	0.0343	0.0114	0.0276	0.032	0.019	0.033	0.032	0.02	0.032
Control Strategy	Peak force	J_{12x}	0.00198	0.00198	0.00198	0.002	0.002	0.004	0.003	0.002	0.004
		J_{12z}	-	-	-	0	0	0	0	0	0
	Dev. stroke	J_{13x}	0.886	0.812	1.36	0.835	1.409	4.449	1.163	1.356	5.683
		J_{13z}	-	-	-	0.002	0.003	0.002	0.002	0.002	0.002
	Peak pow.	J_{14x}	0.00552	0.00657	0.00998	0.005	0.009	0.021	0.006	0.01	0.024
		J_{14z}	-	-	-	0	0	0	0	0	0
	Total pow.	J_{15x}	0.00021	0.00021	0.00023	0.001	0.001	0.002	0.001	0.001	0.003
		J_{15z}	-	-	-	0	0	0	0	0	0

Table 5.2: Phase I [5] -II - Comparison of the results achieved by elasto-plastic parameters. The snow action is not included. The columns 15° and 45° refer to two different angles of incidence of the seismic action

B-Wen parameters			Phase I			Phase II Type 1					
Snow			K_1=80000 K_2=10 KN/m			yes			yes		
Incidence angle			V_y=1000 KN			15°			45°		
Accelerogram			EIC	Mex	Geb	EIC	Mex	Geb	EIC	Mex	Geb
Peak responses	Base shear	J_{1x}	0.346	0.538	0.365	0.348	0.438	0.38	0.449	0.428	0.377
		J_{1z}	-	-	-	1.02	1.121	1.039	0.99	1.033	0.997
	Deck shear	J_{2x}	1.08	1.1	1.13	0.97	1.223	1.604	0.864	1.165	1.732
		J_{2z}	-	-	-	0.963	1.006	0.993	0.985	0.985	0.991
	Base mom.	J_{3x}	0.269	0.58	0.389	0.278	0.421	0.76	0.391	0.418	0.878
		J_{3z}	-	-	-	1.095	1.097	1.052	0.981	1.038	0.994
	Deck mom.	J_{4x}	0.664	0.36	0.949	0.624	0.897	2.769	0.76	0.813	2.786
		J_{4z}	-	-	-	1.009	0.993	1.001	0.996	1.001	1.002
	Cable tens.	J_5	0.216	0.0479	0.13	0.266	0.15	0.354	0.274	0.153	0.328
	Deck displ.	J_6	1.35	1.61	2.48	1.393	2.595	10.506	2.17	2.989	13.331
Normed responses	Base shear	J_{7x}	0.493	1.07	0.677	0.283	0.335	0.366	0.289	0.372	0.416
		J_{7z}	-	-	-	1.013	1.053	1.05	0.979	1.004	1.026
	Deck shear	J_{8x}	1.97	1.81	3.21	1.16	1.205	1.977	1.138	1.264	2.254
		J_{8z}	-	-	-	0.979	0.998	0.993	0.993	0.973	1.003
	Base mom.	J_{9x}	0.522	1.14	0.99	0.307	0.397	0.931	0.329	0.454	1.161
		J_{9z}	-	-	-	1.006	1.05	1.038	0.983	0.998	1.023
	Deck mom.	J_{10x}	1.31	1	4.3	0.839	0.997	3.129	0.94	1.081	3.83
		J_{10z}	-	-	-	1.002	1.004	1.003	1.003	1.003	1.005
	Cable tens.	J_{11}	0.0343	0.0114	0.0276	0.032	0.019	0.033	0.032	0.02	0.033
Control Strategy	Peak force	J_{12x}	0.00198	0.00198	0.00198	0.002	0.002	0.004	0.003	0.002	0.004
		J_{12z}	-	-	-	0	0	0	0	0	0
	Dev. stroke	J_{13x}	0.886	0.812	1.36	0.863	1.441	4.584	1.135	1.392	5.92
		J_{13z}	-	-	-	0.002	0.003	0.002	0.002	0.002	0.002
	Peak pow.	J_{14x}	0.00552	0.00657	0.00998	0.005	0.008	0.022	0.006	0.01	0.025
		J_{14z}	-	-	-	0	0	0	0	0	0
	Total pow.	J_{15x}	0.00021	0.00021	0.00023	0.001	0.001	0.002	0.001	0.001	0.003
		J_{15z}	-	-	-	0	0	0	0	0	0

Table 5.3: Phase I [5] -II - Comparison of the results achieved by elasto-plastic parameters. The snow action is included. The columns 15° and 45° refer to two different angles of incidence of the seismic action

record,

- the last seven criteria consider the requirements of the control system itself.

The simulations with snow extra load presents more onerous outputs but they are similar to the ones obtained in the case without snow. The snow action is neglected in Tables 5.4 and 5.5.
Table 5.4 presents the comparison among the performances achieved by the first four devices in Table 5.1. In the first three cases the deck displacements J_6 is inversely proportional to the device elastic limit. When a perfectly-plastic behaviour (Type 4) is considered for the device a bit of increment in the displacements is obtained. The hysteretic cycle of the last device is similar to the one of the electro-inductive tested in laboratory as detailed in a dedicated chapter and introduced in [1].

Figures 5.3 and 5.4 present the hysteretic cycles for elasto-plastic and elasto-perfectly-plastic behaviour of the device in the longitudinal direction. They are related to a device of Type 1 located at Pier 2. The Gebze earthquake is considered with incidence angle of 15° without snow. Table 5.4 emphasizes how a better performance is achieved at the cost of higher deck displacements.
Figure 5.5 presents a trend of deck longitudinal displacement to Bent 1, Pier 2, 3, 4. The are always uniform but not coincident (v. Figure 5.6).

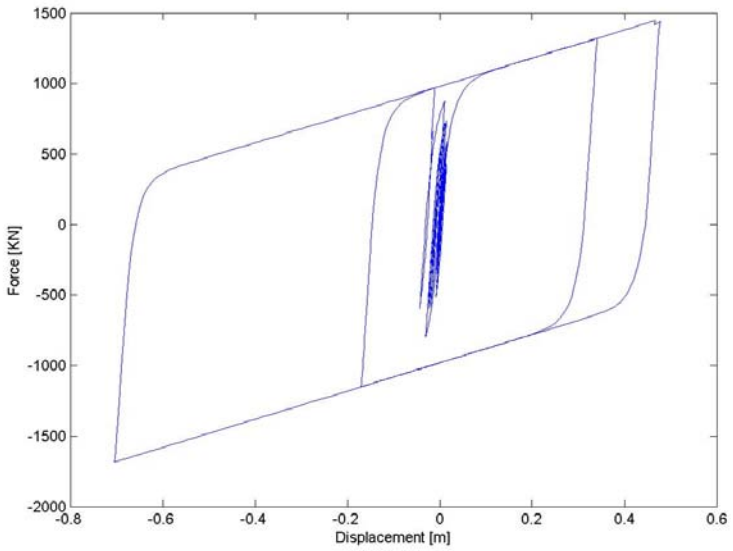

Figure 5.3: Gebze earthquake. Longitudinal device of Type 1 connecting nodes 84-313, elasto-plastic behaviour

5.4 Improving the response

Plotting in a diagram (Figure 5.7) the longitudinal and transversal displacements of the deck relative to Pier 2 more than one order of magnitude of difference between them is showed. Also evaluating the transversal resulting force (Figure 5.8) and the hysteretic cycle, the dissipative behaviour is approximatively negligible. This means that the transversal devices are likely to be unnecessary. Some results are presented in Table 5.5 where several devices and characteristics are discussed. The conclusion that no transversal devices are necessary is achieved.

Following the remarks of [6], Table 5.6 shows the performance of a set of passive devices at different intensities of seismic excitation. It is evident that

B-Wen param.			Type 1			Type 2			Type 3			Type 4		
Accelerogram			EIC	Mex	Geb	EIC	Mex	Geb	EIC	Mex	Geb	EIC	Mex	Geb
Peak responses	Base shear	J_{1x}	0.3	0.382	0.379	0.294	0.414	0.423	0.331	0.474	0.498	0.328	0.47	0.498
		J_{1z}	1.015	1.122	1.039	1.022	1.112	1.046	1.013	1.112	1.041	1.013	1.112	1.041
	Deck shear	J_{2x}	0.966	1.192	1.6	1.033	1.223	1.451	1.148	1.265	1.054	1.142	1.257	1.058
		J_{2z}	0.963	1.006	0.992	0.963	1.016	0.991	0.963	1.025	0.996	0.963	1.026	0.995
	Base mom.	J_{3x}	0.27	0.407	0.742	0.298	0.433	0.661	0.376	0.585	0.461	0.371	0.579	0.457
		J_{3z}	1.095	1.082	1.052	1.089	1.075	1.048	1.08	1.073	1.035	1.08	1.074	1.036
	Deck mom.	J_{4x}	0.642	0.892	2.693	0.713	0.881	1.898	0.811	0.959	0.81	0.803	0.909	0.82
		J_{4z}	1.009	0.993	1.001	1.01	0.993	1	1.01	0.991	1	1.01	0.991	1
	Cable tens.	J_5	0.271	0.149	0.346	0.281	0.149	0.264	0.286	0.155	0.188	0.286	0.155	0.188
	Deck displ.	J_6	1.364	2.587	10.195	1.62	2.531	7.195	2.286	4.191	2.559	2.26	4.255	2.589

Table 5.4: Phase II - Seismic input angle 15° - no snow. Comparison of the performance achieved by adopting devices of different type

B-Wen Longitudinal			Type 2			Type 2			Type 2		
B-Wen Transversal			Type 5			Type 6			Type 7		
Accelerogram			EIC	Mex	Geb	EIC	Mex	Geb	EIC	Mex	Geb
Peak responses	Base shear	J_{1x}	0.294	0.414	0.423	0.294	0.414	0.423	0.294	0.414	0.423
		J_{1z}	1.022	1.112	1.046	1.022	1.112	1.046	1.021	1.112	1.046
	Deck shear	J_{2x}	1.033	1.223	1.451	1.033	1.223	1.451	1.033	1.223	1.451
		J_{2z}	0.963	1.016	0.991	0.962	1.016	0.991	0.962	1.015	0.991
	Base mom.	J_{3x}	0.298	0.433	0.661	0.298	0.433	0.661	0.298	0.433	0.661
		J_{3z}	1.089	1.075	1.048	1.089	1.075	1.048	1.089	1.075	1.048
	Deck mom.	J_{4x}	0.713	0.881	1.898	0.713	0.881	1.898	0.713	0.881	1.898
		J_{4z}	1.01	0.993	1	1.01	0.993	1	1.01	0.993	1
	Cable tens.	J_5	0.281	0.149	0.264	0.281	0.149	0.264	0.281	0.149	0.264
	Deck displ.	J_6	1.62	2.531	7.195	1.62	2.531	7.195	1.62	2.531	7.195

Table 5.5: Phase II - Seismic input angle 15° no snow, different devices in the longitudinal and transversal directions

Input Multiplier			1			0.6			0.3		
Accelerogram			EIC	Mex	Geb	EIC	Mex	Geb	EIC	Mex	Geb
Peak responses / Type 2	Base shear	J_{1x}	0.294	0.414	0.423	0.308	0.446	0.465	0.354	0.517	0.512
		J_{1z}	1.022	1.112	1.046	1.021	1.106	1.043	1.016	1.116	1.04
	Deck shear	J_{2x}	1.033	1.223	1.451	1.092	1.246	1.201	1.181	1.266	0.992
		J_{2z}	0.963	1.016	0.991	0.963	1.023	0.993	0.963	1.026	0.996
	Base mom.	J_{3x}	0.298	0.433	0.661	0.335	0.488	0.537	0.402	0.667	0.478
		J_{3z}	1.089	1.075	1.048	1.081	1.069	1.04	1.079	1.078	1.031
	Deck mom.	J_{4x}	0.713	0.881	1.898	0.774	0.938	1.128	0.804	0.908	0.74
		J_{4z}	1.01	0.993	1	1.01	0.993	1	1.009	0.992	1
	Cable tens.	J_5	0.281	0.149	0.264	0.286	0.151	0.206	0.284	0.161	0.19
	Deck displ.	J_6	1.62	2.531	7.195	1.954	3.412	3.914	2.586	5.008	2.724
Peak responses / Type 1	Base shear	J_{1x}	-	-	-	0.291	0.405	0.409	0.308	0.446	0.465
		J_{1z}	-	-	-	1.021	1.12	1.044	1.021	1.106	1.043
	Deck shear	J_{2x}	-	-	-	1.016	1.216	1.515	1.092	1.246	1.201
		J_{2z}	-	-	-	0.962	1.013	0.991	0.963	1.023	0.993
	Base mom.	J_{3x}	-	-	-	0.291	0.423	0.685	0.335	0.488	0.537
		J_{3z}	-	-	-	1.091	1.081	1.047	1.081	1.069	1.04
	Deck mom.	J_{4x}	-	-	-	0.693	0.863	2.143	0.774	0.938	1.128
		J_{4z}	-	-	-	1.01	0.993	1	1.01	0.993	1
	Cable tens.	J_5	-	-	-	0.278	0.149	0.29	0.286	0.151	0.206
	Deck displ.	J_6	-	-	-	1.534	2.526	8.203	1.954	3.412	3.914
Peak responses / Type 8	Base shear	J_{1x}	-	-	-	-	-	-	0.291	0.405	0.409
		J_{1z}	-	-	-	-	-	-	1.021	1.12	1.044
	Deck shear	J_{2x}	-	-	-	-	-	-	1.016	1.216	1.515
		J_{2z}	-	-	-	-	-	-	0.962	1.013	0.991
	Base mom.	J_{3x}	-	-	-	-	-	-	0.291	0.423	0.685
		J_{3z}	-	-	-	-	-	-	1.091	1.081	1.047
	Deck mom.	J_{4x}	-	-	-	-	-	-	0.693	0.863	2.143
		J_{4z}	-	-	-	-	-	-	1.01	0.993	1
	Cable tens.	J_5	-	-	-	-	-	-	0.278	0.149	0.29
	Deck displ.	J_6	-	-	-	-	-	-	1.534	2.526	8.203

Table 5.6: Phase II - Scaled accelerograms, seismic incidence angle of 15°, no snow, semi-active solution performance

Load conditions			15° no snow			15° snow			45° no snow			45° snow		
Accelerogram			EIC	Mex	Geb	EIC	Mex	Geb	EIC	Mex	Geb	EIC	Mex	Geb
Peak responses / Type 9	Base shear	J_{1x}	-	-	-	0.346	0.469	0.483	-	-	-	0.452	0.524	0.48
		J_{1z}	-	-	-	1.014	1.108	1.043	-	-	-	0.998	1.033	0.996
	Deck shear	J_{2x}	-	-	-	1.092	1.263	1.148	-	-	-	0.953	1.199	1.33
		J_{2z}	-	-	-	0.964	1.026	0.993	-	-	-	0.988	0.987	0.99
	Base mom.	J_{3x}	-	-	-	0.353	0.557	0.545	-	-	-	0.494	0.609	0.557
		J_{3z}	-	-	-	1.08	1.085	1.038	-	-	-	0.988	1.035	0.992
	Deck mom.	J_{4x}	-	-	-	0.784	0.902	1.073	-	-	-	0.787	0.832	1.072
		J_{4z}	-	-	-	1.01	0.992	1	-	-	-	0.997	1.001	1.001
	Cable tens.	J_5	-	-	-	0.281	0.153	0.201	-	-	-	0.297	0.173	0.193
	Deck displ.	J_6	-	-	-	2.048	3.853	3.706	-	-	-	2.235	4.597	4.444
Peak responses / Type 3	Base shear	J_{1x}	0.331	0.474	0.498	0.36	0.507	0.506	0.408	0.525	0.491	0.467	0.567	0.503
		J_{1z}	1.013	1.112	1.041	1.015	1.11	1.046	1.006	1.043	0.997	1.001	1.034	0.997
	Deck shear	J_{2x}	1.148	1.265	1.054	1.117	1.27	1.115	0.97	1.228	1.204	0.977	1.199	1.278
		J_{2z}	0.963	1.025	0.996	0.964	1.028	0.994	0.99	0.99	0.992	0.989	0.987	0.991
	Base mom.	J_{3x}	0.376	0.585	0.461	0.38	0.613	0.489	0.477	0.65	0.536	0.511	0.673	0.565
		J_{3z}	1.08	1.073	1.035	1.079	1.087	1.038	0.99	1.033	0.992	0.989	1.035	0.992
	Deck mom.	J_{4x}	0.811	0.959	0.81	0.814	0.873	0.95	0.804	0.855	0.861	0.835	0.813	0.953
		J_{4z}	1.01	0.991	1	1.01	0.991	1	0.996	1.001	1.002	0.997	1.001	1.002
	Cable tens.	J_5	0.286	0.155	0.188	0.283	0.157	0.188	0.293	0.173	0.195	0.301	0.177	0.201
	Deck displ.	J_6	2.286	4.191	2.559	2.272	4.449	2.762	2.29	5.056	3.442	2.236	5.301	3.821

Table 5.7: Phase II - Snow load, semi-active solution performance, seismic incidence angle of 15°

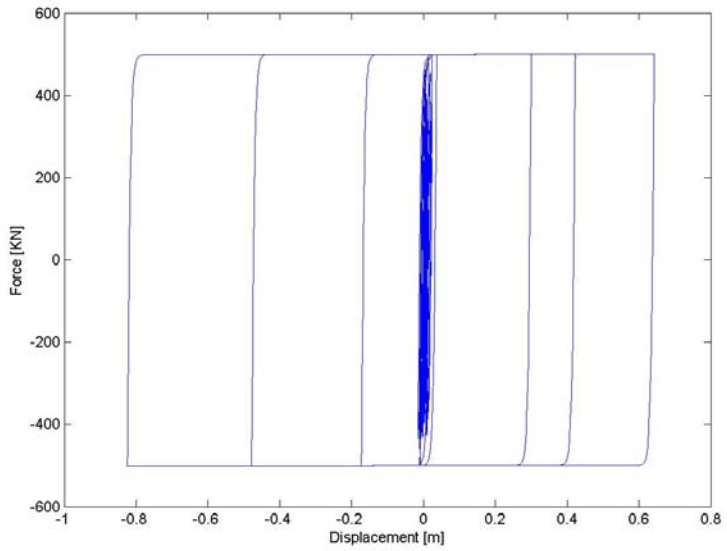

Figure 5.4: Gebze earthquake. Longitudinal device of Type 1 connecting nodes 84-313, elasto-perfectly-plastic (with $\alpha = 0.00001$) behaviour

the efficiency decreases with the intensity of the seismic excitation. But, if a semi-active control system is implemented in the device, and the force limit value is tuned on the seismic excitation intensity, one can pursue similar performances for different seismic excitation intensities. Analogously, Tables 5.7 compares the performances in the two cases of snow and no snow for the two incidence angle of the seismic excitation, 15° and 45°. Also in this case, the availability of a semi-active adaptor allows one to pursue the same efficiency in the two cases.

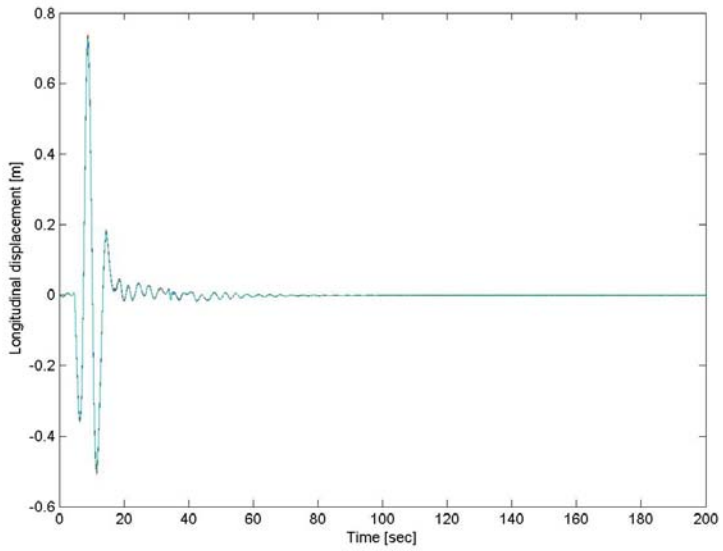

Figure 5.5: Uniform deck longitudinal displacements to Bent 1, Pier 2, 3, 4 (node 134, 118, 84, 68)

5.5 Remarks on the wind load on the benchmark cable-stayed bridge

The seismic load showed a modest transversal response in the bridge benchmark so that the relevant passive control devices resulted rather ineffective. Attention is therefore focused on the wind load.

5.5.1 Simulating a wind load record

The Italian recommendations [5] drives the designer in the evaluation of the wind pressure on a structure. In particular it is possible to evaluate the mean value of the wind pressure and the peak value. This last is influenced by the gust effect.

Two considerations at first have to be done:

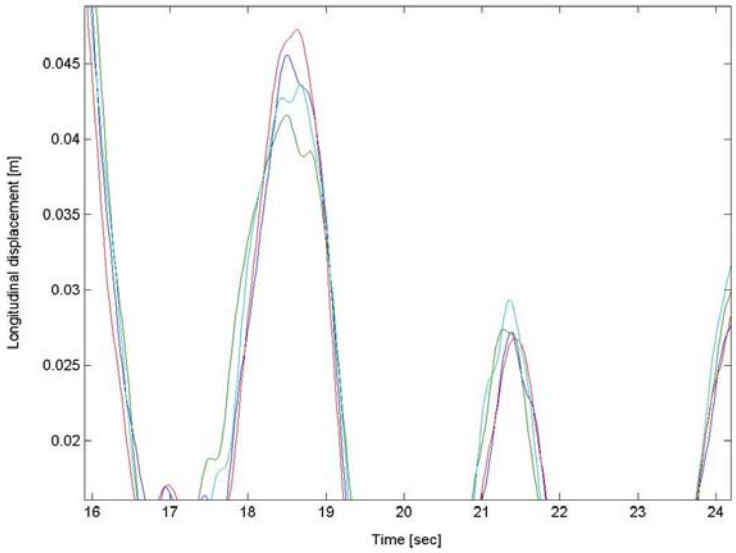

Figure 5.6: Details Figure 5.5

- the cables and the towers can be considered a local problem and they can be analyzed separately from this study,
- only the deck response is here evaluated.

The mean value p_m of the wind pressure is function of the distances z of the structure from the ground. The deck is located at 50 m of height so the mean wind pressure can be expressed as follow

$$p_m(z) = \frac{v_m^2}{1.6} \tag{5.3}$$

$$v_m(z) = v_{ref}\alpha_t\alpha_r\alpha_z \tag{5.4}$$

where v_m is the mean wind velocity, v_{ref} is the reference value of the wind velocity and without specific statistic observations can be setted to 30 m/sec, α_t is the topography coefficient and it is evaluated 1.1 for a unfavourable

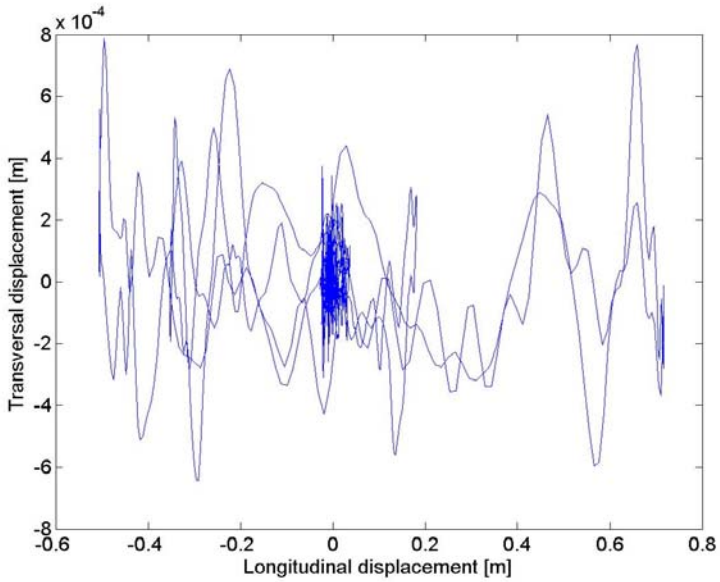

Figure 5.7: Longitudinal vs. transversal displacement, connection devices deck-Pier 2 (nodes 313, 84), Gebze record

assumtion, α_r is the return coefficient and considering a period of 1000 years it is assumed 1.23, α_z is the profile coefficient and for the position assumed of 50 m from the ground it consists in 1.13. So the mean wind velocity results $v_m = 45.8m/sec$, the mean wind pressure $p_m = 1.31KN/m^2$.
The peak value of the wind pressure can be calculated as $p_m G$ where G is the coefficient representing the gust influence. G can be processed as

$$G = 1 + 1.12\frac{\alpha_d}{\alpha_z} = 1.62 \tag{5.5}$$

where α_z has the same value previuosly used and α_d is the dynamic coefficient and can be calculated as 0.63 depending on the structural geometry.
This values of wind pressure will be used to generate a wind pressure time history from a basic signal with the frequency content shows in Figure 5.9

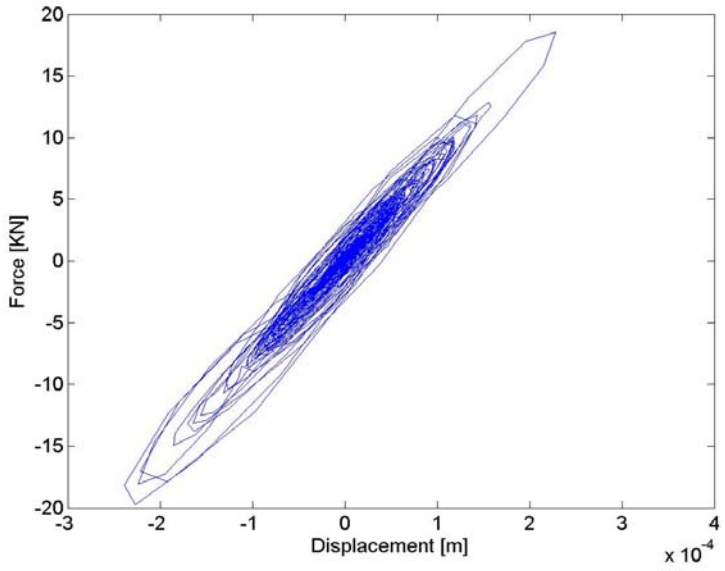

Figure 5.8: Force vs. transversal displacement, transversal device deck-Pier 2 (nodes 313-84), Gebze record

[11]. The wind pressure is transformed in forces considering the lateral surface of the deck between two nodes of the finite element model (it consists of about 45 m^2). So 65 nodes along the deck are loaded with the time history in Figure 5.10. The wind forces will be applied uniformly to all the deck nodes in the horizontal direction normal to the deck axis.

5.5.2 Wind time history on the cable-stayed bridge model

The bridge benchmark control problem considers only the seismic load as detailed in Appendix B, so the implementation of the wind load required special developements. The seismic load was removed. The benchmark statement allows to define forces in every node of the all structure. So 65 new force time hystories are defined and included by an external data file

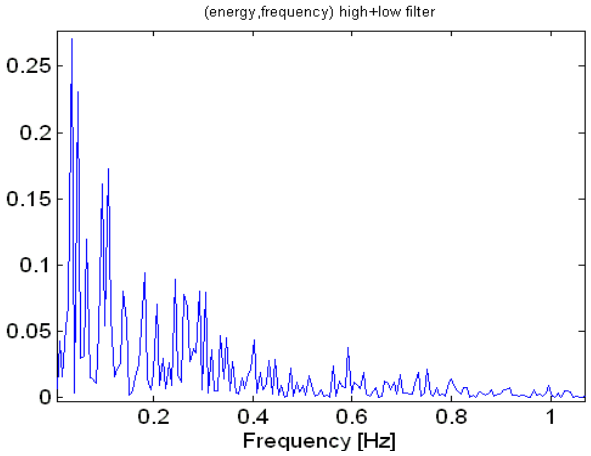

Figure 5.9: Frequency content of the basic signal for the wind pressure simulation

as wind force on the cable-stayed bridge. Then simulated wind forces are saved in a .mat data file composed by 66 rows. The first one contains the time vector and the other 65 are the wind forces applied to the 65 nodes along the bridge deck. The wind forces are incorporated in the model as they were produced by an external device connected to the deck and the ground. Figure 5.11 reassumes the model block in Simulink [7] where the wind load is implemented. It is possible to see how the seismic load is setted to zero. The wind load comes from the .mat file at the first time step of calculation. The control forces have one step of delay because they must to be processed.

5.5.3 Numerical simulation and results

The passive control devices applied to the cable-stayed bridge for the wind load simulation are Type 1 with elastic limit of 1000 KN, this typology is

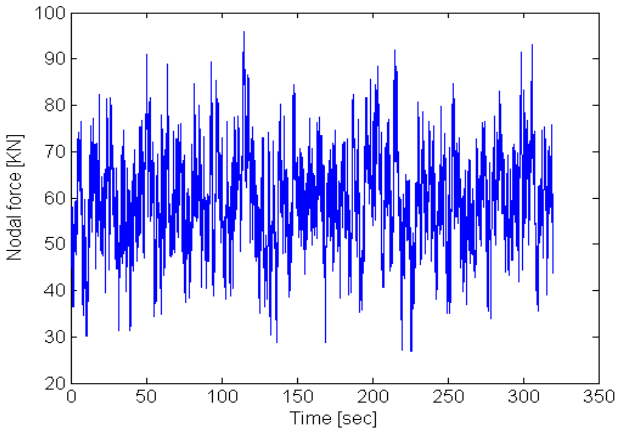

Figure 5.10: Wind history, nodal forces on the finite element model

extended to all the devices in longitudinal and transversal direction. Figure 5.12 depicts the hysteretic cycle of the passive transversal device at Pier 2. Like previously found for the seismic load, also for the wind load the dissipative behaviour is negligible. This means that the transversal devices are likely to be unnecessary also for the wind load.

Figure 5.13 presents the transversal displacement versus the longitudinal one for the passive device at Pier 2. The wind load transversal to the deck appears without influence also in longitudinal direction.
The other devices at Bent 1, Pier 3 and 4 presents similar negligible dissipative effects.

5.6 Summary of Chapter 5

This chapter is part of the international cable-stayed bridge benchmark and covers the moving from Phase I to Phase II (Appendix B). It mainly consists in considering a bi-directional nature of the seismic excitation. Passive

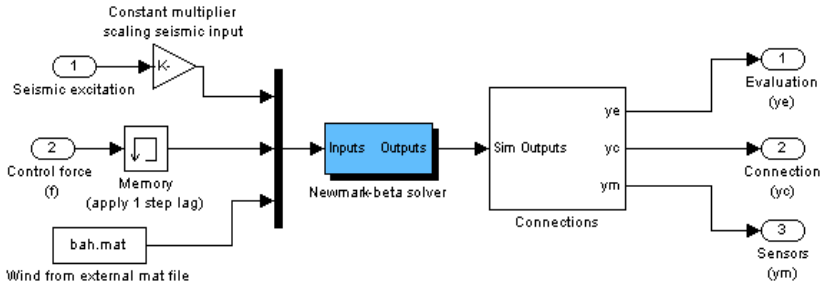

Figure 5.11: Implementation of the wind load, developed in this work, for the bridge Simulink model

devices solutions and simple open loop semi-active control designs were investigated. An extension of the benchmark problem to the wind load is also included.

Table 5.8 maps the principal results.

Notation

All symbols used in this chapter have been defined chronologically, as they appear in the text.

Results	**Contents**
Tables 5.2 and 5.3	They show the passage from Phase I (mono-directional seismic excitation) to Phase II (bi-directional) with similar passive dissipative devices. The results are comparable.
Table 5.4	It shows the responses of different passive dissipative devices to the same input excitation. The deck displacement is inversely proportional to the device elastic limit. Better performance is achieved at the cost of higher displacement.
Table 5.5 and Figures 5.7 - 5.8	Under bi-directional seismic excitation, the dissipative behaviour shown by transversal devices is negligible.
Table 5.6 and 5.7	Open-loop semi-active control system. The limit value is tuned on the seismic excitation intensity or on the presence of extra load. One can pursue similar performances.
Figures 5.12 - 5.13	Under wind excitation, the dissipative behaviour of transversal devices is negligible.

Table 5.8: Map of results in Chapter 5

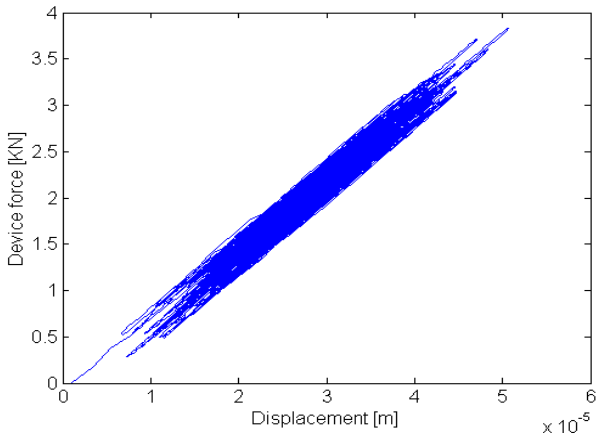

Figure 5.12: Hysteretic cycle under wind load at Pier 2, transversal behaviour, device Type 1

z	auxiliary variable controlling the hysteretic behaviour
y	displacement
$A, \beta, \alpha, \gamma, n$	parameters defining the amplitude and the shape of the hysteretic cycles in th Bouc-Wen model
u	control force
k	device stiffness
J_i	evaluation criteria (i=1,..18)
p_m	mean value of wind pressure
v_m	mean value of wind velocity
v_{ref}	reference value of wind velocity
α_t	topography coefficient
α_r	return coefficient
α_z	profile coefficient
α_d	dynamic coefficient
G	gust coefficient for the wind pressure peak value

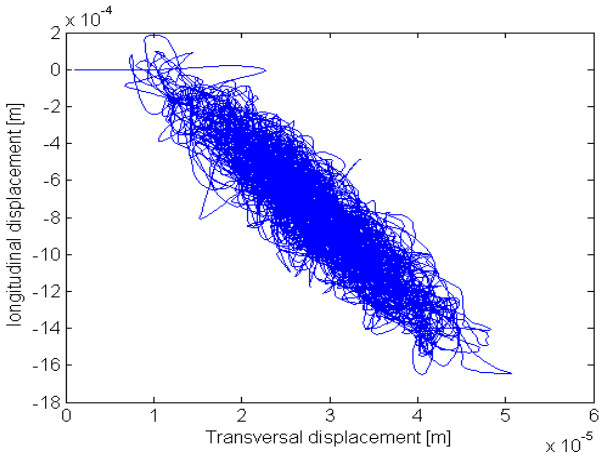

Figure 5.13: Transversal vs longitudinal displacement, passive device Type 1 at Pier 2, wind load

Bibliography

[1] Battaini M., Casciati F., Domaneschi M., 2003
Electro-inductive passive and semi-active control devices,
System-based Vision for Strategic and Creative Design (ISEC02), Bontempi (eds.), 23-26, September 2003 Rome, Italy, Kluwer, pp.2085-2090.

[2] F. Casciati, M. Domaneschi, 2004
Confinement of Vibration Applied to a Benchmark Problem
Proc. Of Second European Workshop on Structural Health Monitoring, Monaco (D), July 7-9, 2004, pp 811-818.

[3] Caicedo J.M., Dyke S.J., Moon S.J., Bergman L., Turan G., Hague S., 2003
Phase II Benchmark Control Problem for Seismic Response of Cable Stayed Bridges,
Journal of Structural Control, 10:137-168.

[4] Caicedo J.M., Dyke S.J., Moon S.J., Bergman L., Turan G., Hague S., 2003
Phase II Benchmark Control Problem for Seismic Response of Cable

Stayed Bridges
http://wusceel.cive.wustl.edu/quake/.

[5] Bontempi F., Casciati F., Giudici M., 2003
Seismic response of a cable-stayed bridge: active and passive control systems (Benchmark Problem),
Journal of Structural Control, 10:169-185.

[6] Casciati F., Faravelli L., Battaini M., 2000
Ultimate vs. Serviceability Limit State in Designing Bridge Energy Dissipation Devices,
Earthquake Engineering Frontiers in the New Millenium, Spencer B.F. Jr and Hu Y.X. Eds., Beijing, China, 8-11 November 2000, pp. 293-297.

[7] *Matlab and Simulink*, 2002
The Mathworks Inc., Natick, MA.

[8] *Control System Toolbox*, 2002
The Mathworks Inc., Natick, MA.

[9] Casciati F., Domaneschi M., Faravelli L., 1998
Some Remarks on the Drift of Elasto-Plastic Oscillators Under Stochastic Excititon,
Stochastic Structural Dynamics, Spencer B.F. Jr and Johnson E.A. Eds., Notre Dame, Indiana, USA, 6-8 August 1998, pp. 545-550.

[10] CNR - 10012, 1985
Instructions for the evaluation of the external actions on structures (in Italian),
Italian Research National Council.

[11] Augusti G., Baratta A., Casciati F., 1984
Probabilistic Methods in Structural Engineering,
Chapman and Hall Ltd, ISBN 0-412-22230-2.

Chapter 6

Decentralized control solution for the bridge benchmark

6.1 Introduction

This chapter pursues the development of an innovative semi-active, totally decentralized control system for the cable stayed bridge benchmark introduced in the previous chapter.

The decentralized strategy is referred in the literature as potentially useful for the systematic reliable control design of different kinds of real world large scale systems [1]. Thus, the application to the cable-stayed bridge benchmark with diffuse sensors and devices appears suitable. The decentralization is thought as "total" in the sense that neither control device depends on any other. Seismic excitation only is considered in the study.

This chapter also discusses the implementation of semi-active devices which use a low order control scheme for their decentralization from the nodes where they are located.

A comparison of the decentralized semi-active control system is done with

passive and active control systems. Eventually, this chapter considers robustness with regard to local failures, as well as the ability of decentralized semi-active systems to cope with different levels of seismic intensity.

6.2 A decentralized semi-active control system

The development of a semi-active decentralized control system first of all requires summarizing a few theoretical developments.

6.2.1 Decentralized control

The cable-stayed bridge benchmark problem investigated in this study deals with a long span, cable-stayed bridge with two main towers and over a hundred cables attached to it. A decentralized setting is suggested for the control design, due to the large dimension of the bridge. In fact, control devices and the sensors are at hundreds of meters distance among each other, with predictable complications in term of connecting and processing. The problem of decentralization is widely studied in several works [1] [2] [3] [4] [5], with particular emphasis on active cases. The performances of the decentralization, when applied to flexible structures, are slightly worse than the centralized control system but they lie into acceptable ranges.
On the other side, the decentralization of the control systems, compared to its centralization, presents several good points, of which two in particular have to be underscored:

- system decentralization performs satisfactorily even under adverse conditions. Local failures can be examined and if the system decentralization is totally distributed, none of the device depends on any

other. It is therefore acceptable to foresee the failures of one control device at a time.

- Furthermore, the advantages of designing decentralized control schemes result from the reduction of transmission costs within the feedback loops, the reduction of the overall computational efforts and the possibility of a more effective power supply of the devices.

6.2.2 Semi-active choice

Cable-stayed bridges are very complex systems not only for the understanding of their dynamical behaviour but also in terms of design and implementation of feedback. Moreover, they may require a significant number of sensors and actuators installed at appropriate locations for effective control, and these may strongly interact with the bridge dynamics [5] [6].
Passive devices were proved in Chapter 5 to be useful in the seismic protection of the bridge. Moreover, they do not require external energy supply and feedback processes. However the induced forces can be significantly powerful, thus resulting in high forces transmitted to the structures, on the connections.
Semi-active approaches for cable-stayed structures present several good points in comparison with passive and active solutions, which should be underlined:

- a semi-active approach allows one to improve passive solutions by online adjustments of the damping or stiffness of adaptable devices; this is done according to feedback signals and control commands.

- semi-active control strategies simplify the design and implementation of the control system in comparison with active solutions; this is also

due to the requirements of low power supply and low maintenance costs.

Reference [9] reports a semi-active low order scheme for a simple short two-span bridge. The scheme is low order in the sense that it uses feedback only from the nodes which are directly influenced by the devices. Usually, the design of semi-active controllers is based on the assumption of an ideally fast response of the controllable devices. A first order actuator dynamics allows one to incorporate a delayed response of the device to the feedback control signal. This is a more realistic approach to the control design in real operational conditions.

6.2.3 Semi-active algorithm

Each semi-active device is implemented by using a simple on/off skyhook control law. The device is controlled by two force levels. This control law is developed so as to have a lower vibration amplitude between the two points to which the device is connected.
Considering that the device is connected between the tower (or the bent) and the deck, the choice between a high or low a response level of the device is based on the following control law: the control force u is chosen depending on the product of the relative velocity v_{rel} between the two connected nodes and the absolute velocity of the device connection node on the deck. If the product is positive or zero, the control force u is adjusted to its high level. Otherwise u is set to the low level. This concept is summarized by:

$$\dot{y}_b v_{rel} \geq 0 \Rightarrow u \Rightarrow high \tag{6.1}$$

$$\dot{y}_b v_{rel} < 0 \Rightarrow u \Rightarrow low \tag{6.2}$$

Consequently, a high control force value is used only while needed, otherwise the lowest possible force value is adopted [3].

6.2.4 Mathematical model

Appendix B reports the main details of the benchmark control problem statement. The model resulting from finite element formulation has the form

$$M\ddot{\mathbf{y}} + C\dot{\mathbf{y}} + K\mathbf{y} = -M\Gamma\ddot{y}_g + \Lambda\mathbf{u} \tag{6.3}$$

where $\ddot{\mathbf{y}}$ is the second time derivative and $\dot{\mathbf{y}}$ the first time derivative of the response vector $\mathbf{y}$ with dimension 909. M, C and K are the mass and stiffness matrices of the structure, $\mathbf{u}$ is the vector of the control force inputs, $\ddot{y}_g$ is the seismic ground acceleration, Γ is a vector of zeros and ones defining the loading of the ground acceleration to the structure, and Λ is a matrix defining how the forces produced by the control devices act in the structure. In order to make the model more manageable, the high frequency dynamics is neglected and the model is reduced from 909 to 419 d.o.f.

The dynamic equations of the structural model are integrated directly. For each step, one has the desired output in order to implement the semi-active algorithm in eqs. 6.1 and 6.2. Considering that $\dot{y}_{id}$ is the velocity of the deck node to which the ith device is connected, $\dot{y}_{ib}$ is the velocity of the support node for the same ith device. The semi-active control law can be expressed as:

$$(\dot{y}_{id} - \dot{y}_{ib})\dot{y}_{id} \geq 0 \Rightarrow u \Rightarrow high \tag{6.4}$$

$$(\dot{y}_{id} - \dot{y}_{ib})\dot{y}_{id} < 0 \Rightarrow u \Rightarrow low \tag{6.5}$$

From eq. 5.2 one can state for the ith device

$$u_i = (1-\alpha)kz_i + \alpha k(y_{id} - y_{ib}) \tag{6.6}$$

where z_i is processed for each device (see eq. 5.1)

$$\dot{z}_i = A(\dot{y}_{id} - \dot{y}_{ib}) - \beta(\dot{y}_{id} - \dot{y}_{ib})|z_i|^n - \gamma|(\dot{y}_{id} - \dot{y}_{ib})|z_i|z_i|^{n-1} \tag{6.7}$$

The control forces have thus been defined by two processes: the Bouc-Wen model [12] and the semi-active skyhook control law. Figure 6.1 presents a detail of the finite element mesh with the semi-active control device between Pier 2 (node 314) and the deck (node 151); the control forces in the longitudinal and the transversal direction are depicted.

The low order decentralized control scheme consists in 8 sub-systems se-

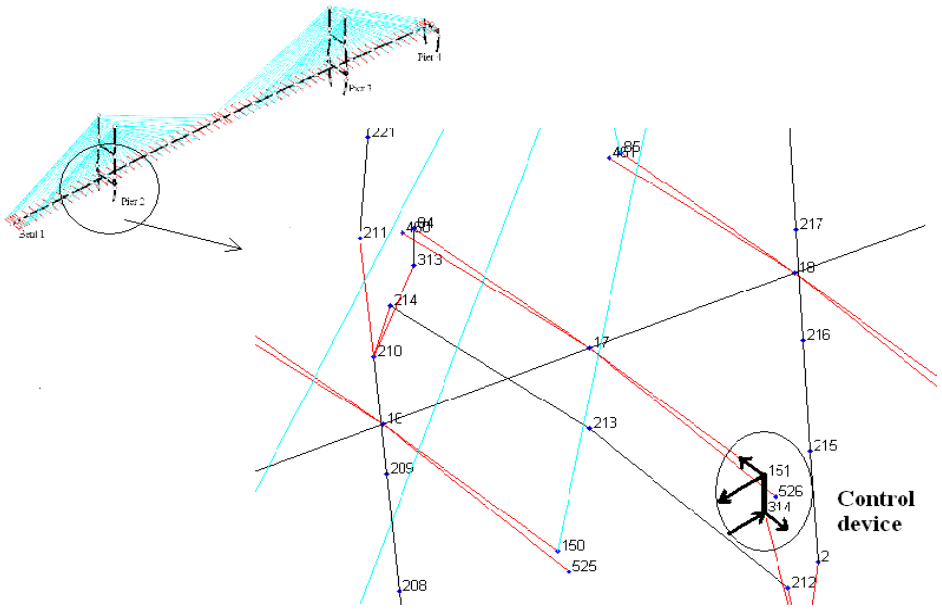

Figure 6.1: Detail of the semi-active control device implementation between Pier 2 (node 314) and the deck (node 151), control forces

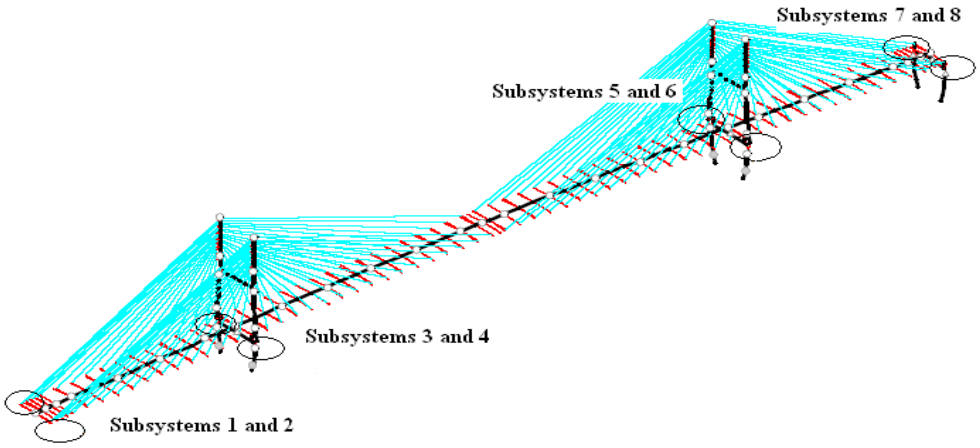

Figure 6.2: Structure decomposition, 8 sub-systems

lected by the positions of the control devices along the bridge structure. Figure 6.2 depicts the sub-systems distribution. Each sub-system processes independently its own control forces, in the longitudinal and transversal directions, having feedback only from the nodes where the devices are connected.

The dynamic equations of the system 6.1 could also be managed by a transfer function approach (Chapter 2 introduces, as an example, a system equipped with a feedback process, see eq. 2.13). The transfer function of the bridge model can be written as follows

$$(Ms^2 + Cs + K)\mathbf{y}(s) = -M\Gamma s^2 y_g(s) \tag{6.8}$$

$$\mathbf{y}(s) = -\frac{M\Gamma s^2}{(Ms^2 + Cs + K)} y_g(s) \tag{6.9}$$

The control forces expressed by eq. 6.6 represent the control feedback of the process. So one could consider the whole system as

$$\mathbf{y}(s) = \frac{-\frac{M\Gamma s^2}{(Ms^2+Cs+K)}}{1-(-\frac{M\Gamma s^2}{(Ms^2+Cs+K)})(W_u)} y_g(s) \tag{6.10}$$

where W_u is the transfer function of the system producing the control forces. In this specific study, however, it is not possible to explicitate W_u because the control system shows strongly non linear components. Figure 6.3 depicts the nonlinear term (NL block in the scheme) as expressed by eq. 6.7.

The bridge benchmarck model with the non linear vibration protection

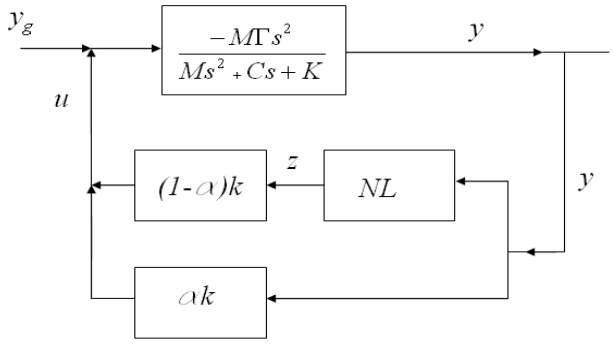

Figure 6.3: Transfer function scheme with a non linear term

strategy has to be solved by integrating the differential equations directly and considering the non linear behaviour separately. Its implementation is presented in the remaining part of the chapter.

6.2.5 Implementation of the semi-active total decentralized control system

In this chapter the cable-stayed bridge is equipped with 8 semi-active devices in the longitudinal direction and 8 in the transversal one. The po-

sitions where the devices are located are the same as those used for the passive control system, discussed in Chapter 5. The devices working in the longitudinal direction are located symmetrically with respect of the deck longitudinal axis under the bridge deck: two devices between the ground and Bent 1, two devices between Pier 2 and the deck, two devices between Pier 3 and the deck, two devices between Pier 4 and the deck. The same arrangement is used for the devices working in the transversal direction. These 16 devices together are able to guarantee the energy dissipation in the two horizontal orthogonal directions, the one along the deck and the other in the direction transversal to it.

The devices are semi-active in the sense that they are able to change their hysteretic dissipative cycles by increasing or decreasing the elastic limit force. The hysteretic behaviour is determined by the Bouc-Wen model, the same as the one used for the passive control system of Chapter 5.

The model of the total decentralized semi-active control system is implemented in Matlab and Simulink [13]. The implementation is not immediate and covers a great number of blocks and sub-blocks of the Simulink code. Some figures try to describe the basic ideas.

Figure 6.4 depicts the global Simulink flow scheme, where the semi-active devices are implemented with potential different characteristics in the longitudinal and transversal directions. For the implementation of the Skyhook on/off algorithm the inputs of the semi-active devices blocks account for the absolute and relative velocity values of the nodes where the devices are connected. The relative values of the displacement are also included, as they serve for the implementation of the Bouc-Wen model.

The distribution of the 8 devices in the longitudinal direction is shown

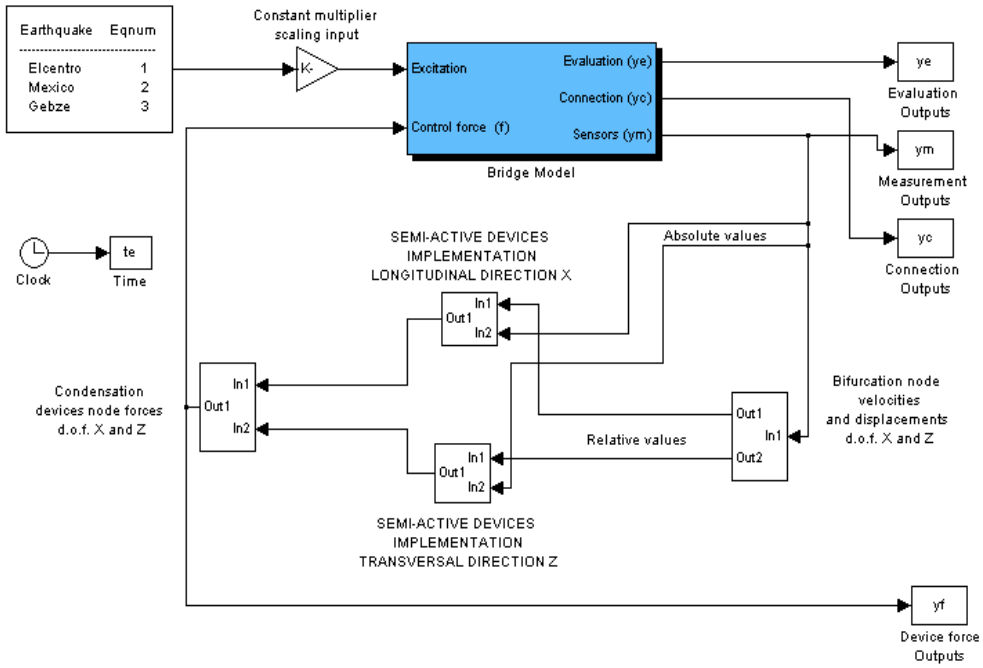

Figure 6.4: Simulink flow diagram developed in this work, level 0 blocks

in Figure 6.5. The inputs account for the absolute and relative velocity values and the displacement of the nodes where the devices are connected. The Bouc-Wen model is implemented separately for each device as Figure 6.6 clarifies. The Bouc-Wen parameters for the different configurations of the semi-active devices throughout this chapter are summarized in Table 6.1. The device parameters are defined by an external Matlab script file. The parameter regulating the elastic limit force of the hysteretic cycle is processed by the Skyhook on/off algorithm implemented by a switch as depicted in Figure 6.7.

The possibility to select different parameters for the devices is a must. Consider the devices at Bent 1. They are connected directly to the ground, so the velocity is just absolute. In other words, the relative velocity between

	A	**N**	α	$\beta = \gamma$	**K**$[KN/m]$
Type 1	1	1	0.02	40 ($V_y = 1000KN$)	80000
Type 2	1	1	0.02	20 ($V_y = 2000KN$)	80000
Type 3	1	1	0.02	8 ($V_y = 5000KN$)	80000
Type 4	1	1	0.00001	8 ($V_y = 5000KN$)	80000
Type 5	1	1	0.02	160 ($V_y = 250KN$)	80000
Type 6	1	1	0.02	40000 ($V_y = 1KN$)	80000
Type 7	1	1	0.00001	40000 ($V_y = 1KN$)	80000
Type 8	1	1	0.02	80 ($V_y = 500KN$)	80000
Type 9	1	1	0.02	10 ($V_y = 4000KN$)	80000
Type 10	1	1	0.02	320 ($V_y = 125KN$)	80000

Table 6.1: Semi-active parameters

the connection nodes multiplied by the velocity of the deck nodes yealds either a positive value or a zero (see eq. 7.2). At any rate the Skyhook algorithm produces a high level of control forces. To manage this local behaviour, lower elastic limit values for the devices are implemented.

6.3 Summary of Chapter 6

In this chapter, issues concerning the application of decentralized control solutions for large structures are discussed. A semi-active decentralized control system is implemented for the cable-stayed bridge benchmark control problem. In Chapter 7, numerical simulations are performed and bases for a comparison with different control techniques are introduced.

Notation

All symbols used in this chapter have been defined chronologically, as they appear in the text.

u	control force
v_{ref}	relative velocity
y	displacement
M, C, K	matrices of mass, damping and stiffness
$\mathbf{y}$	vector of displacement
$\mathbf{u}$	vector of control forces
Γ	vector of zeros and ones defining the loading of the ground acceleration on the structure
Λ	matrices defining how the control forces act in the structure
y_{ref}	ground displacement
z	auxiliary variable controlling the hysteretic behaviour
$A, \beta, \alpha, \gamma, n$	parameters defining the amplitude and the shape of the hysteretic cycles in th Bouc-Wen model
k	device stiffness
s	Laplace variable
W_u	transfer function matrix of the system producing the control forces
NL	nonlinear operator

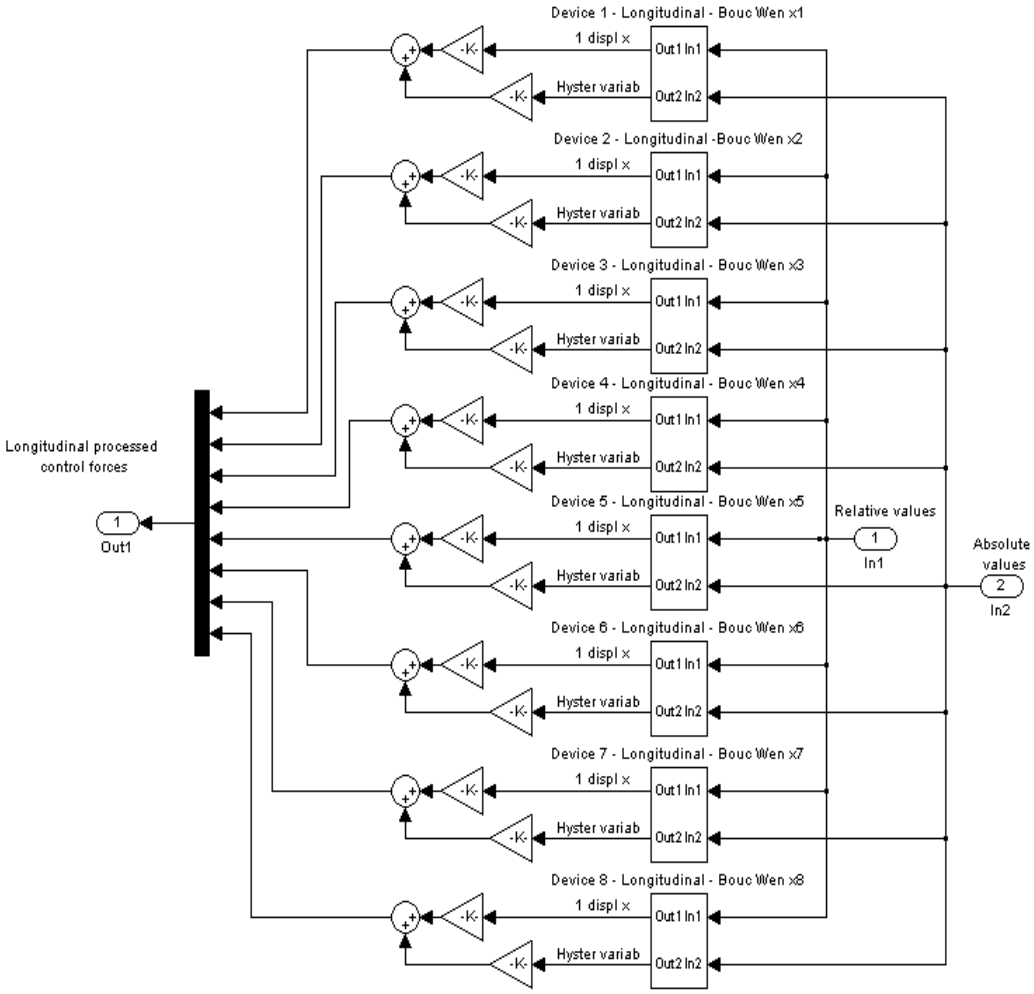

Figure 6.5: Simulink flow diagram developed in this work, level 1 blocks

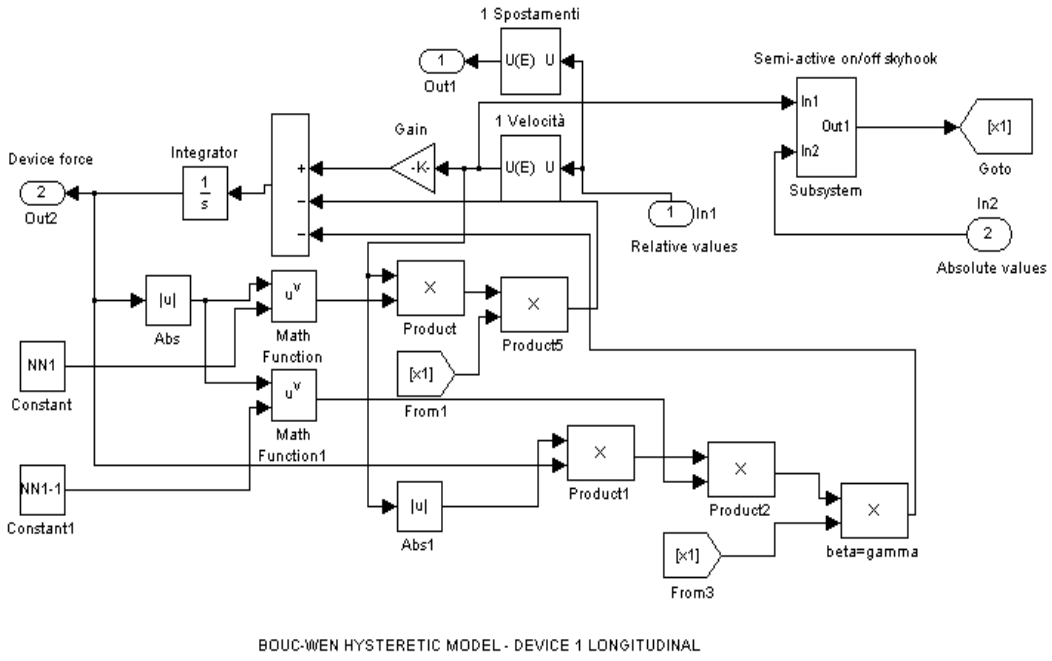

Figure 6.6: Simulink flow diagram developed in this work, level 2 blocks

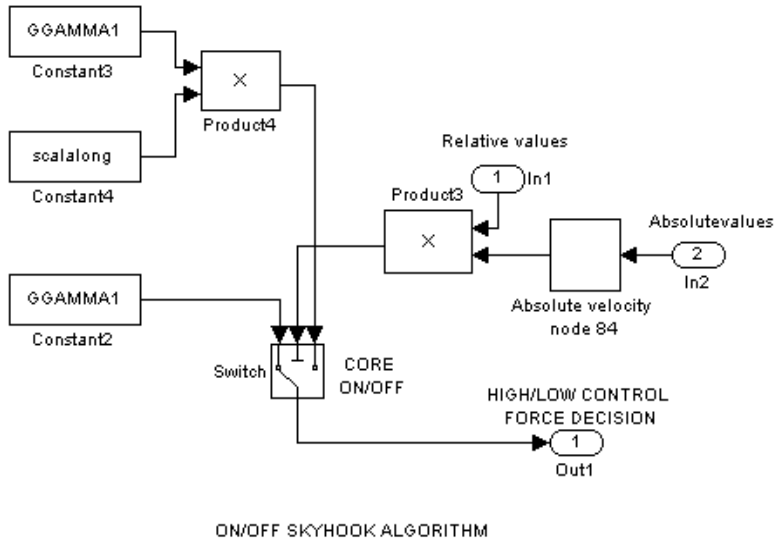

Figure 6.7: Simulink flow diagram developed in this work, level 3 blocks

Bibliography

[1] Bakule L., Paulet-Crainiceau F., Rodellar F., Rossel J.M., 2005
Overlapping Reliable Control for a Cable-Stayed Bridge Benchmark
IEEE Transactions on Control Systems Technology, Vol. 13, No. 4.

[2] Bakule L., Paulet-Crainiceau F., Rodellar J., 2004
Decentralized control design for a cable-stayed bridge benchmark
Proc. of the 2002 American Control Conference, IEEE, Piscataway, NJ, 2002, pp.3046-3051.

[3] Bakule L., Paulet-Crainiceau F., Rodellar J., 2004
Reliable control design for a cable-stayed bridge benchmark
Proc. of the 2002 American Control Conference, IEEE, Piscataway, NJ, 2002, pp.5040-5045.

[4] Luo N., Rodellar J., de la Sen M., Veí J., 2002
Decentralized active control of a class of uncertain cable-stayed flexible structures
International Journal of Control, vol. 75 (4), pp. 285-296.

[5] Rodellar J., Manosa V., Monroy C., 2002
An active tendon control scheme for cable-stayed bridges with model

uncertainties and seismic excitation
Journal of Structural Control, Vol. 9, 75-94.

[6] Magana M.E., Rodellar J., Casas J.R., Mas J., 1999
Active control of cable-stayed bridges
J. Holnicki-Szulc and J. Rodellar eds., Smart Structures, Kluwer, pp. 193-202.

[7] Amini F., 2002
Predictive Active Control Using Pole Assignment Method for Seismic Structures
Proc. of Third World Conference on Structural Control, Vol. 3, John Wiley & sons, 2002, pp. 101-106.

[8] Monroy C., Rodellar J., Magana M.E., 2000
Performance analysis of a robust local active control scheme of cable-stayed bridges
Proc. of 2nd European Conference on Structural Control, Paris, July 2000.

[9] Luo N., Rodellar J., Villarmizar R., Veí J., 2004
Robust control law for a friction-based semi-active controller of a two-span bridge
Proc. of SPIE's 10th Int. Symposium SMART Structures and Materials, 2-6 March 2003, San Diego, California, USA.

[10] Caicedo J.M., Dyke S.J., Moon S.J., Bergman L., Turan G., Hague S., 2003
Phase II Benchmark Control Problem for Seismic Response of Cable

Stayed Bridges
http://wusceel.cive.wustl.edu/quake/.

[11] Marazzi F., 2002
Semi-active control of civil structures: implementation aspects,
Ph.D. Thesis, Structural Mechanics Dept., University of Pavia.

[12] Casciati F., Domaneschi M., Faravelli L., 1998
Some Remarks on the Drift of Elasto-Plastic Oscillators Under Stochastic Excitation,
Stochastic Structural Dynamics, Spencer B.F. Jr and Johnson E.A. Eds., Notre Dame, Indiana, USA, 6-8 August 1998, pp. 545-550.

[13] *Matlab and Simulink*, 2002
The Mathworks Inc., Natick, MA.

Chapter 7

Semi-active protection of cable stayed bridges

7.1 Introduction

This chapter summarizes the results achieved by the implementation of the semi-active decentralized control system discussed in Chapter 6.
Different numerical simulations using the proposed decentralized semi-active control have been conducted. The results have been discussed with the aid of two utility functions. Eventually, an active control strategy has been developed with the aim of defining a target for the performance evaluation.

7.2 Utility functions

The utility functions c_1 and c_2 have been introduced herein to provide an improved tool of system evaluation. They are defined in the below general form

$$c = \frac{\sum_{i=1}^{6} p_i J_{i,x-z}}{\sum_{i=6}^{n} p_i} \tag{7.1}$$

Index	**Weights c_1**	**Weights c_2**
J_{1x} Base shear longitudinal direction	30	15
J_{1z} Base shear transversal direction	1	1
J_{2x} Deck shear longitudinal direction	1	15
J_{2z} Deck shear transversal direction	1	1
J_{3x} Base moment longitudinal direction	30	15
J_{3z} Base moment transversal direction	1	1
J_{4x} Deck moment longitudinal direction	1	15
J_{4z} Deck moment transversal direction	1	1
J_5 Cables tension	30	21
J_6 Deck displacement	4	15

Table 7.1: Weights for two utility functions of the form 7.1

where p_i are the weights and $J_{i,x-z}$ the evaluation criteria with $i = 1, ..6$ for the directions x and z. In Table 7.1 the weights adopted for the calculus of the utility functions are listed. The first one emphasizes base shear, base moment in longitudinal direction and cable tension, while the second function is more general. It is worth underling that c_2 with a weight of 15 in J_6 is more onerous for a vibration protection system which reduces the internal actions by managing the displacements (passive and semiactive ones).

In the remaining part of this chapter, all the numerical results for c_1 and c_2 have been reported (see Tables 7.2, 7.4, 7.5, 7.6, 7.7, 7.8, 7.9); c_1 has also been reported in the histograms (see Figures 7.2, 7.3, 7.7, 7.8, 7.9, 7.10, 7.11).

7.3 Active control results as target

An active control scheme based on a linear quadratic gaussian regulator (LQG) has been introduced in order to define a target for further simula-

tions. The LQG active control system, suggested by the benchmark problem statement [1] [2], shows the same location of the control devices as those discussed in Chapter 5. This will make a comparison of the different control strategies consistent.

In [3] the LQG active control algorithm has been widely discussed. It consists in a technique developed from the LQR (linear quadratic regulation) scheme [4], for a stochastic external excitation. In LQG control, the regulation performance is measured by a quadratic function of the form

$$\Xi(\mathbf{u}) = \int_0^\infty (\mathbf{y}^T Q\mathbf{y} + 2\mathbf{y}^T N\mathbf{u} + \mathbf{u}^T R\mathbf{u})dt \tag{7.2}$$

The weighting matrices Q, N, and R have been specified by the user and define the trade-off between regulation performance and control effort. The first design step seeks a state-feedback law $\mathbf{u} = -K\mathbf{y}$ that minimizes the cost function Ξ. The minimizing gain matrix K is obtained by solving an algebraic Riccati equation. This gain is called the LQ-optimal gain [5] [6]. In this study, the best configuration for LQG control parameters for the bridge benchmark control problem was obtained by numerical simulations and the results have been used in the following steps as a target.

Figure 7.1 depicts the implemented Simulink flow diagram. The a/d-d/a converter where the problem of hardware saturation is included and the sensors block in which a noise presence is added should be taken into account for a more realistic approach to the control problem.

7.4 Numerical simulations

The bridge benchmark statement (Phase II) comes with an example serving as a guide to the benchmark participant. This example is a standard

centralized active control applied to the benchmark problem. The active controller implements a LQG (linear quadratic Gaussian) regulator with longitudinal actuators placed between deck and Bent 1, Towers 2-3, Pier 4. The proposed control strategy has also been compared to the passive solution, to provide a broader perspective with regard to quality. Table 7.2 shows the results of the active solution and the main passive solutions for the case of 15° of seismic incidence, without any extra snow load. Table 7.3 reports some details of the semi-active simulations and Table 7.4 the respective results. They serve for a comparison of an active strategy to the total decentralized semi-active one. Only peak values in the evaluation criteria have been reported, together with the two newly introduced additional utility functions.

Figures 7.2, 7.3 depict histograms with the variation of the utility function c_1 for the different solutions.

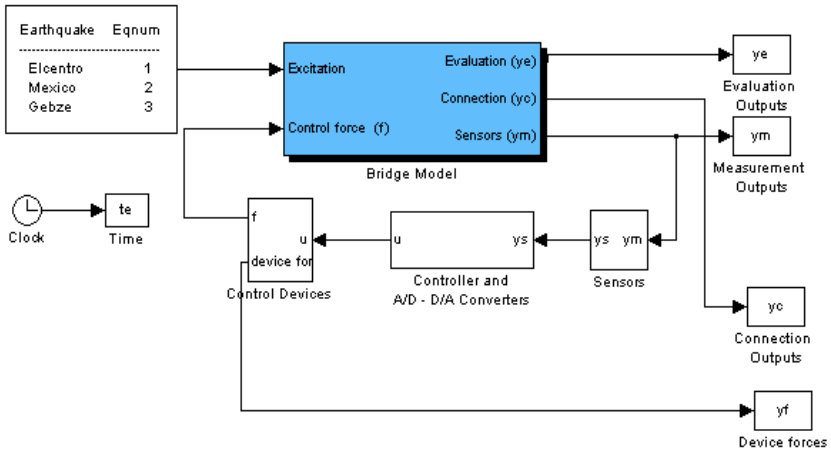

Figure 7.1: Simulink flow diagram for the active control implementation

The configurations of the semi-active devices cover several scenarios.

Criteria		Active			Passive Type 1			Passive Type 2			Passive Type 3		
Accelerogram		EIC	Mex	Geb	EIC	Mex	Geb	EIC	Mex	Geb	EIC	Mex	Geb
Base	**J1x**	0.331	0.415	0.474	0.300	0.382	0.379	0.294	0.414	0.423	0.331	0.474	0.498
Shear	**J1z**	1.022	1.117	1.037	1.015	1.122	1.039	1.022	1.112	1.046	1.013	1.112	1.041
Deck	**J2x**	0.810	0.828	0.941	0.966	1.192	1.600	1.033	1.223	1.451	1.148	1.265	1.054
shear	**J2z**	0.967	0.998	0.994	0.963	1.006	0.992	0.963	1.016	0.991	0.963	1.025	0.996
Base	**J3x**	0.324	0.396	0.456	0.270	0.407	0.742	0.298	0.433	0.661	0.367	0.585	0.461
Mom.	**J3z**	1.097	1.079	1.046	1.095	1.082	1.052	1.089	1.075	1.048	1.080	1.073	1.035
Deck	**J4x**	0.612	0.766	0.955	0.642	0.892	2.692	0.713	0.881	1.898	0.811	0.959	0.810
Mom.	**J4z**	1.009	0.992	1.001	1.009	0.993	1.001	1.010	0.993	1.000	1.010	0.991	1.000
tens.	**J5**	0.248	0.121	0.182	0.271	0.149	0.346	0.281	0.149	0.264	0.286	0.155	0.188
disp.	**J6**	1.028	1.783	2.403	1.364	2.587	10.195	1.620	2.531	7.195	2.286	4.191	2.559
	c_1	0.367	0.409	0.489	0.364	0.448	0.932	0.385	0.463	0.767	0.447	0.596	0.506
	c_2	0.559	0.695	0.863	0.629	0.892	2.455	0.694	0.896	1.840	0.842	1.196	0.888

Table 7.2: Active and passive results - no snow, incidence angle 15°

Simulation A	**high control force**	**low control force**	**NOTE**
longitudinal dev.	Type 1 (Vy=1000KN)	Type 8 (Vy=500KN)	Bent 1: devices type 1 for the two directions
transversal dev.	Type 1 (Vy=1000KN)	Type 8 (Vy=500KN)	
Simulation B	**high control force**	**low control force**	**NOTE**
longitudinal dev.	Type 2 (Vy=2000KN)	Type 8 (Vy=500KN)	Bent 1: devices type 2 for the two directions
transversal dev.	Type 2 (Vy=2000KN)	Type 8 (Vy=500KN)	
Simulation C	**high control force**	**low control force**	**NOTE**
longitudinal dev.	Type 8 (Vy=500KN)	Type 5 (Vy=250KN)	Bent 1: devices type 8 for the two directions
transversal dev.	Type 8 (Vy=500KN)	Type 5 (Vy=250KN)	
Simulation D	**high control force**	**low control force**	**NOTE**
longitudinal dev.	Type 8 (Vy=500KN)	Type 5 (Vy=250KN)	Bent 1: devices type 10 for the two directions
transversal dev.	Type 8 (Vy=500KN)	Type 5 (Vy=250KN)	
Simulation E	**high control force**	**low control force**	**NOTE**
longitudinal dev.	Type 3 (Vy=5000KN)	Type 2 (Vy=2000KN)	Bent 1: devices type 2 for the two directions
transversal dev.	Type 3 (Vy=5000KN)	Type 2 (Vy=2000KN)	

Table 7.3: Simulations details

Simulation cases A, B and C present rather low values of the elastic limit of the Bouc-Wen model. Actually at Bent 1 the devices parameters are always set on high force levels for formally discussed reasons. The simulation case D was introduced to study the possibility of achieving a better response by setting a lower elastic limit for the devices at Bent 1. The result was positive.

Figure 7.4 presents the intensities of the three records. The worst among

Criteria		Simulation A			Simulation B			Simulation C			Simulation D			Simulation E		
Accelerogram		EIC	Mex	Geb	EIC	Mex	Geb	EIC	Mex	Geb	EIC	Mex	Geb	EIC	Mex	Geb
Base Shear	**J1x**	0.311	0.375	0.377	0.313	0.366	0.382	0.320	0.397	0.348	0.320	0.393	0.351	0.301	0.432	0.423
	J1z	1.027	1.117	1.041	1.023	1.124	1.041	1.073	1.138	1.083	1.072	1.135	1.097	1.023	1.085	1.048
Deck shear	**J2x**	0.906	1.160	1.986	1.299	2.738	2.446	0.941	1.138	2.069	0.948	1.122	1.797	1.057	1.235	1.452
	J2z	0.960	0.995	0.995	0.956	0.999	0.998	0.983	0.972	0.978	0.984	0.966	0.977	0.962	1.025	0.991
Base Mom.	**J3x**	0.246	0.365	0.906	0.668	1.606	1.162	0.238	0.380	0.959	0.240	0.385	0.843	0.308	0.444	0.662
	J3z	1.092	1.078	1.055	1.089	1.087	1.056	1.139	1.094	1.025	1.138	1.092	1.037	1.089	1.100	1.050
Deck Mom.	**J4x**	0.597	0.793	3.446	2.579	5.206	4.839	0.555	0.865	3.692	0.550	0.957	3.305	0.728	0.972	1.901
	J4z	1.009	0.992	1.001	1.009	0.993	1.001	1.022	1.050	0.991	1.022	1.048	0.991	1.010	0.992	1.000
Cable tens.	**J5**	0.265	0.152	0.408	0.375	0.375	0.441	0.265	0.158	0.419	0.267	0.154	0.402	0.284	0.157	0.264
Deck disp.	**J6**	1.640	1.987	12.835	11.698	22.815	17.163	1.342	2.136	13.280	1.338	2.495	12.576	1.686	2.953	7.204
	c_1	0.368	0.409	1.116	0.954	1.738	1.396	0.358	0.428	1.147	0.359	0.443	1.074	0.394	0.492	0.767
	c_2	0.652	0.776	3.059	2.603	5.031	4.032	0.607	0.813	3.181	0.608	0.877	2.956	0.713	0.980	1.843

Table 7.4: Semi-active results - no snow, incidence angle 15°

them, due to the effects it implies, is represented by Gebze one.

Figure 7.5 shows the semi-active processed force at Pier 2 in the longitudinal direction under the El Centro record for the simulation D, Figure 7.6 for the simulation E. The parameters of simulation E are too high to show a semi-active behaviour of the device. The semi-active simulation case D appears to be the best performing of all the tested cases. Device setting Type 2 in Table 7.2 shows the best results among passive solutions. The semi-active simulation D and the passive solution set with Type 2 parameters are compared with the active target, for all the load cases available in the benchmark.

Figures 7.7, 7.8, 7.9 and 7.10 present the comparison in terms of utility function c_1. Tables 7.5, 7.6 detail the numerical results of benchmark evaluation criteria for peak responses. The simulation results show the good performance of the semi-active total decentralized control system. In the light of El Centro and Mexico, it is close to the active solution (in some cases even better) and, generally, much better than the passive solution. In case of Gebze noise, the effectiveness of the semi-active system is not so

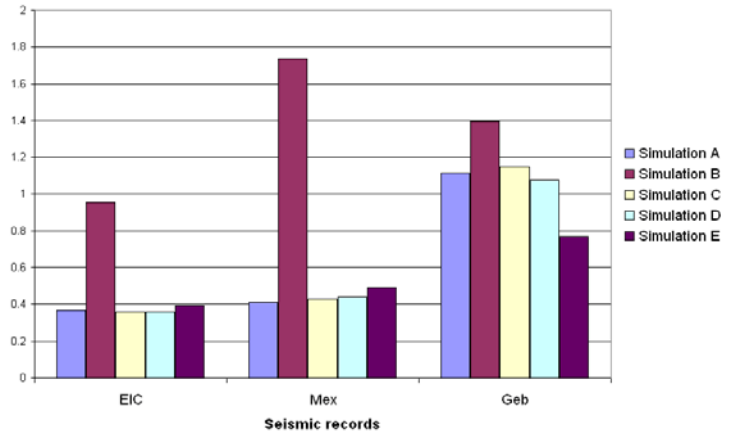

Figure 7.2: Utility function c_1 for the different semi-active solutions - no snow, incidence angle 15° (ElC=El Centro input, etc.)

evident but it remains within good ranges. To improve this lack of performance, a higher elastic limit of the device could be more suitable.

7.5 System efficiency for different seismic intensities

Theoretically the most evident quality of a semi-active control system is its ability to adapt its configuration to the level of external excitation. For passive systems, it is evident that their efficiency decreases as the seismic excitation intensity increases. By contrast, the semi-active strategy is able to tune the force limit value on the seismic excitation intensities. Table 7.7 shows the performances of the semi-active simulation case D at different intensities of the seismic excitation: the availability of the semi-active protection system allows one to pursue the same efficiency in all the cases.

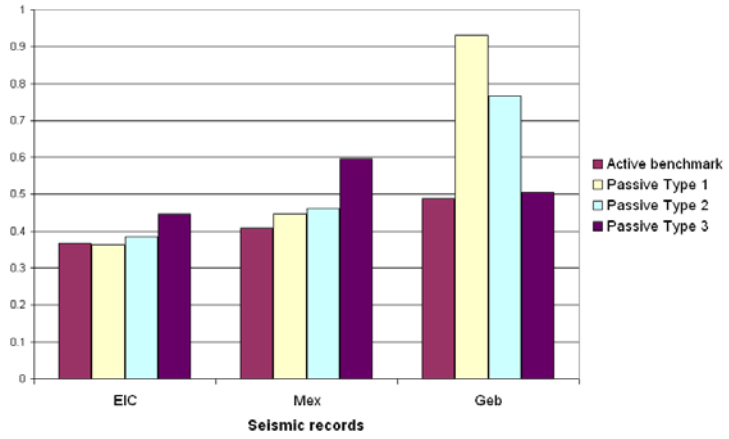

Figure 7.3: Utility function c_1 for active and passive solutions - no snow, incidence angle 15° (ElC=El Centro input, etc.)

Figure 7.11 underlines the good performance achieved by the semi-active solution in terms of utility function c_1 for different seismic intensities.

7.6 Robustness considerations

The semi-active control system implemented in this chapter, for its decentralized nature with devices independent from each other, suggests to check the robustness in the occurrence of local failures. The failure is simulated by reducing the device stiffness from 80000 KN/m to 800 KN/m. So three simulations are processed with an incidence angle of 15°, without the extra load of snow. The three failures considered are at Bent 1, Pier 2 and Pier 4, respectively. The results are reported in Table 7.8.

The control behaviour remains satisfactory in all cases. Only for the Gebze seismic record, a better response in terms of utility function c_1 is reported. This is an interesting result. It can be justified by a redistribution of the

effect induced by the failed device on the global geometry of the bridge. This effect results in a loss of symmetry in the problem. The evaluation criteria in the transversal direction compensate the failure effects, resulting in a better performance.

7.7 Remarks on improving responses

Case D performs suitable responses very close to the active solution, sometimes even better. When noise intensity is reduced by a multiplier 0.6 or 0.3, the performances are very good. So case D can be considered suitable for sites where a hazard analysis indicates at rather light frequent seismic excitations.

In order to improve the response shown by simulation D, the high level of on/off Skyhook algorithm (see Chapter 6) [7] is set with Type 1 parameters. The elastic limit so increases from the level of $V_y = 500KN$ to $1000KN$. Table 7.9 details the evaluation criteria for the load case with 15° of seismic incidence angle, without snow extra load and with two values of multipliers of the input, 1 and 0.3. The response is effectively improved.

Figures 7.12, 7.13, 7.14 and 7.15 present the structural responses in terms of acceleration for the El Centro input signal. In particular Figure 7.12 and 7.14 are relatives to the deck in the longitudinal and transversal directions, respectively. The longitudinal direction is strongly involved in the seismic motion.

Figure 7.13 and 7.15 present the results for the top of the tower at Pier 2, the intensity of the accelerations is much greater than the one at the deck.

7.8 Summary of Chapter 7

In this chapter a semi-active, decentralized solution is applied to a cable-stayed bridge benchmark control problem. This control strategy is compared with a passive and an active solution. It results close to the latter (at times even better) and generally better than the former solution. In particular, a semi-active configuration, referred in this work as case D, shows good performances.

A robustness study has also been conducted with the semi-active solution and it reveals suitable robustness against local failures of the control devices.

Finally a new semi-active configuration has been tested in order to find the best tuning of the device parameters and to improve the performances of case D.

Notation

All symbols used in this chapter have been defined chronologically, as they appear in the text.

J_i	evaluation criteria (i=1,..18)
c_i	utility function (i=1,2)
p_i	weights
$\mathbf{y}$	displacement
$\mathbf{u}$	control force
Ξ	LQG quadratic function
Q, N, R	weights matrices
K	gain matrix
t	time
V_y	yelding level

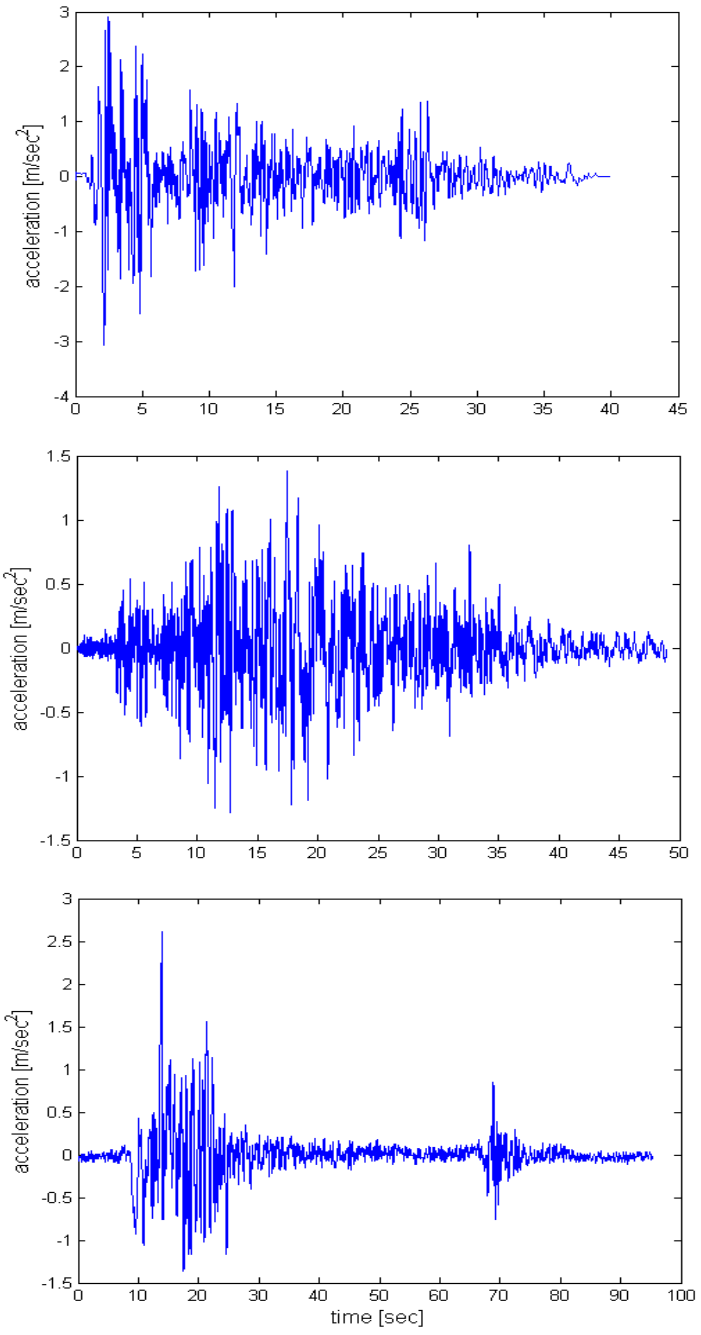

Figure 7.4: El Centro, Mexico, Gebze record

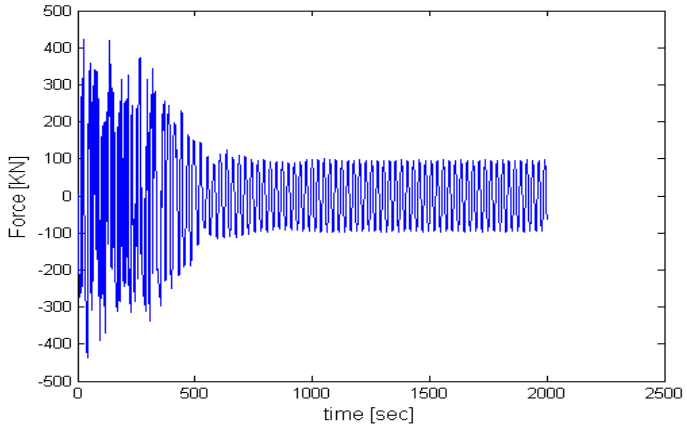

Figure 7.5: Semi-active device at Pier 2, El Centro record, simulation D

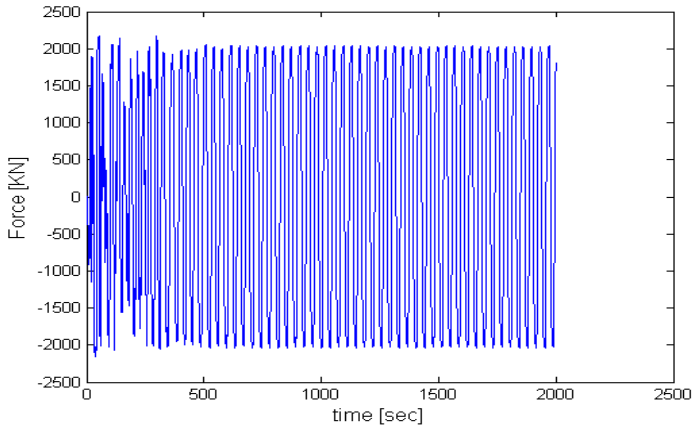

Figure 7.6: Semi-active device at Pier 2, El Centro record, simulation E

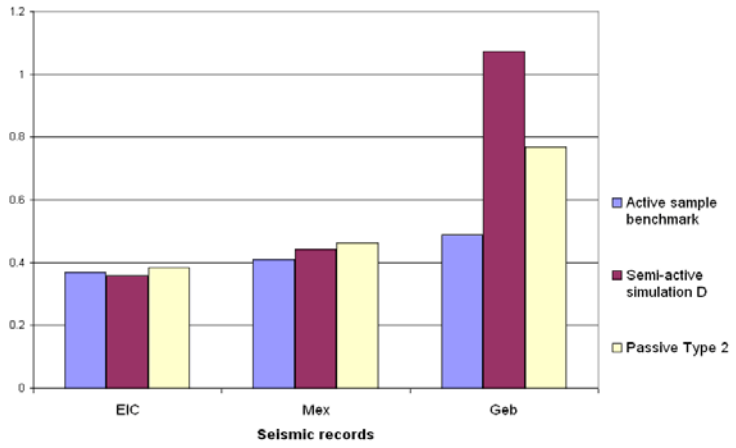

Figure 7.7: Utility function c_1 - no snow, incidence angle 15° (ElC=El Centro input, etc.)

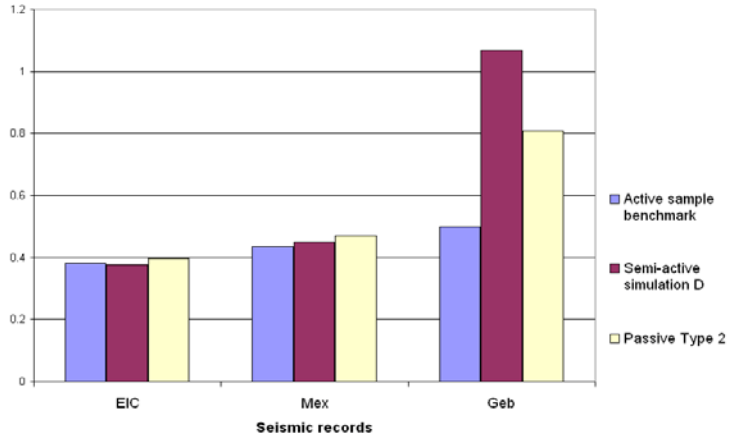

Figure 7.8: Utility function c_1 - snow, incidence angle 15° (ElC=El Centro input, etc.)

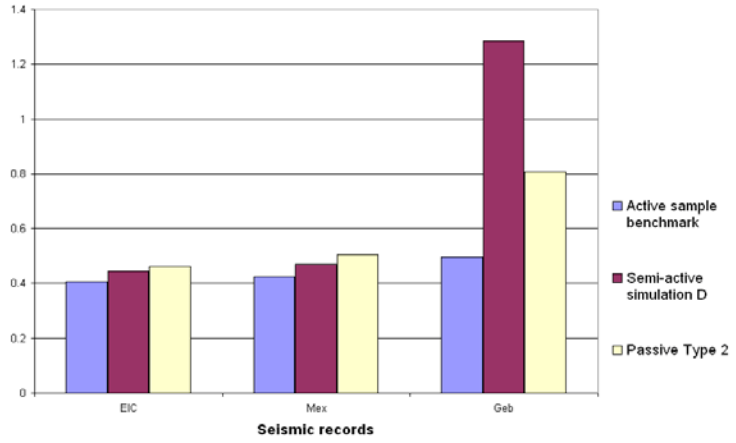

Figure 7.9: Utility function c_1 - no snow, incidence angle 45° (ElC=El Centro input, etc.)

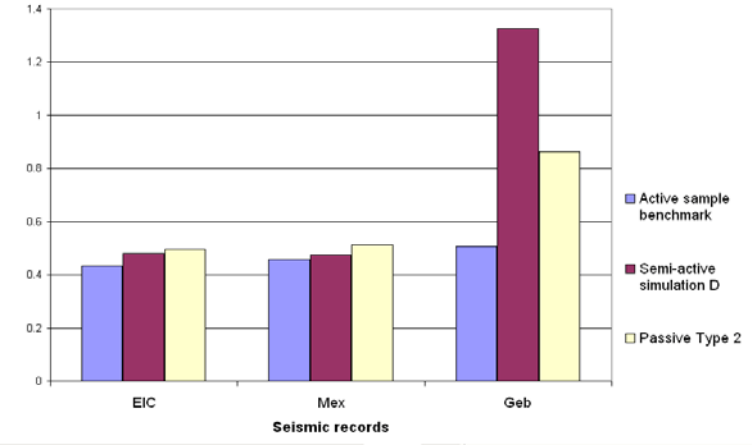

Figure 7.10: Utility function c_1 - snow, incidence angle 45° (ElC=El Centro input, etc.)

Criteria		Active			Semi-active D			Passive Type 2		
		Incidence angle 15° no snow								
		EIC	Mex	Geb	EIC	Mex	Geb	EIC	Mex	Geb
Base Shear	**J1x**	0.331	0.415	0.474	0.320	0.393	0.351	0.294	0.414	0.423
	J1z	1.022	1.117	1.037	1.072	1.135	1.097	1.022	1.112	1.046
Deck shear	**J2x**	0.810	0.828	0.941	0.948	1.122	1.797	1.033	1.223	1.451
	J2z	0.967	0.998	0.994	0.984	0.966	0.977	0.963	1.016	0.991
Base Mom.	**J3x**	0.324	0.396	0.456	0.240	0.385	0.843	0.298	0.433	0.661
	J3z	1.097	1.079	1.046	1.138	1.092	1.037	1.089	1.075	1.048
Deck Mom.	**J4x**	0.612	0.766	0.955	0.550	0.957	3.305	0.713	0.881	1.898
	J4z	1.009	0.992	1.001	1.022	1.048	0.991	1.010	0.993	1.000
Cable tens.	**J5**	0.248	0.121	0.182	0.267	0.154	0.402	0.281	0.149	0.264
Deck disp.	**J6**	1.028	1.783	2.403	1.338	2.495	12.576	1.620	2.531	7.195
	c_1	0.367	0.409	0.489	0.359	0.443	1.074	0.385	0.463	0.767
	c_2	0.559	0.695	0.863	0.608	0.877	2.956	0.694	0.896	1.840
		Incidence angle 15° snow								
		EIC	Mex	Geb	EIC	Mex	Geb	EIC	Mex	Geb
Base Shear	**J1x**	0.358	0.485	0.480	0.364	0.435	0.347	0.340	0.438	0.421
	J1z	1.022	1.115	1.037	1.079	1.133	1.089	1.022	1.110	1.044
Deck shear	**J2x**	0.853	0.861	0.973	0.948	1.149	1.856	1.033	1.242	1.495
	J2z	0.967	0.999	0.994	0.984	0.964	0.976	0.962	1.015	0.991
Base Mom.	**J3x**	0.336	0.416	0.463	0.258	0.377	0.837	0.307	0.438	0.687
	J3z	1.095	1.093	1.045	1.136	1.105	1.029	1.090	1.088	1.047
Deck Mom.	**J4x**	0.642	0.771	0.979	0.569	0.945	3.304	0.699	0.866	2.039
	J4z	1.009	0.993	1.001	1.024	1.048	0.991	1.010	0.992	1.000
tens.	**J5**	0.246	0.113	0.178	0.264	0.153	0.400	0.273	0.150	0.280
Deck disp.	**J6**	1.054	1.822	2.546	1.342	2.447	12.512	1.562	2.508	7.866
	c_1	0.380	0.435	0.499	0.377	0.451	1.068	0.397	0.471	0.807
	c_2	0.579	0.719	0.894	0.620	0.878	2.953	0.689	0.897	1.976

Table 7.5: Comparison benchmark evaluation criteria peak values - incidence angle 15°, snow and not

Criteria		Active			Semi-active D			Passive Type 2		
		Incidence angle 45° no snow								
Accelerogram		EIC	Mex	Geb	EIC	Mex	Geb	EIC	Mex	Geb
Base Shear	**J1x**	0.371	0.415	0.428	0.386	0.386	0.424	0.358	0.447	0.364
	J1z	0.991	1.044	0.998	1.145	1.095	0.942	0.999	1.042	0.996
Deck shear	**J2x**	0.690	1.028	0.937	0.864	1.297	2.144	0.895	1.194	1.244
	J2z	0.984	0.970	0.989	1.056	1.050	1.033	0.987	0.982	0.990
Base Mom.	**J3x**	0.362	0.404	0.491	0.337	0.411	1.114	0.422	0.465	0.667
	J3z	0.979	1.027	0.993	1.118	1.112	0.923	0.984	1.038	0.993
Deck Mom.	**J4x**	0.600	0.681	0.736	0.807	0.873	3.419	0.719	0.805	1.867
	J4z	0.997	1.000	1.002	0.992	1.004	1.011	0.996	1.000	1.002
Cable tens.	**J5**	0.285	0.122	0.185	0.285	0.155	0.370	0.280	0.158	0.245
Deck disp.	**J6**	1.243	2.126	2.701	2.084	3.028	15.443	2.223	3.060	8.857
	c_1	0.408	0.425	0.495	0.445	0.471	1.285	0.463	0.504	0.808
	c_2	0.589	0.764	0.872	0.775	0.974	3.498	0.791	0.969	2.041
		Incidence angle 45° snow								
Accelerogram		EIC	Mex	Geb	EIC	Mex	Geb	EIC	Mex	Geb
Base Shear	**J1x**	0.431	0.494	0.433	0.471	0.407	0.434	0.442	0.465	0.366
	J1z	0.987	1.036	0.998	1.142	1.096	0.943	0.994	1.032	0.996
Deck shear	**J2x**	0.735	1.052	0.964	0.869	1.331	2.225	0.903	1.192	1.297
	J2z	0.982	0.974	0.989	1.052	1.052	1.032	0.986	0.984	0.989
Base Mom.	**J3x**	0.384	0.430	0.505	0.371	0.404	1.165	0.440	0.466	0.716
	J3z	0.980	1.027	0.993	1.116	1.113	0.924	0.983	1.037	0.992
Deck Mom.	**J4x**	0.633	0.696	0.763	0.817	0.862	3.604	0.755	0.767	2.048
	J4z	0.997	1.000	1.002	0.991	1.002	1.011	0.996	1.000	1.002
Cable tens.	**J5**	0.282	0.119	0.179	0.287	0.155	0.375	0.277	0.161	0.258
Deck disp.	**J6**	1.258	2.152	2.873	2.042	2.976	15.924	2.261	3.100	9.721
	c_1	0.432	0.457	0.507	0.480	0.473	1.327	0.494	0.512	0.864
	c_2	0.615	0.789	0.908	0.789	0.972	3.621	0.818	0.973	2.216

Table 7.6: Comparison benchmark evaluation criteria peak values - incidence angle 45°, snow and not

Input multiplier		1			0.6			0.3		
Criteria		Incidence angle 15° no snow								
Accelerogram		ElC	Mex	Geb	ElC	Mex	Geb	ElC	Mex	Geb
Base Shear	**J1x**	0.320	0.393	0.351	0.187	0.215	0.223	0.090	0.111	0.112
	J1z	1.072	1.135	1.097	0.613	0.680	0.636	0.306	0.337	0.312
Deck shear	**J2x**	0.948	1.122	1.797	0.560	0.688	0.976	0.292	0.353	0.476
	J2z	0.984	0.966	0.977	0.577	0.603	0.601	0.289	0.303	0.297
Base Mom.	**J3x**	0.240	0.385	0.843	0.145	0.231	0.437	0.078	0.126	0.219
	J3z	1.138	1.092	1.037	0.655	0.656	0.629	0.328	0.325	0.316
Deck Mom.	**J4x**	0.550	0.957	3.305	0.355	0.575	1.646	0.196	0.278	0.794
	J4z	1.022	1.048	0.991	0.606	0.595	0.602	0.303	0.298	0.300
Cable tens.	**J5**	0.267	0.154	0.402	0.160	0.093	0.219	0.082	0.046	0.101
Deck disp.	**J6**	1.338	2.495	12.576	0.807	1.609	6.388	0.423	0.800	2.989
	c_1	0.359	0.443	1.074	0.214	0.264	0.570	0.109	0.136	0.274
	c_2	0.608	0.877	2.956	0.366	0.543	1.521	0.191	0.272	0.722

Table 7.7: Comparison benchmark evaluation criteria peak values for different seismic intensity - no snow, incidence angle 15°

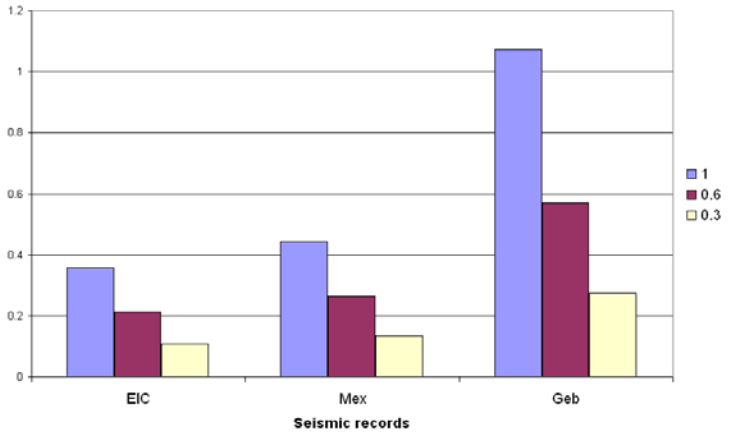

Figure 7.11: Utility function c_1 for different seismic intensity - no snow, incidence angle 15° (ElC=El Centro input, etc.)

Input multiplier		Device failed at Bent 1			Device failed at Pier 2			Device failed at Pier 4		
Criteria		Incidence angle 15° no snow								
Accelerogram		EIC	Mex	Geb	EIC	Mex	Geb	EIC	Mex	Geb
Base Shear	**J1x**	0.318	0.354	0.476	0.320	0.361	0.357	0.323	0.356	0.426
	J1z	1.023	1.122	1.648	1.018	1.123	1.123	1.022	1.122	1.199
Deck shear	**J2x**	0.917	1.134	2.036	0.910	1.132	1.310	0.908	1.163	1.523
	J2z	0.966	1.006	1.245	0.966	1.005	1.019	0.965	1.008	1.041
Base Mom.	**J3x**	0.237	0.381	0.732	0.240	0.373	0.492	0.242	0.379	0.480
	J3z	1.100	1.083	1.385	1.100	1.084	1.058	1.106	1.083	1.125
Deck Mom.	**J4x**	0.576	0.970	1.956	0.554	0.919	1.892	0.556	0.942	1.846
	J4z	1.008	0.992	0.992	1.008	0.990	0.993	1.008	0.991	1.022
Cable tens.	**J5**	0.267	0.156	0.334	0.267	0.159	0.268	0.275	0.165	0.267
Deck disp.	**J6**	1.395	2.627	7.679	1.337	2.446	6.470	1.300	2.519	6.376
	c_1	0.358	0.436	0.863	0.357	0.428	0.668	0.359	0.434	0.685
	c_2	0.613	0.895	2.055	0.601	0.860	1.676	0.598	0.880	1.698

Table 7.8: Comparison benchmark evaluation criteria for failed device in different locations - no snow, incidence angle 15°

Input multiplier		15°, no snow - input multiplier 1			15°, no snow - input multiplier 0.3		
Criteria		Simulation case D improved by Type 1					
Accelerogram		EIC	Mex	Geb	EIC	Mex	Geb
Base Shear	**J1x**	0.317	0.358	0.337	0.090	0.112	0.112
	J1z	1.022	1.130	1.145	0.308	0.333	0.312
Deck shear	**J2x**	0.919	1.158	1.006	0.294	0.359	0.476
	J2z	0.960	1.006	1.039	0.289	0.303	0.297
Base Mom.	**J3x**	0.236	0.367	0.477	0.079	0.129	0.219
	J3z	1.086	1.092	1.075	0.328	0.322	0.316
Deck Mom.	**J4x**	0.569	0.969	1.814	0.195	0.293	0.794
	J4z	1.010	0.992	1.036	0.303	0.298	0.300
Cable tens.	**J5**	0.265	0.159	0.284	0.082	0.046	0.101
Deck disp.	**J6**	1.339	2.700	6.205	0.420	0.878	2.991
	c_1	0.355	0.437	0.649	0.109	0.140	0.274
	c_2	0.604	0.908	1.578	0.191	0.288	0.722

Table 7.9: Comparison benchmark evaluation criteria for improved high semi-active limit - no snow, incidence angle 15°, multiplier 1 and 0.3

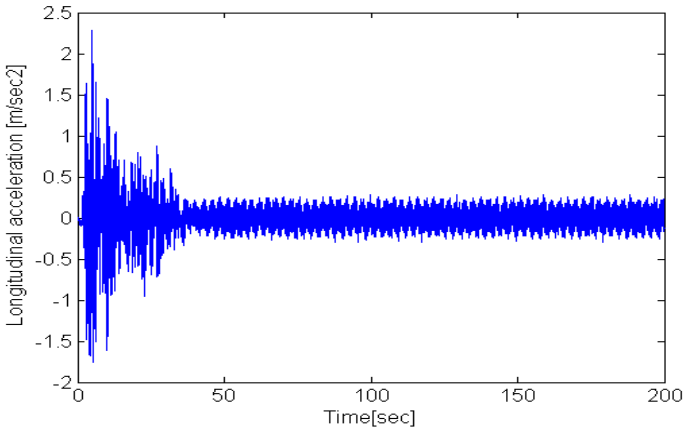

Figure 7.12: Deck longitudinal acceleration at Pier 2, El Centro record without snow load and 15° of incidence, simulation D improved, multiplier 1

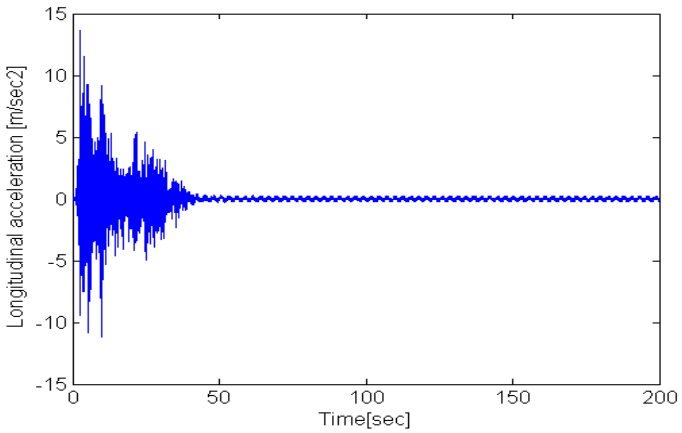

Figure 7.13: Tower (top) longitudinal acceleration at Pier 2, El Centro record without snow load and 15° of incidence, simulation D improved, multiplier 1

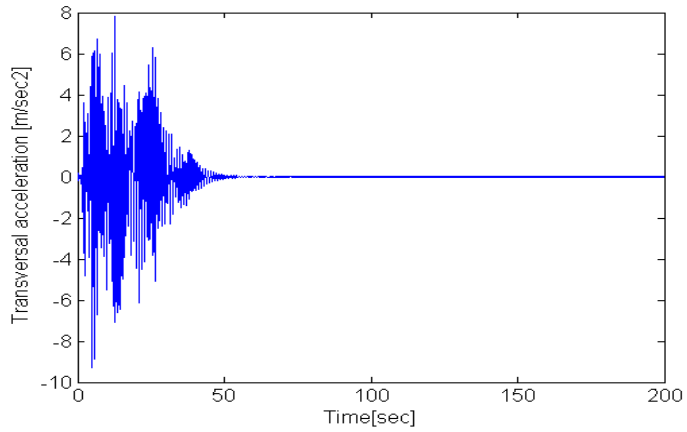

Figure 7.14: Deck transversal acceleration at Pier 2, El Centro record without snow load and 15° of incidence, simulation D improved, multiplier 1

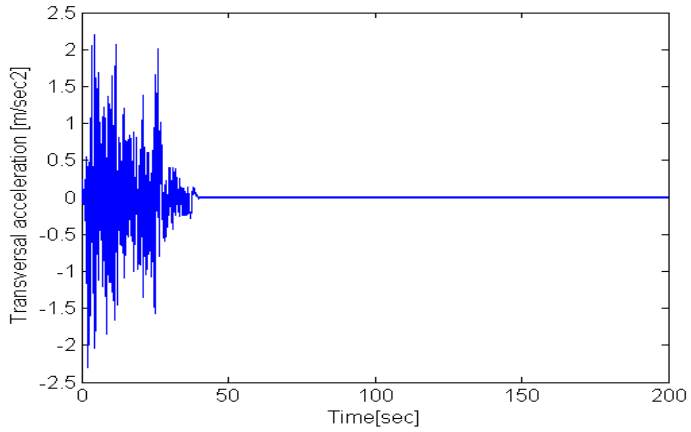

Figure 7.15: Tower (top) transversal acceleration at Pier 2, El Centro record without snow load and 15° of incidence, simulation D improved, multiplier 1

Bibliography

[1] Caicedo J.M., Dyke S.J., Moon S.J., Bergman L., Turan G., Hague S., 2003
Phase II Benchmark Control Problem for Seismic Response of Cable Stayed Bridges,
Journal of Structural Control, 10:137-168.

[2] Caicedo J.M., Dyke S.J., Moon S.J., Bergman L., Turan G., Hague S., 2003
Phase II Benchmark Control Problem for Seismic Response of Cable Stayed Bridges
http://wusceel.cive.wustl.edu/quake/.

[3] Battaini M., 1998
Sistemi strutturali controllati: progettazione ed affidabilitá,
Ph.D. Thesis (in Italian), Structural Mechanics Dept., University of Pavia.

[4] Casciati F., Domaneschi M., Faravelli L., 2004
Active Control Schemes for Managing Nonlinear Passive Devices,
Proc. of the Third European Conference on Structural Control, R.

Flesch, H. Irschik, M. Kommer (eds.), Vienna, Austria, July 2004, Vol. II, pp. from S1-23 to S1-26, ISBN-3-901167-90-0.

[5] *Matlab and Simulink*, 2002
The Mathworks Inc., Natick, MA.

[6] *Control System Toolbox*, 2002
The Mathworks Inc., Natick, MA.

[7] Marazzi F., 2002
Semi-active control of civil structures: implementation aspects,
Ph.D. Thesis, Structural Mechanics Dept., University of Pavia.

Chapter 8

Control solutions for suspended bridges

8.1 Introduction

This chapter extends the control experiences collected for the cable-stayed bridge benchmark to a single span suspended bridge model. A commercial finite element code furnishes the tool for numerical implementations.
The wind is regarded as the most aggressive dynamic external excitation, in terms of displacement and internal actions [1] [2].

8.2 Main geometry

The global geometry for the suspended bridge is freely ispired by the Shimotsui-Seto Bridge in Japan, spanning from the Mt. Washu side to the Hitsuishi-jima Island side. This bridge is a *single span truss−stiffened suspension bridge with overhanging span* type. The main dimensions can be summarized as follows:

- length, 1446 m;

- tower height, 149 m;
- vertical distance of the main girder quote from the towers foundation quote, 31 m;
- main girder section: 30 m for width and 13 m for thickness.

The main girder is a steel frame, the towers have been built in concrete and the main cables with suspenders are also in steel. Figure 8.1 shows the bridge profile and the deck section. These informations were taken from the website [3].

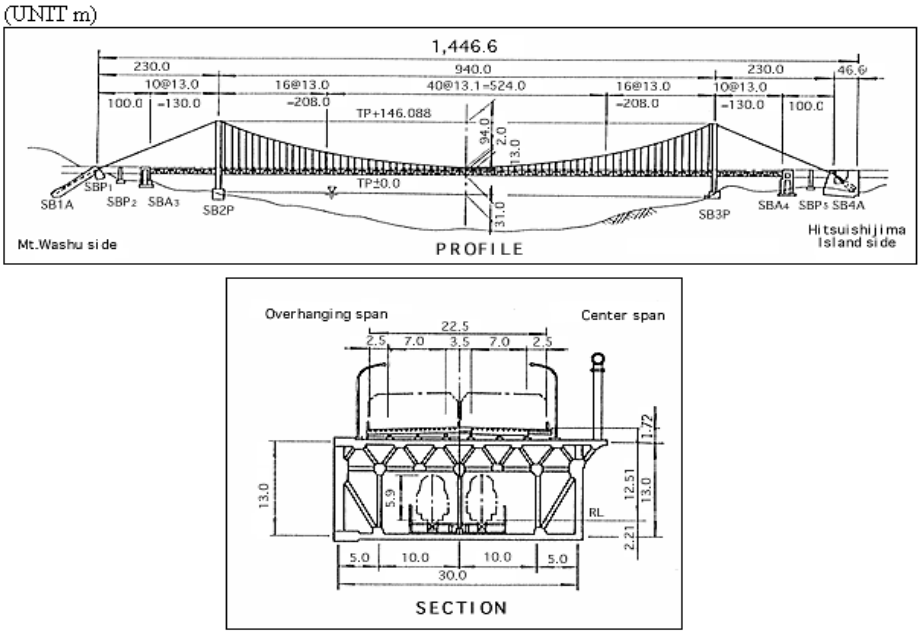

Figure 8.1: Shimotsui-Seto bridge: profile and deck section, main dimensions

8.3 Structural model

A finite element model has been implemented by the commercial code ANSYS CivilFEM [4]. For the aim of this control study, the following considerations have been introduced:

- The constitutive law is linear elastic for all the materials.
- The deck can be discretized by an equivalent girder.
- The dynamic excitation considered is the wind load. The static effect of the materials weight has also been accounted for.

Three types of elements have been used in the basic (uncontrolled) numerical model:

- beams for the towers,
- trusses for the cable and the suspenders,
- shells for the deck.

The sections geometry adopted for the model elements can be summarized as given below:

- the towers are composed of vertical beams of varied rectangular sections (from 20x10m and 12x6m) and of horizontal beams of a square section (6 m).
- The main cables truss has a circular section with a diameter of 0.62 m; the suspenders have a diameter of 0.12 m.
- The deck shell elements are 5 m thick.

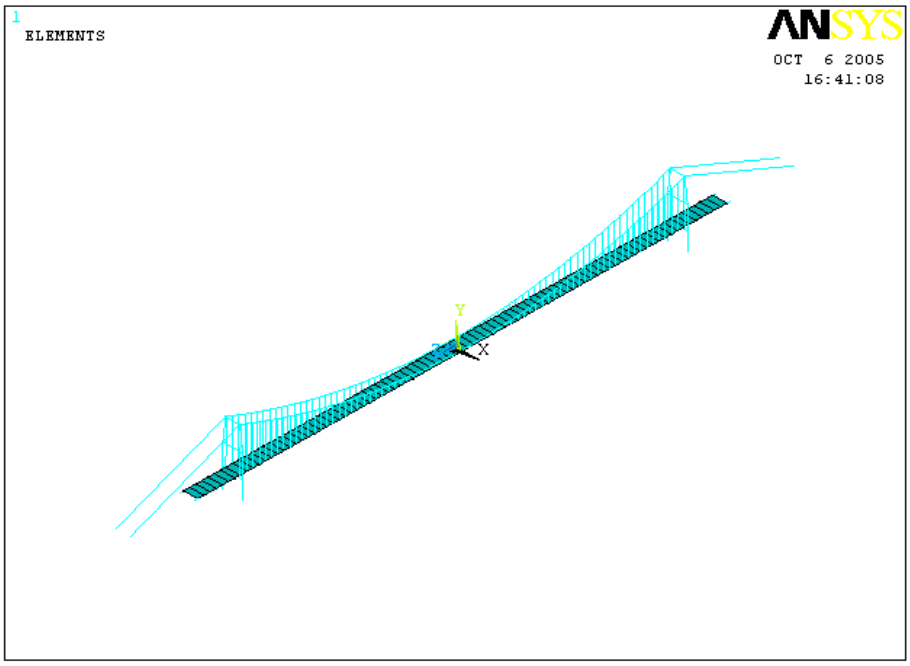

Figure 8.2: The Shimotsui-Seto bridge: finite element mesh

Figure 8.2 depicts the bridge mesh; it consists of 464 elements and 392 nodes.

8.3.1 Boundary conditions and materials

The whole model is fixed to the ground (by assigning zero displacements in three directions) at the bottom of the towers, at the edges of the main cables and at the deck's ends. In the uncontrolled model, the towers are rigidly linked to the bridge deck.

The loads considered are the gravity load and the external wind load, applied uniformly along the deck, in the horizontal direction transversal to the deck axis. The mean wind pressure is calculated as presented in Chapter 5

for the cable-stayed bridge, following [5]:

$$p_m = 1.31 KN/m^2 \tag{8.1}$$

In this case, the gust coefficient is also $G = 1.62$.

Considering the wind pressure on the steel frame girder of the deck, it is possible to calculate the nodal forces applied to the shell nodes in the finite element model. The distance between the nodes is $13m$; the equivalent width of the steel frame girder is $5m$.

The wind signal is simulated as a white noise segment sampled at the time interval of $0.5sec$. The frequency content is limited to 1 Hz (see Figure 8.3). Figure 8.4 depicts the whole nodal force time history selected for the numerical simulations. The initial ramp from 0 to the mean value of the force moves the deck in 10 sec from the initial static configuration to the mean value of the random noise which acts for a total duration of 35 sec.

Figure 8.5 reports the boundary condition as applied to the bridge model.

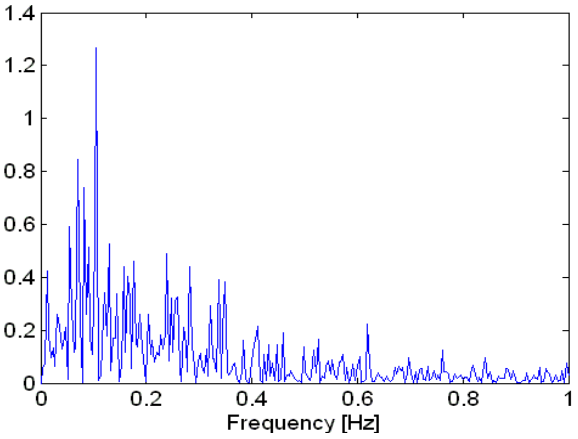

Figure 8.3: Wind load frequency content

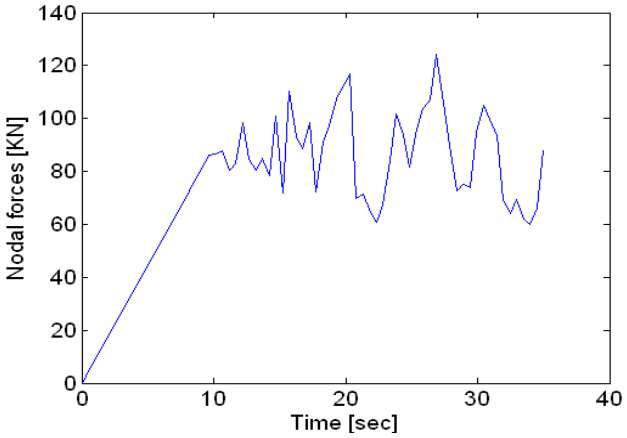

Figure 8.4: Wind load time history

Table 8.1 reports material parameters (Young and Poisson modulus, mass density) associated with the elements in the finite element model.

It is worth noting that the mass density value for the deck girder has

Structural element and material	**Young modulus** $[KN/m^2]$	**Poisson modulus**	**Mass density** $[KN/m^3g]$
Tower beams (high performance concrete)	50000000	0.2	2.4
Cables trusses (steel)	210000000	0.3	7.0
Deck shells	900000	0.3	0.1

Table 8.1: Material parameters

been selected considering a linear weigh of 150 KN/m of the deck [1]. The Poisson modulus is the steel one. The elastic Young modulus of the girder has been fixed after several runs of modal analysis on the uncontrolled model so as to tune the natural frequency for the horizontal displacement of the deck in the transversal direction.

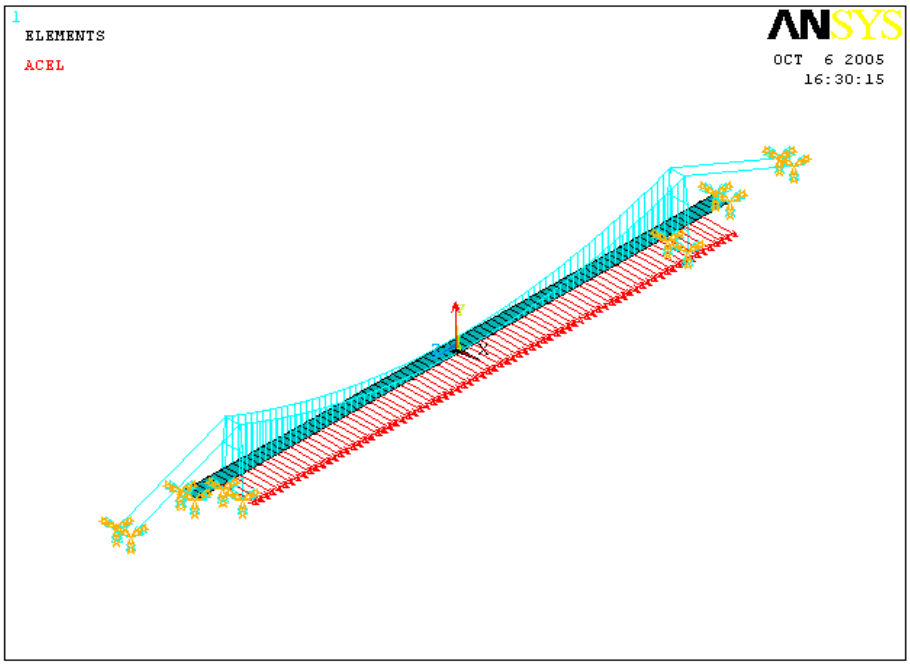

Figure 8.5: Bridge boundary conditions

8.3.2 Structural verifications values

For the purpose of this control issue, some structural verifications have been considered:

- the maximum tension in the main cables and in the suspenders,
- the shear in the transversal direction at the base of the tower,
- the bending moment in the transversal direction at the tower base,
- the bending moment in the transversal direction of the deck in the proximity of the tower.

The corrisponding limit values are:

- The cable wire strenght is assumed to be 1800 MPa, according to [1]. Therefore, for the main cable, maximum tension is 540000 KN (for each one of the two main cables) and for the suspenders 20000 KN (for each of the 150 suspenders).

- The limit value for the shear at the base of the towers in the transversal direction is calculated, according to [6], as 160000 KN, without any specific shear steel reinforces. The positive contribution of the compression in the tower is not considered with its static values of 610000 KN but with its minimum value under the dynamic condition simulated in this study. The fluctuation of the wind load can reduce the compression down to 200000 KN.

- The bending moment limit value in the transversal direction at the tower base is calculated as 900000 KNm including the interaction with the axial compression, this without any specific longitudinal steel reinforcement.

- It is not possible to collect specific technical details for the deck. It is assumed with reference to [1], that the longitudinal connection in the deck structure is equivalent to six steel beams of square section $(0.6m)$. The beams are placed as shown in Figure 8.6. Considering a design yelding tension for the steel of 320 MPa, the limit bending moment for the transversal displacement of the deck is 700000 KNm.

Table 8.2 reports a summary of these limit values.

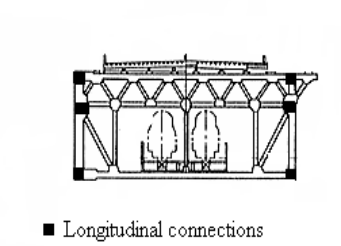

Figure 8.6: Longitudinal steel beams locations

Main cable tension limit	540000 KN
Suspender tension limit	20000 KN
Transversal shear, tower base	160000 KN
Transversal bending moment, tower base	900000 KNm
Transversal bending moment, deck	700000 KNm

Table 8.2: Limit values adopted in the structural verifications

8.3.3 Static analysis

The uncontrolled model is initially implemented in a linear static analysis with the mass density of structural materials. The resulting displacements field could be used to correct the nodes positions in the overall bridge model: the nodes vertical coordinate is lifted up to the same vertical displacement resulting from the analysis. With this procedure the configuration of the bridge coincides with the design problem and includes also the initial stress state induced by the mass density.

In Table 8.3 the tension in some bridge cables evaluated in different positions along the main span is reported. They are far from their limit values. The shear and the bending moment checks are omitted because they are not influenced by the static load.

Position	**Static tension in the main cable** $[KN]$	**Static tension in the suspender** $[KN]$
Near the tower	46000	704
Quarter-span	24000	950
Mid-span	497	780

Table 8.3: Static tension in the cables

8.3.4 Modal analysis

Usually, the bridge structures show usually low natural frequencies in its first mode of vibration. For this particular bridge model, it was necessary to tune the stiffness parameters in order to move the structure toward a real behaviour. A modal analysis has been performed and the elastic Young modulus of the shells the main girder is composed of is tuned to the value reported in Table 8.1. Actually this elastic modulus is compatible with the longitudinal steel connection guessed for the deck (see Figure 8.6).
With this introduction the bridge presents a frequency of $0.1017Hz$ and a period of $9.83sec$ in the mode shape excited by the transversal horizontal wind action. Figure 8.7 depicts the deformed shape of the bridge.

As a matter of fact the model for the extraction of the natural frequencies is set by fixing down the mass density of the cables to zero. This procedure has been adopted in order to exclude the cables mode shapes which are numerous and could distort or over-charge the calculus. The mode shape extraction is performed by the Lanczos method [4].

8.4 Transient analysis in large displacements

The geometry of the bridge and the boundary conditions suggest to perform the transient analyses with the time history of Figure 8.4 in large displace-

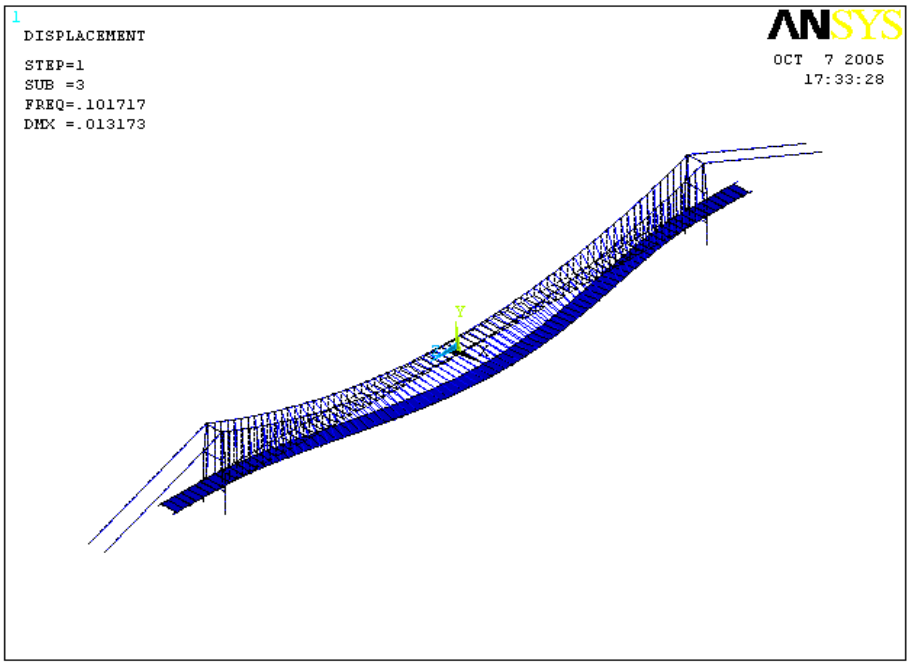

Figure 8.7: Bridge natural mode shape in transversal horizontal direction, deformed and undeformed

ments establishing the equilibrium on the deformed shape. It means that the relation between displacements and strains in the structure is not linear and the solution is determined by numerical iterations with a tangent stiffness method (Newton Rapson) [7] [8].

The first runs on the finite element model show low values of the structural response in terms of displacements. In particular, the horizontally transversal displacements in the mid span are restricted to 1-2 m. In order to push the bridge's horizontally transversal displacements towards more significant values and to assess the structure in extremely heavy conditions, a series of back-analyses have been performed. The displacements were eventually set

in the bridge mid span, 4-9 m, by means of a 2.5 multiplier of the original wind signal [9].

8.4.1 Control schemes implemented

This control matter concerns certain previously presented issues with regard to the cable-stayed bridge. Attention is focused on the reliability and robustness of the control solutions, on the reduction of computational efforts and on the simplification of data transmission connections [10] [11].
Passive control strategies have been implemented herein for the protection of the suspended bridge model and compared with the uncontrolled ones. Figures 8.8 and 8.9 depict the control devices typologies applied on the bridge structure. The former simulate a bumper device, the latter a bumper with a damper contribute.
Due to the implemented control schemes, the deck is free to translate longitudinally with respect to its axis and it is limited to move by bumper devices within ± 1.5 m. The dynamic forces have been applied in the transversal direction; the control devices have been located between the towers and the deck and have been simulated with different characteristics, summarized in Table 8.4. The bumper device have been simulated by a linear element

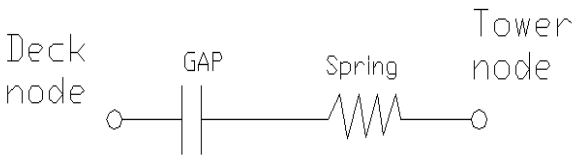

Figure 8.8: Control device with gap and spring

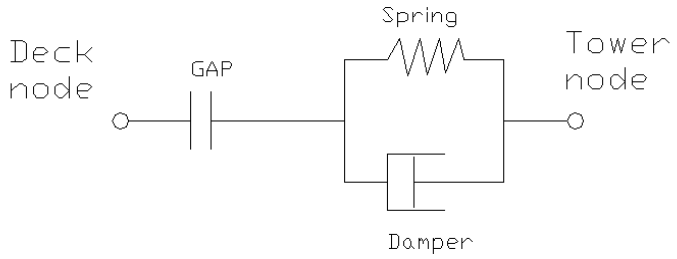

Figure 8.9: Transversal control device with gap, spring and damper

Name	**Gap** $[m]$	**Spring** $[KN/m]$	**Damper**
GAPlargeDAMPED	1	15000	0.15
GAPmediumDAMPED	0.5	15000	0.15
GAPlargeUNDAMPED	1	25000	-

Table 8.4: Devices connecting deck and towers, characteristics

available in the element library of the finite element code [4] connecting one node on the deck and another node on the tower, directly. This element is *contac*52. It is able to simulate the contact between two surfaces and simulate a spring, as well.

For the damped bumpers, it was necessary to couple two linear elements: *contac*52, with a rigid spring, and, in a series, the linear element *combin*14 which simulates a spring and a damper in parallel. A frame structure is built to combine these two elements (see Figure 8.10).

8.4.2 Comparison between different solutions and structural verifications

Several simulations were performed on the bridge model in different configurations in order to analyse its response under the wind signal. Only

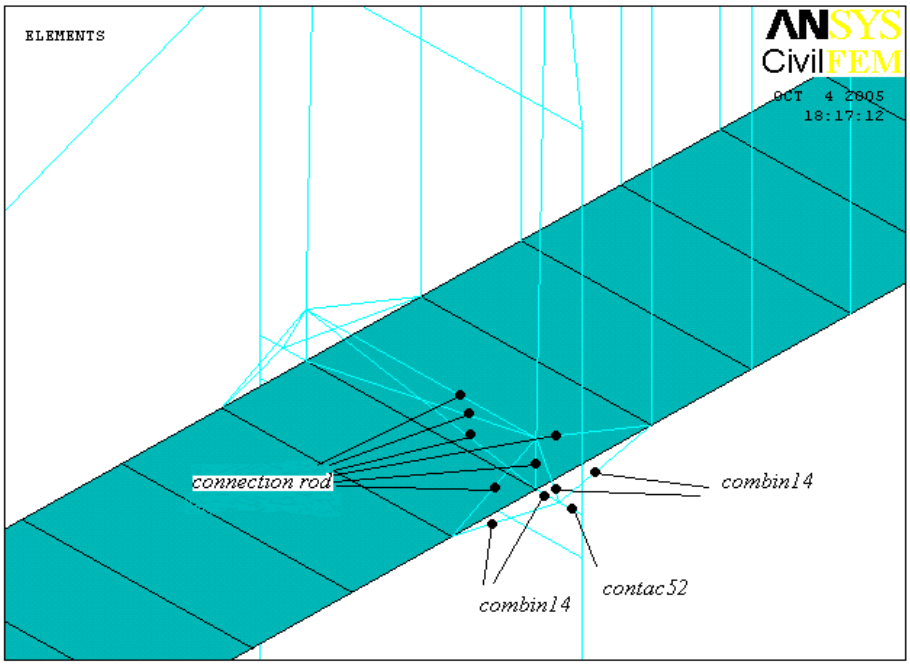

Figure 8.10: Micro-structure on the deck to couple linear elements *contac*52 and *combin*14

the most significant have been presented herein. The values of the internal actions are always far from the limit values in Table 8.2.

Some pictures not only summarise the results but also compare the responses of the uncontrolled configuration (rigid link) and the three selected control schemes to the transversal passive devices in Table 8.4. As previously mentioned, the controlled models always see bumpers in the longitudinal direction at the deck extremities with gap 1.5 m.

Figure 8.11 shows the positive effects of the control devices in reducing the bending moment in the deck structure near the tower positions. The damping contribution in the devices increases the positive effects. The bending

moment is reduced also in the mid-span (see Figure 8.12). The sign of the bending moment in the controlled cases has been inverted because the curvature is opposite, as one can see in the last figures of this chapter.

Figures 8.13 and 8.14 reports the curves for the tower base bending mo-

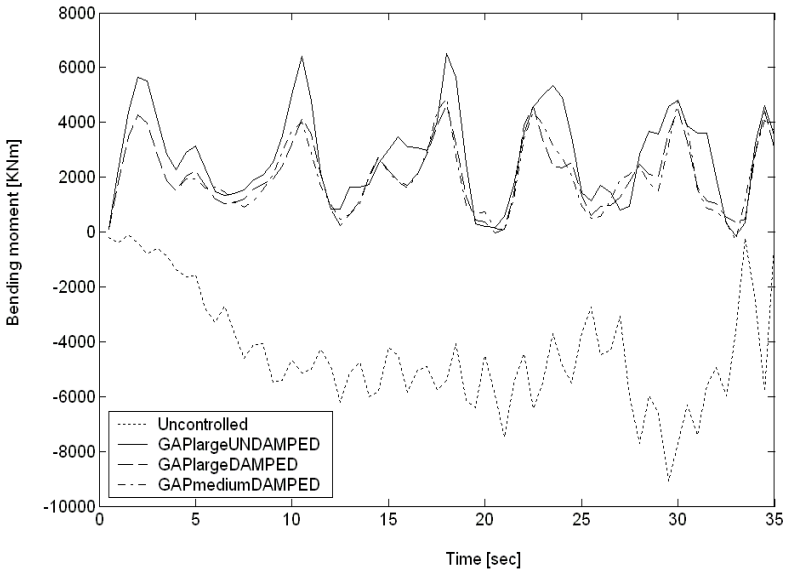

Figure 8.11: Bending moment in the deck plane near to the tower

ment in the plane transversal to the deck axis and the shear force transversal to the deck axis. The moments remain at similar levels for the controlled and uncontrolled models; the shears appear sensibly reduced by the control devices. The best responses are influenced by the gap presence.

The transient in the tension forces of the cables is reported in the pictures below. Moreover Figures 8.15 and 8.16 consider the forces in the suspenders near the towers and in the mid-span, respectively. With rigid links, the suspenders forces near the tower are around zero. For the controlled case, they appear to be similar. In the mid-span, the controlled solutions show effects

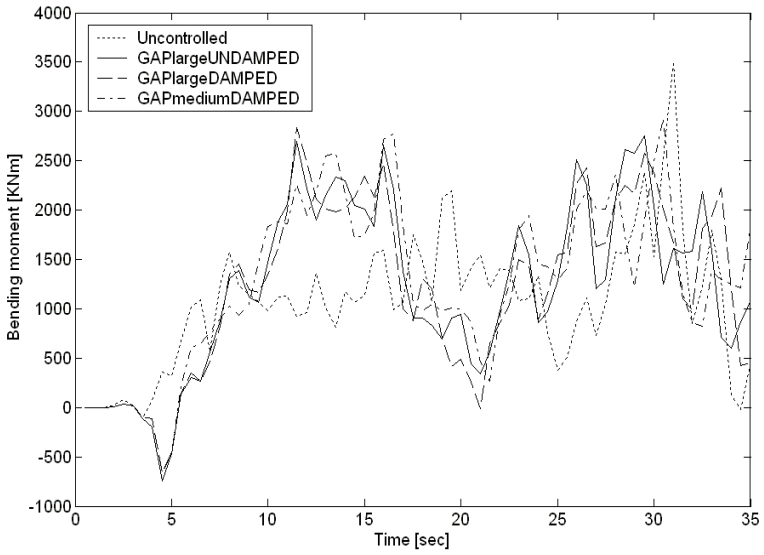

Figure 8.12: Bending moment in the deck plane on the mid-span

close to the uncontrolled. An amplification is reported in the last 10 seconds of the signal for the device with gap 0.5 m.

Figure 8.17 reports the main cable tension forces in its most stressed position, near the tower. In this case the presence of rigid links for the uncontrolled case reduce the tension in the cable.

Figure 8.18 reports the deck transversal displacements on the mid-span. They have been increased for the controlled solutions but they remain within the acceptable range for a flexible structure. Figure 8.19 depicts the transversal displacements of the deck near the tower, the effects of the gap on the control devices and the contribution of the spring and the damper (when in function).

Finally Figures 8.20 and 8.21 give the top view of the deformed shape of the bridge under the wind load. The effect of the control device has been

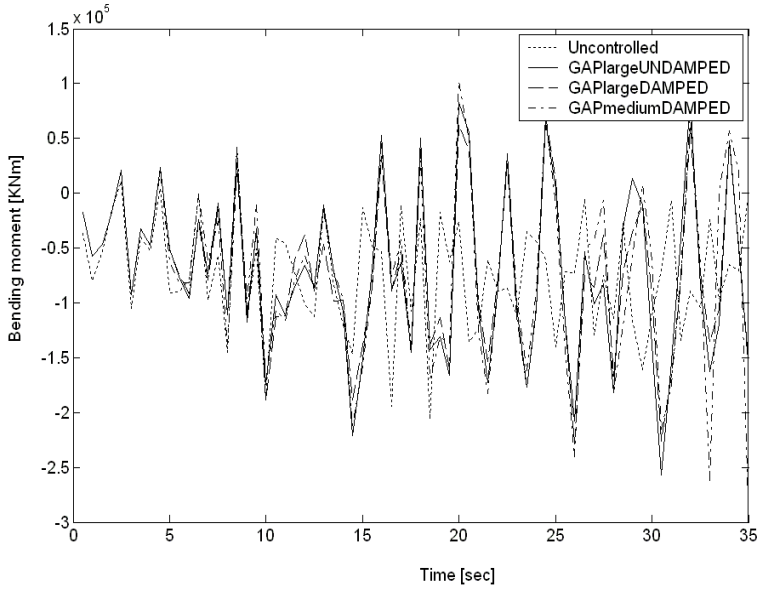

Figure 8.13: Tower base bending moment in the plane transversal to the deck axis

represented in a different structural scheme of the bridge. It appears to be more regular in its curvature for the controlled cases, with a positive effect on the crossing traffic.

8.5 Summary of Chapter 8

In this chapter passive control solutions have been applied on a long span suspended bridge in order to mitigate the dynamic effects of the wind load. Several strategies have been compared with each other and with the uncontrolled configuration. The performance of different solutions results similar, but the positive contributions of the damping arises from several factors. The controlled configurations of the bridge result more effective than the uncontrolled ones, in particular for the wind effects on the deck, but also

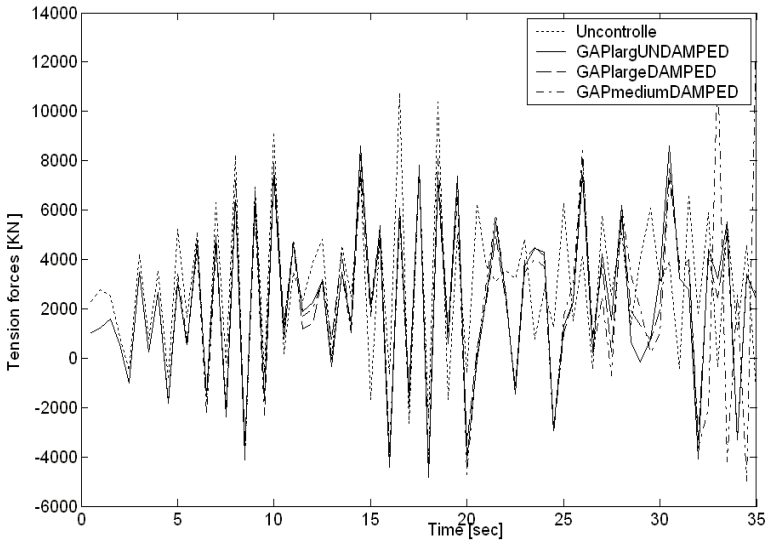

Figure 8.14: Shear force in the tower base transversal to the deck axis

on the shear forces at the tower base. The internal actions are always far from their design limit values.

Notation

All symbols used in this chapter have been defined chronologically, as they appear in the text.

p_m	mean value of wind pressure
G	gust coefficient for the wind pressure peak value

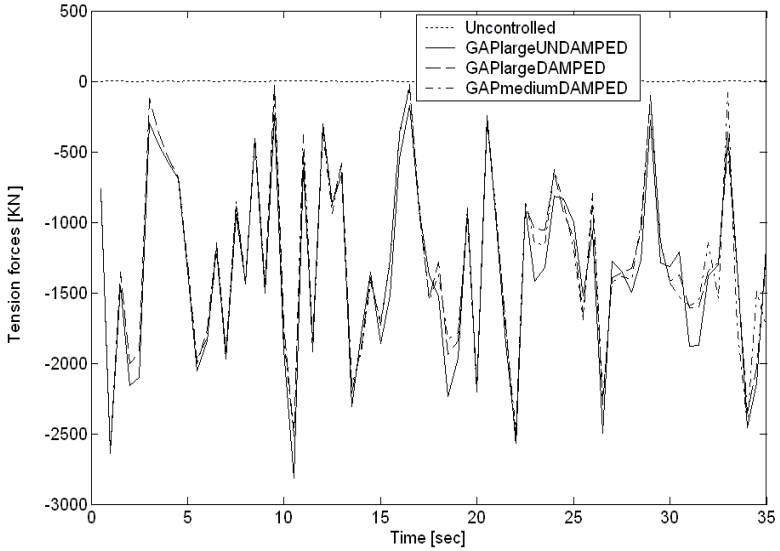

Figure 8.15: Tension force in the suspender near to the tower

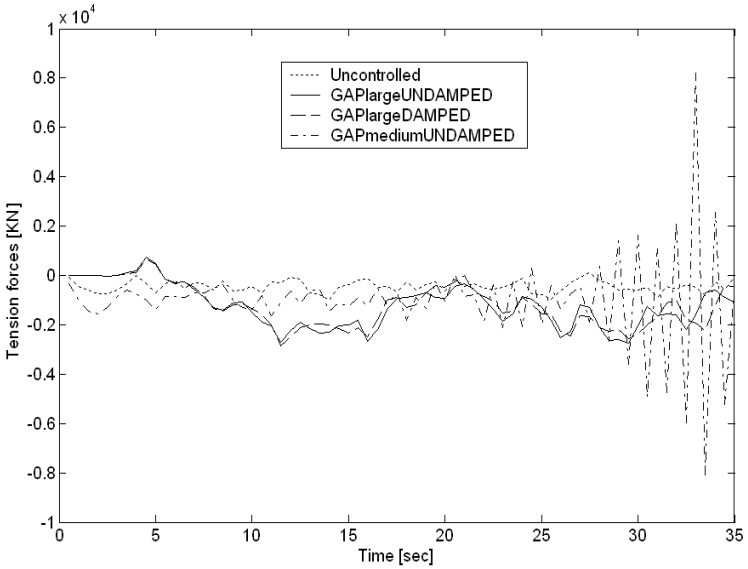

Figure 8.16: Tension force in the suspender in the mid-span

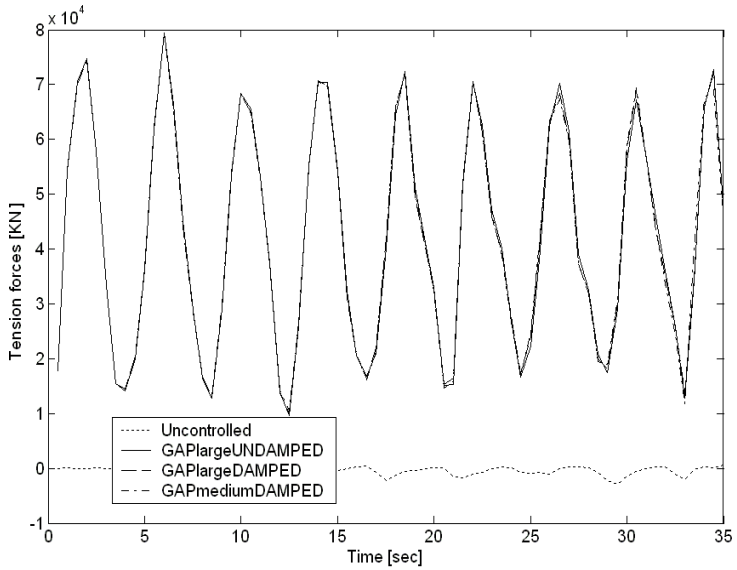

Figure 8.17: Tension force in the main cable near to the tower

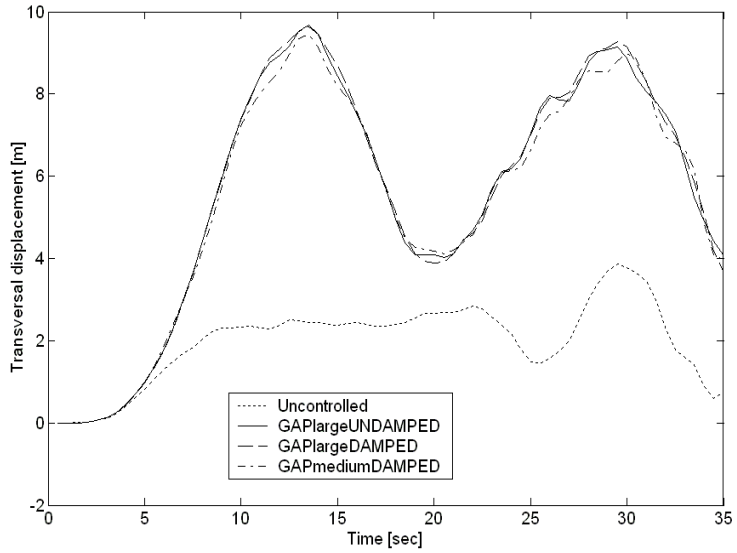

Figure 8.18: Horizontal displacement of the deck in the mid-span transversal to the deck axis

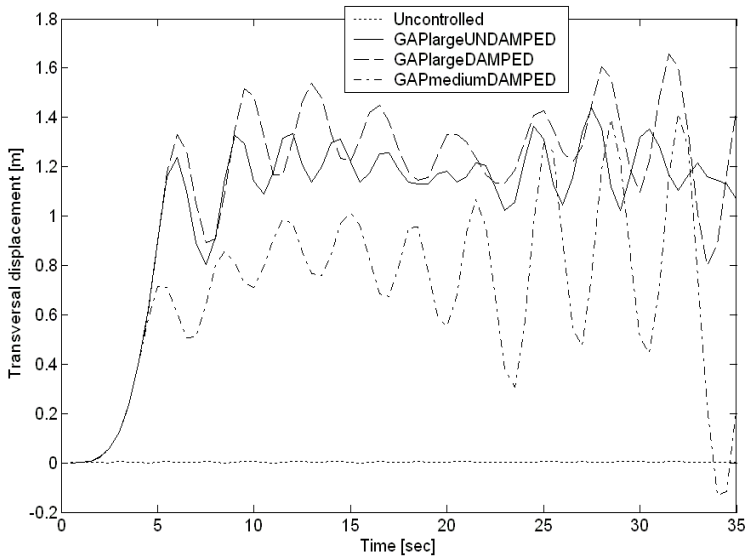

Figure 8.19: Horizontal displacement of the deck near the tower transversal to the deck axis

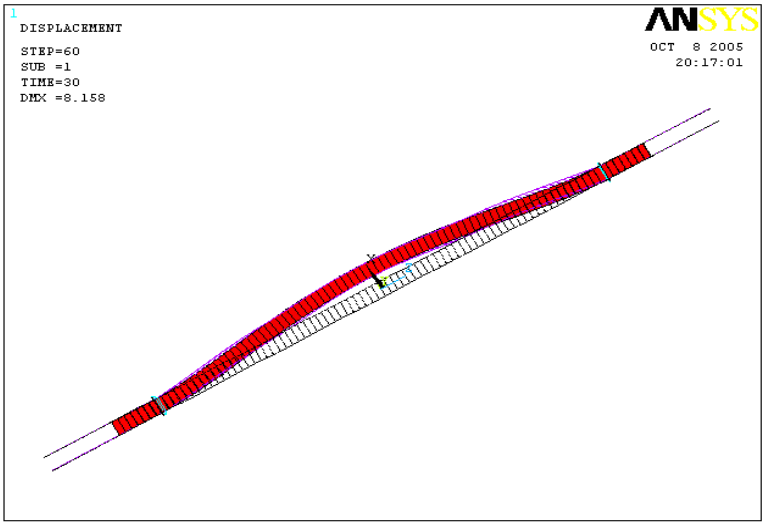

Figure 8.20: Top wiew of the deformed shape of the bridge with rigid links

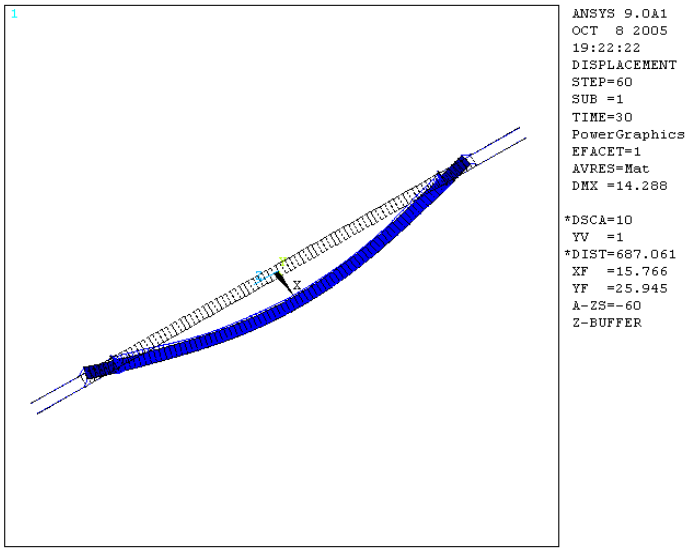

Figure 8.21: Top wiew of the deformed shape of the bridge with control a device (GAP=1m)

Bibliography

[1] Kitagawa M., 2004
Technology of the Akashi Kaikyo Bridge,
Structural Control and Health Monitoring, Vol. 11, pp. 75-90.

[2] Ostenfeld K. H., 2004
The Storebelt East Bridge,
Structural Control and Health Monitoring, Vol. 11, pp. 125-139.

[3] http://www.hsba.go.jp/bridge/e-simotu.htm, 2005.

[4] *ANSYS and CivilFEM 9.0 User Manual*, 2005
ANSYS Inc, USA. CivilFEM Ingeciber s.a., Madrid, Spain.

[5] CNR - 10012, 1985
Instructions for the evaluation of the external actions on structures (in Italian),
Italian Research National Council.

[6] Eurocode No. 2, 1992
Design of Concrete Structures,
ENV 1992-1-1.

[7] Bontempi F., 2000
Metodi computazionali per l'analisi non lineare di strutture in CA e CAP,
Lectures notes (in Italian), April-July, 2000, Structural Mechanics Dept., University of Pavia.

[8] Giudici M., 2003
Progettazione in regime non lineare di strutture in CAP a cavi aderenti e non aderenti,
Ph.D. Thesis (in Italian), Structural Mechanics Dept., University of Pavia.

[9] Cimellaro G.P., Casciati F., Domaneschi M., 2005
Fragility of a benchmark problem,
Proc. of The Tenth International Conference on Civil, Structural and Environmental Engineering Computing, B.H.V. Topping, (Ed.), Civil-Comp press, Stirling, United Kingdom, paper 241, 2005.

[10] Wong K.Y., 2004
Instrumentation and health monitoring of cable-supported bridges,
Structural Control and Health Monitoring, Vol. 11, pp. 91-124.

[11] Bergmann D., Starossek U., 2004
Numerical-experimental simulation of active flutter control for bridges,
Structural Control and Health Monitoring, Vol. 11, pp. 141-156.

Chapter 9

Conclusions

This document deals with control systems of cable supported bridges. In each of the solutions offered herein, robustness and simplicity are given priority. Accordingly, emphasis is put on passive and semi-active control systems and a decentralized control solution is investigated.

Furthermore, when it comes to the cable-stayed bridge benchmark, two kinds of dynamic loads are taken into consideration, namely the seismic and the wind effects. This study provided useful elements which were subsequently applied in the analysis of the impact of wind on the suspension bridge structure.

The possibility of simulating control solutions for large structures by means of commercially available and accessible finite element codes is also worth promoting. This should facilitate structural control as a regular activity in civil engineering, and pave the path towards further innovations in structural design.

Appendix A

Laplace transforms

A.1 Introduction

The definition of the Laplace transform is achieved by the expression:

$$F(s) = L[f(t)] = \int_0^\infty f(t)e^{-st}dt \tag{A.1}$$

where $f(t)$ is any function of the independent variable t (usually denoting the time). $F(s)$ is function of the Laplace variable s [1] [2].

Conventionally one marks the original function of time with a lower case letter, while the function in the s-domain is shown by the same letter in upper case. The transform starts at $t = 0$.

For example, the transform $f(t)$ of the step function jumping to the value $A = 5$ at time $t = 0sec$ can be evaluated as

$$F(s) = \int_0^\infty f(t)e^{-st}dt = \int_0^\infty 5e^{-st}dt = -\frac{5}{s}e^{-st}|_0^\infty = \frac{5}{s} \tag{A.2}$$

The first order derivative transform is

$$G(s) = L[g(t)] = L[\frac{d}{dt}f(t)] = \int_0^\infty (d/dt)f(t)e^{-st}dt \tag{A.3}$$

$$g(t) = df(t)/dt \tag{A.4}$$

by integration by parts and going backward, one introduces the relation

$$\int_a^b udv = uv|_a^b - \int_a^b vdu \tag{A.5}$$

Then with $u = f(t)$, and $v = e^{-st}$, one writes

$$L[\frac{d}{dt}f(t)] = -f(0) + sL[f(t)] \tag{A.6}$$

In systems initially undeflected and at rest, the Laplace variable s can directly replace the d/dt (or D) operator in differential equations.

$$D = s \tag{A.7}$$

with $s = \sigma + j\omega$ and j the imaginary unit. It is a superset of the phasor representation in that it has both a complex part, for the steady state response, but also a real part, representing the transient part.
If the real part is neglected the frequency response is provided and the system is characterized not in its transient but as stabilized. The Laplace variable s is related to the rate of change in the system.
Table A.1, A.2, A.3 provide the most popular transforms and the related relations.

A.2 Applying Laplace transforms

The process of applying Laplace transforms to analyze a linear system involves the basic steps listed below [1] [2].

- Convert the system transfer function, or differential equation, to the s-domain by replacing D with s (note: If any of the initial conditions are non-zero these must be also added).

Time domain	**Frequency domain**
$f(t)$	$f(s)$
$Kf(t)$	$KL[f(t)]$
$f_1(t) + f_2(t) + f_3(t) + ..$	$f_1(s) + f_2(s) + f_3(s) + ..$
$\frac{df(t)}{dt}$	$sL[f(t)] - f(0^-)$
$\frac{d^2f(t)}{dt^2}$	$s^2L[f(t)] - sf(0^-) - \frac{df(0^-)}{dt}$
$\frac{d^nf(t)}{dt^n}$	$s^nL[f(t)] - s^{n-1}f(0^-) - s^{n-2}\frac{df(0^-)}{dt} - ... - \frac{d^{n-1}f(0^-)}{dt^n}$
$\int_0^t f(t)\ \mathrm{dt}$	$\frac{L[f(t)]}{s}$
$f(t-a)u(t-a), a > 0$	$e^{-as}L[f(t)]$
$e^{-at}f(t)$	$f(s-a)$
$f(at), a > 0$	$\frac{1}{a}f(\frac{s}{a})$
$tf(t)$	$-\frac{df(s)}{ds}$
$t^nf(t)$	$(-1)\frac{nd^nf(s)}{ds^n}$
$\frac{f(t)}{t}$	$\int_s^\infty f(u)du$

Table A.1: Laplace transform table

- Convert the input function(s) to the s-domain using the transform tables.
- Algebraically combine the input and transfer function to find an output function.
- Use partial fractions to reduce the output function to simpler components.
- Convert the output equation back to the time-domain using the tables.

A.3 Applications of the tables

Some examples clarify the application of the tables presented above.

Time domain	**Frequency domain**
$\delta(t)$ unit impulse	1
A step	$\frac{A}{s}$
t ramp	$\frac{1}{s^2}$
t^2	$\frac{2}{s^3}$
$t^n, n > 0$	$\frac{n!}{s^{n+1}}$
e^{-at} exponential decay	$\frac{1}{s+a}$
$sin(\omega t)$	$\frac{\omega}{s^2+\omega^2}$
$cos(\omega t)$	$\frac{s}{s^2+\omega^2}$
te^{-at}	$\frac{1}{(s+a)^2}$
t^2e^{-at}	$\frac{2!}{(s+a)^3}$

Table A.2: Laplace transform table

Time domain	**Frequency domain**
$e^{-at}sin(\omega t)$	$\frac{\omega}{(s+a)^2+\omega^2}$
$e^{-at}cos(\omega t)$	$\frac{s+a}{(s+a)^2+\omega^2}$
$e^{-at}sin(\omega t)$	$\frac{\omega}{(s+a)^2+\omega^2}$
$e^{-at}[Bcos\omega t + (\frac{C-aB}{\omega})sin(\omega t)]$	$\frac{Bs+C}{(s+a)^2+\omega^2}$
$2\|A\|e^{-at}cos(\beta t + \theta)$	$\frac{A}{s+\alpha-\beta j} + \frac{A^{c.conjugate}}{s+\alpha+\beta j}$
$2t\|A\|e^{-at}cos(\beta t + \theta)$	$\frac{A}{(s+\alpha-\beta j)^2} + \frac{A^{c.conjugate}}{(s+\alpha+\beta j)^2}$
$\frac{(c-a)e^{-at}-(c-b)e^{-bt}}{b-a}$	$\frac{s+c}{(s+a)(s+b)}$
$\frac{e^{-at}-e^{-bt}}{b-a}$	$\frac{1}{(s+a)(s+b)}$

Table A.3: Laplace transform table

- A differential equation is converted to the s-domain as follows

$$L[\ddot{x} + 7\dot{x} + 8x = 9] = [s^2 + 7s + 8 = \frac{9}{s}] \tag{A.8}$$

  If the initial conditions are non-zero, say $\ddot{x}(0) = 1$, $\dot{x}(0) = 2$, $x(0) = 3$, they must be added. So eq. A.9 results

$$L[\ddot{x} + 7\dot{x} + 8x = 9] = [s^2 + 7s + 8 - 39 = \frac{9}{s}] \tag{A.9}$$

- The equation

$$f(t) = 5sin(5t + 8) = 5cos8sen5t + 5sen8cos5t \tag{A.10}$$

  is converted from the time to the s-domain by writing

$$L[f(t)] = 5cos8\frac{5}{s^2 + 25} + 5sen8\frac{s}{s^2 + 25} \tag{A.11}$$

- going from the s-domain to the time domain, the function

$$F(s) = \frac{5}{s} + \frac{6}{s + 7} \tag{A.12}$$

  can be processed into

$$f(t) = 5 + 6e^{-7t} \tag{A.13}$$

A.4 Modelling the transfer function in the s-domain

The transfer functions of mechanical and electrical systems can be converted to the s-domain, as shown in the following mass-spring-damper example depicted in Figure A.1. In this case one assumes that the system starts undeflected and at rest, so that the D operator may be directly replaced with the Laplace s. If the system did not start at rest and undeflected, the

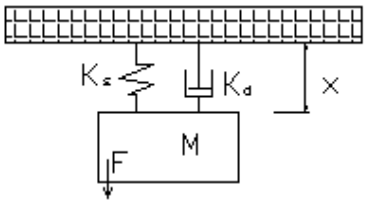

Figure A.1: Mass-spring-damper system

D operator would be replaced with an expression which includes the initial conditions.

$$f = MD^2x + K_dDx + K_sx \tag{A.14}$$

$$\frac{f(t)}{x(t)} = MD^2 + K_dD + K_s \tag{A.15}$$

$$L[\frac{f(t)}{x(t)}] = \frac{F(s)}{X(s)} = Ms^2 + K_ds + K_s \tag{A.16}$$

In the equations above the operator D is simply replaced with s. Indeed it is only valid if the initial conditions are zero, otherwise the following more complex form must be used

$$L[\frac{d^nf(t)}{dt^n}] = s^nL[f(t)] - s^{n-1}f(0^-) - s^{n-2}\frac{df(0^-)}{dt} - ... - \frac{d^nf(0^-)}{dt^n} \tag{A.17}$$

A.5 Finding the output equation

The input to a system is normally expressed as a function of time which can be converted to the s-domain. As an example of this conversion, consider a step function jumping to the value A starting at time $t = 0$ sec is

$$f(t) = 0, t < 0 \tag{A.18}$$

$$f(t) = A, t > 0 \tag{A.19}$$

therefore

$$F(s) = L[f(t)] = \frac{A}{s} \tag{A.20}$$

In the previous section a differential equation, modelling phisical systems, was converted into a transfer function in the s-domain. It is the ratio of the output divided by the input. If the transfer function is multiplied by the input function, both in the s-domain, the result is the system output in the s-domain.

Output functions have complex forms that are not found directly in the transform tables. It is often necessary to simplify the output function before it can be converted back to the time domain. The *partial fraction methods* allow the functions to be broken into smaller, simpler components. The following example shows how to use the partial fraction expansion: the roots of the third order denominator polynomial are first calculated: they provide three partial fraction terms. The residues (numerators) of the partial fraction terms must still be calculated. It is generally done by multiplying the output function by a root term, and then finding the limit of the product as s approaches the root.

Given,

$$\frac{X(s)}{F(s)} = \frac{1}{Ms^2 + K_d s + K_s} \tag{A.21}$$

$$F(s) = \frac{A}{s} \tag{A.22}$$

the output is

$$X(s) = (\frac{X(s)}{F(s)})F(s) = (\frac{1}{Ms^2 + K_d s + K_s})\frac{A}{s} \tag{A.23}$$

Assume, $K_d = 3000Ns/m$, $K_s = 2000N/s$, $M = 1000Kg$, $A = 1000N$: eq. A.23 becomes

$$X(s) = \frac{1}{(s^2+3s+2)s} \tag{A.24}$$

The values of the parameters A, B, C in the following equation are required in order to reduce the function in a simpler form and to convert it back to the time domain

$$X(s) = (\frac{1}{(s^2+3s+2)s}) = \frac{1}{(s+1)(s+2)s} = \frac{A}{s} + \frac{B}{s+1} + \frac{C}{s+2} \tag{A.25}$$

$$A = \lim_{s\to 0}[s(\frac{1}{(s+1)(s+2)s})] = \frac{1}{2} \tag{A.26}$$

$$B = \lim_{s\to -1}[(s+1)(\frac{1}{(s+1)(s+2)s})] = -1 \tag{A.27}$$

$$C = \lim_{s\to -2}[(s+2)(\frac{1}{(s+1)(s+2)s})] = \frac{1}{2} \tag{A.28}$$

The output has now the following simpler form

$$X(s) = (\frac{1}{(s^2+3s+2)s}) = \frac{0.5}{s} + \frac{-1}{s+1} + \frac{0.5}{s+2} \tag{A.29}$$

After simplification with the partial fraction expansion method, the output function is easily converted back to a function of time as shown below

$$x(t) = L^{-1}[X(s)] = L^{-1}[\frac{0.5}{s} + \frac{-1}{s+1} + \frac{0.5}{s+2}] \tag{A.30}$$

$$x(t) = L^{-1}[\frac{0.5}{s}] + L^{-1}[\frac{-1}{s+1}] + L^{-1}[\frac{0.5}{s+2}] \tag{A.31}$$

$$x(t) = [0.5] + [(-1)e^{-t}] + [(0.5)e^{-2t}] \tag{A.32}$$

$$x(t) = 0.5 - e^{-t} + 0.5e^{-2t} \tag{A.33}$$

A.6 Inverse transforms and partial fractions

The flowchart in Figure A.2 shows the general procedure for converting a function from the s-domain to a function of time. In some cases the function is simple enough to immediately use a transfer function table. Otherwise, the partial fraction expansion is used to reduce the complexity of the function. Figure A.3 shows the basic procedure for the partial fraction expan-

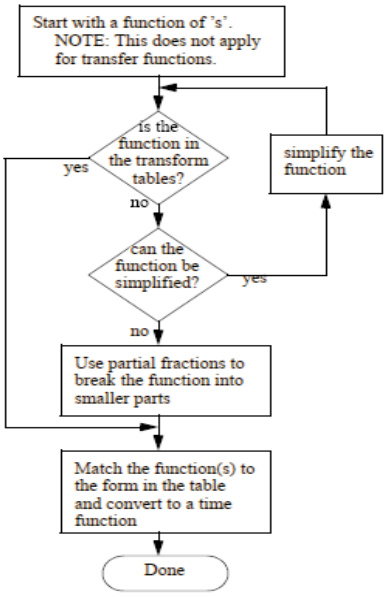

Figure A.2: The methodology for doing an inverse transform of an output function

sion. In the cases where the order of the numerator is greater than the one of the denominator, the overall order of the expression can be reduced by a long division. After this the denominator can be reduced from a polynomial to a product of roots. Calculators or computers are normally used when the order of the polynomial is greater than two. An example in which the order

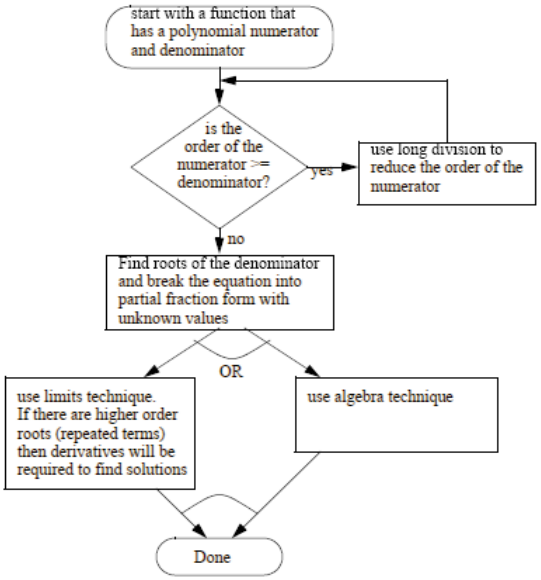

Figure A.3: The methodology for doing an inverse transform of an output function

of the numerator is greater than the one of the denominator is presented below. A long division of the numerator is used to reduce the order of the term until it is low enough to apply partial fraction techniques. It must be noted, however, that this type of output function occurs in systems with extremely fast response rates that are infeasible in practice:

$$X(s) = \frac{5s^3 + 3s^2 + 8s + 6}{s^2 + 4} \tag{A.34}$$

It can not be solved using partial fractions because the numerator is of the 3rd order and the denominator is only of order 2. Therefore a long division can be used to reduce the order of the equation and write it as a new function that has a reduced portion that can be solved with partial

fractions. So eq. A.34 it is reduced in

$$x(s) = 5s + 3 + \frac{-12s - 6}{s^2 + 4} \tag{A.35}$$

and the partial fraction method can be applied to

$$\frac{-12s - 6}{s^2 + 4} \tag{A.36}$$

A.7 Mass-spring-damper vibration: example

A mass-spring-damper system with sinusoidal input is written by its transfer function

$$\frac{X(s)}{F(s)} = \frac{\frac{1}{M}}{s^2 + \frac{K_d}{M}s + \frac{K_s}{M}} \tag{A.37}$$

The parameters values are assigned as $M = 1Kg$, $K_s = 2N/m$, $K_d = 0.5Ns/m$. The sinusoidal input is converted to the s-domain, from

$$f(t) = 5cos(6t) \tag{A.38}$$

to

$$F(s) = \frac{5s}{s^2 + 36} \tag{A.39}$$

This can be combined with the transfer function to obtain the output function,

$$X(s) = F(s)(\frac{X(s)}{F(s)}) = (\frac{5s}{s^2 + 36})(\frac{1}{s^2 + 0.5s + 2}) \tag{A.40}$$

$$X(s) = \frac{5s}{(s^2 + 36)(s^2 + 0.5s + 2)} \tag{A.41}$$

$$X(s) = \frac{A}{s + 6j} + \frac{B}{s - 6j} + \frac{C}{s - 0.25 + 1.39j} + \frac{D}{s - 0.25 - 1.39j} \tag{A.42}$$

The residues for the partial fraction are calculated and converted to a function of time. In this case the roots of the denominator are complex, so the result has a sinusoidal component.

$$A = \lim_{s \to -6j} [\frac{(s+6j)(5s)}{(s-6j)(s+6j)(s^2+0.5s+2)}] = \frac{-30j}{(-12j)(36-3j+2)} \tag{A.43}$$

One finds then B, C and D by the same way: the output function in s-domain is simplified and the result can be converted in function of time.

A.8 Further topics

A.8.1 Input functions

In some cases a system input function consists of many different functions, as shown in Figure A.4.

The step function can be used to switch function on and off to create a

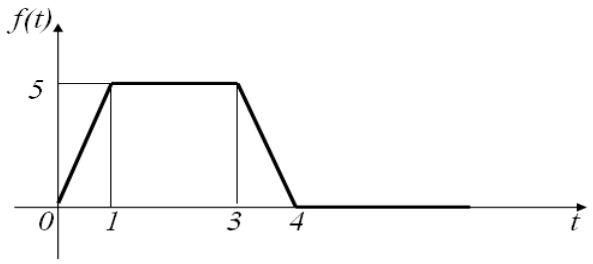

Figure A.4: System input function comprised of many different functions

piecewise function. This is converted by the Laplace transform tables to the s-domain as follow

$$f(t) = 5tu(t) - 5(t-1)u(t-1) - 5(t-3)u(t-3) + 5(t-4)u(t-4) \tag{A.44}$$

$$F(s) = \frac{5}{s^2} - \frac{5e^{-s}}{s^2} - \frac{5e^{-3s}}{s^2} + \frac{5e^{-4s}}{s^2} \tag{A.45}$$

A.8.2 Initial and final value Theorems

The initial and final values an output function can be calculated using the following theorems *Final Value Theorem*

$$x(t \to \infty) = \lim_{s \to 0}[sX(s)] \tag{A.46}$$

Initial Value Theorem

$$x(t \to 0) = \lim_{s \to \infty}[sX(s)] \tag{A.47}$$

A.9 A map of techniques for Laplace analysis

Figure A.5 presents a map to be used to generally identify the use of the various topics covered in this Appendix

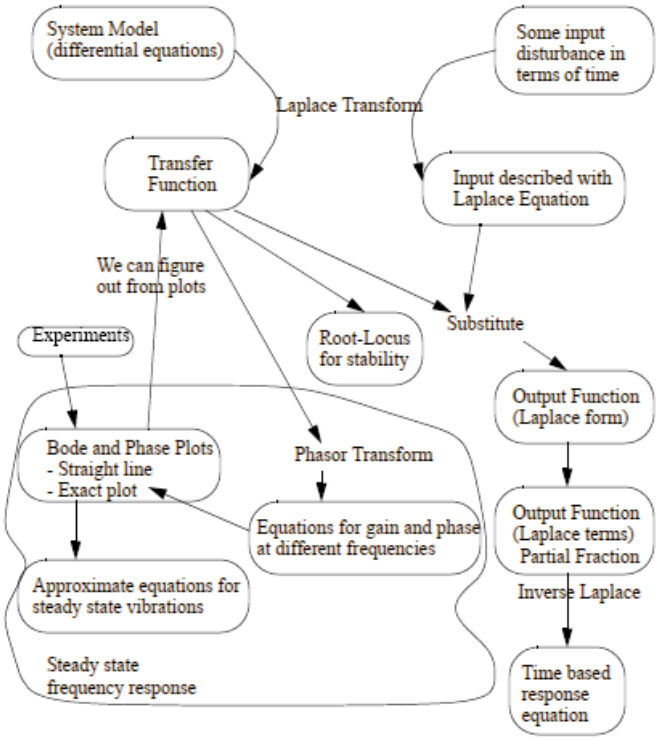

Figure A.5: A map of Laplace analysis technique

Bibliography

[1] Irwin J.D., Graf E.R., 1979
Industrial Noise and Vibration Control",
Prentice Hall Pubblishers.

[2] Close C.M., Frederick D.K., 1995
Modeling and Analysis of Dynamic Systems, second edition
John Wiley and Sons, Inc.

Appendix B

Cable-Stayed Bridge Benchmark Statement

B.1 Introduction

The cable-stayed Emerson Memorial Bridge in Cape Girardeau, Missouri (USA), opened to the road traffic on December 13, 2003 [1] [2]. It was selected as Bridge Benchmark Problem.

From an initial Phase I of the Bridge Benchmark Problem, a new Phase II was established. Although a significant amount of expertises was accumulated during Phase I, the assumptions made regarding the excitation (acting longitudinally and simultaneously) limited the extent to which Phase I modelled a realistic situation. The main characteristic in Phase II of the bridge Benchmark is the bi-directional nature of the seismic excitation. For sake of completeness, a better comprehension, the different aspects of the global model are detailed in next session.

B.1.1 Bridge mechanic characteristics

The mechanical characteristics and the complex behaviour of the full-scale benchmark bridge are simulated [1] [2] by a three-dimensional *evaluation model*.
At the design stage of the Bill Emerson Memorial Bridge, various solutions were considered including full longitudinal restraints at the tower piers, no longitudinal restraints and passive isolation. When the temperature effects were considered, it was found that fully restraining the deck in the longitudinal direction would result in unacceptably large stresses. Based on examination of various designs, it was determined that incorporating force transfer devices would provide the most efficient solution. So the *builted structure* contains the following solutions:

- sixteen 6.67 MN shock transmission devices are employed in the connection between the towers and the deck. These devices are installed in the longitudinal direction to allow for the expansion of the deck due to temperature changes. Under the dynamic load these devices are extremely stiff and are assumed to behave as a rigid link.

- In the transverse direction earthquake restrainers are employed at the connection between the tower and the deck.

- The deck is constrained in the vertical direction at the towers.

- The bearing at Bent 1 and Pier 4, see Figure B.1, are designed to permit the deck the longitudinal displacement and the rotations about the vertical and transversal axes.

The global geometry of the bridge can also be completed describing some other structural elements. The bridge is composed by:

- two towers
- 128 cables
- An approach bridge on 11 piers and Bent 15.
- The total length of the Emerson Memorial Bridge and his approach is 1205.8 m. The bridge approach is 570 m. The main span is 350.6 m, the side spans 142.7 m.
- A cross section of the deck is reported in Figure B.2. The bridge has four lanes plus two narrower bicycle lanes, for a total width of 29.3 m. The deck is composed of steel beams and prestressed concrete slabs. A concrete longitudinal barrier is located in the center of the transversal bridge sections, and a railing is located along the edges of the deck.
- The H shaped towers have the height of 102.4 m at Pier 2 and 108.5 m at Pier 3. Each tower supports a total of 64 cables. The towers are constructed in reinforced concrete, the cross section of each tower varies five times along the height of the tower, as shown in Figure B.3. Section A is used at the top of the legs, Section B in the middle of the legs, and Section E at the bottom of the towers. Some of these elements have variable sections. Section D shows the cross section in the bottom strut, and Section C shows the cross section of the strut located in the middle of the tower.

- The material quantitative details are reported in [1][2].

B.1.2 Load inputs

The external loads acting on the bridge are of different nature: the seismic load, with dynamic influence on the structural skeleton, and the snow load introduced with the aim of investigating the robustness of the control systems proposed. The structural response is determined under the simultaneous action of the three translational components of the ground motion, two in the horizontal plane and one in the vertical direction. The structural response depends on the incidence angle (the angle between the ground motion components and the structural axes). Additionally, the excitation is expected to vary at each of the supports due to the length of the structure. The distance between the supports of the bridge suggests to consider the noncontemporary incidence of the seismic action on all the connections ground-bridge, by introducing a time delay. Phase II was developed to extend the problem to consider such issues.

This Bridge Benchmark Problem furnishes a model where the ground acceleration may be applied in any arbitrary direction using the two horizontal components of historical earthquakes with a specific incidence angle.

Multi-support excitation is also considered in Phase II of the Bridge Benchmark. The prescribed ground motion is assumed to be identical at each support, although it is not applied simultaneously. It is assumed that a support undergoes a specific ground motion, and the motion at the other three supports is identical to this motion but delayed proportionally to the distance between adjacent supports, divided by the speed of the Love-wave of a typical earthquake (nearly 3 Km/sec). The total response of the struc-

ture is obtained by superposition of the responses due to each independent support input [3].

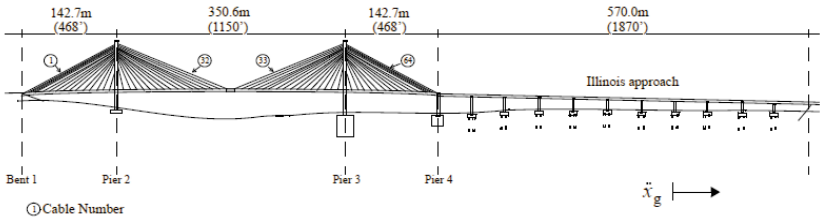

Figure B.1: Bridge Emerson Memorial Bridge

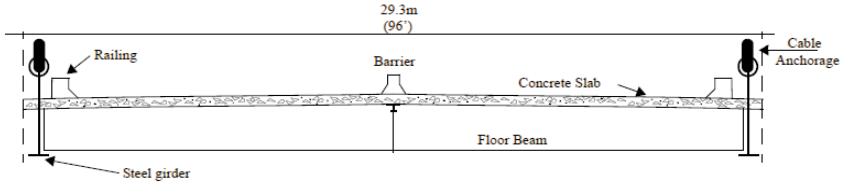

Figure B.2: Transversal section of the bridge deck

B.1.3 Soil characteristics

Writing about the ground and the seismic action, a main aspect concerns the potential amplification due to the soil. In the benchmark problem it is not considered because no layered soil was found and so the bridge is regarded as connected directly on the bedrock [1] [2].

B.2 Evaluation model

In this section some characteristics of the evaluation model are provided. The evaluation model represents the tool used to develop different design

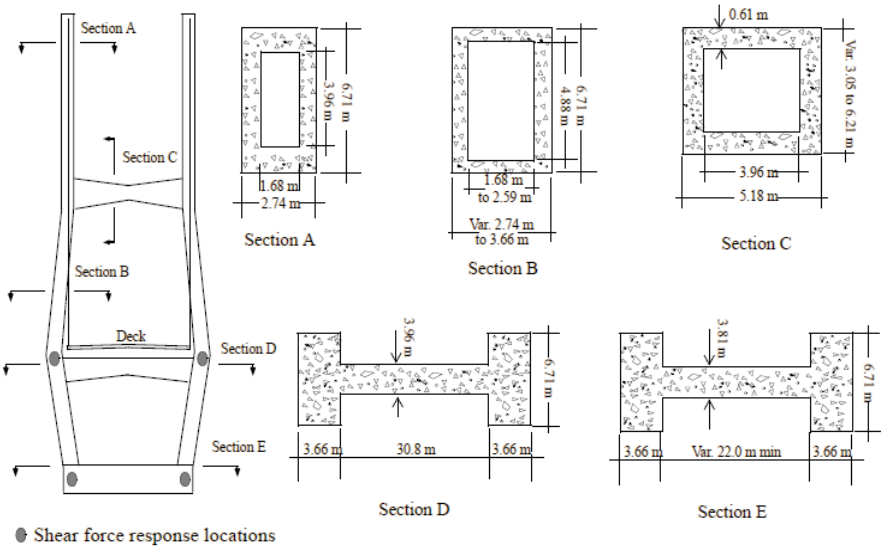

Figure B.3: Cross section of the towers

models. It starts from a finite element method discretization of the real structure. A three dimensional finite element model of the bridge is developed in Matlab [4]. A linear evaluation model is used in the Benchmark study, however, the stiffness matrices used in this linear model are those of the structure determined through *a non-linear static analysis corresponding to the deformed state of the bridge with dead loads* [1] [2].

The finite element model employs beam elements, cable elements and rigid links. The non-linear static analysis is performed in Abaqus [5], and the element mass and stiffness matrices are exported to Matlab for assembly. Then, the constraints are applied, and a reduction is performed to reduce the size of the model to something more manageable. The reduced model finally consists in 419 d.o.f.

To make possible to place control devices between the deck and the tow-

ers the connections are disconnected. The user must define devices at this nodes (between deck and towers).
The nodes deck-towers are not the only ones available for placing the control devices. Note also that the uncontrolled structure used as a basis of comparison for the controlled system, corresponds to the model in which the deck-towers connections are fixed (it does not mean that the node on the towers and on the deck are coincident but that the dynamically stiff shock transmission devices between these nodes are present with their mechanical characteristics).

B.2.1 Finite element model description

The finite element model (fem) is drawn in Figure B.4. It consists of 579 nodes, 420 rigid links, 162 beam elements, 134 nodal masses and 128 cables elements. The towers are modelled using 50 nodes, 43 beam elements and 74 rigid links. Some other details define the fem model:

- constraints applied to Piers 2, 3, 4 to restrict the deck from lateral movements.

- At Pier 1, some boundary conditions restrict the motion to allow only the longitudinal displacement (x) and the rotations about the axes y and z.

- Rigid links (see FigureB.5) are used to connect the cables to the tower and to the deck. The anchorage points are above the neutral axes of towers and deck. So the length and the inclination angle of the cables in the model agree with the design drawings and the cross section of

the deck is infinitely rigid. It is a current hypotesis in the flexible bridge analysis.

- The moment produced in the towers by the the movement of the cables is considered.
- The average value of variable sections is used in the finite element model.
- The cables are modelled by truss elements and the nominal tension is assigned to each cable.

A suitable use of the model is performed considering some items:

- The fem model described above is used directly in cases when the control devices are employed in the longitudinal direction between the deck and the tower. The control devices can be also placed in the transversal direction and not only as a connection between the deck and the towers.

- If the users employ no control devices in longitudinal direction between the deck and the towers, the shock-transmission devices are included and the model is modified by four longitudinally-directed, axially-stiff beam elements that force the deck to move with the tower in the longitudinal direction. The uncontrolled structure used as a basis of comparison corresponds to this last case.

- The program included with the benchmark files detects whether or not the user has placed devices in the longitudinal direction (between

towers and deck), and builds the appropriate model.

The Illinois approach (Figure B.1) is not included in this model (see Figure B.1) because the bearing at Pier 4 does not restrict longitudinal motion and rotation about the x axis of the bridge, the Illinois approach was found to have a negligible effect on the dynamics of the cable-stayed portion of the bridge [1] [2].

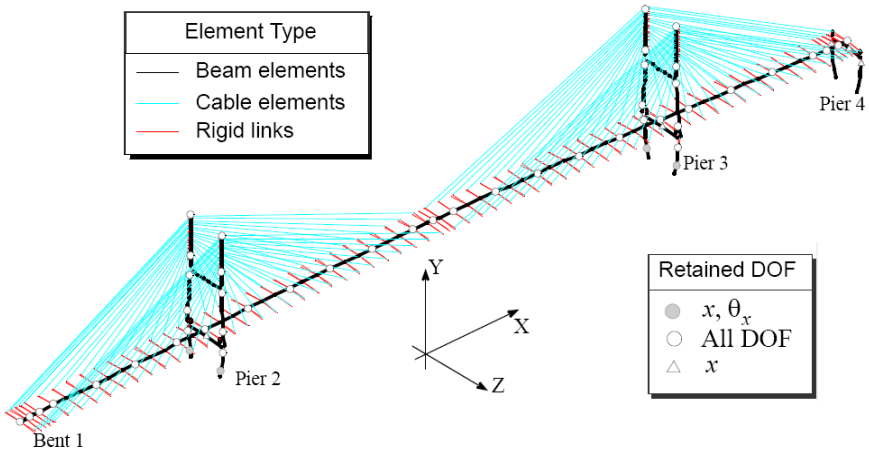

Figure B.4: Finite element model of the benchmark problem

B.2.2 Non linear static analysis

Cable-stayed bridges exhibit nonlinear behaviour due to:

- variations of the catenary shape of the inclined cables
- cable tensions that induce compression forces in the deck and towers
- large displacements

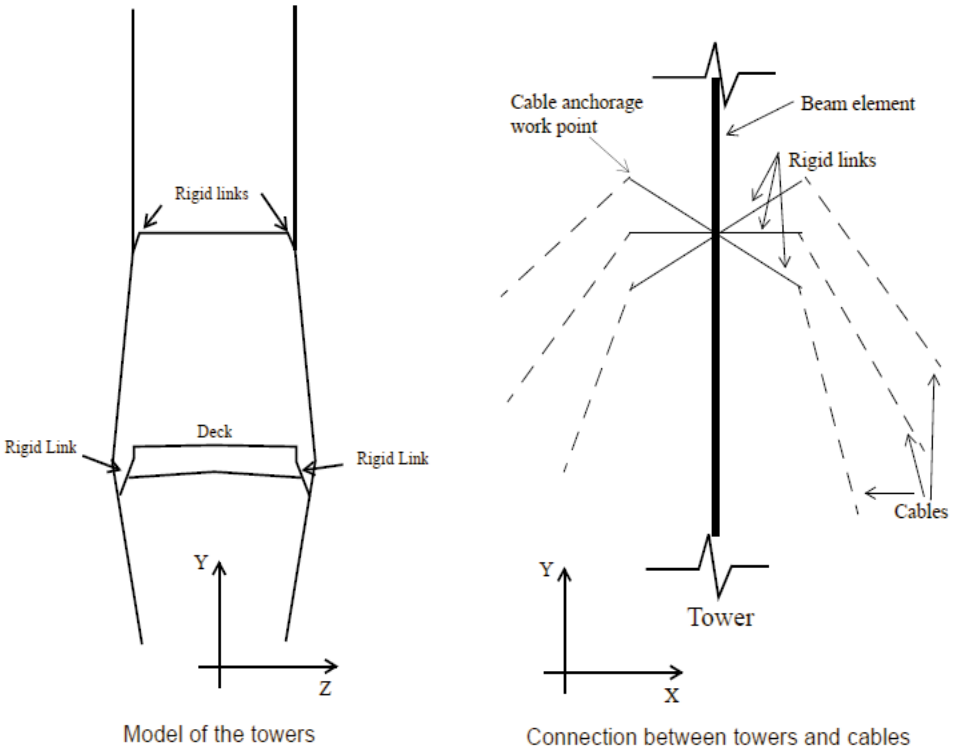

Figure B.5: Tower model

A nonlinear static analysis was performed using the commercial finite element program Abaqus [5], giving the model the tangent stiffness matrix at the deformed equilibrium position.

In modeling the cables, the catenary shape and its variation with the axial force in the cable are modelled using an equivalent elastic modulus [1] [2]. The cable element is a large-displacement truss element that has a modified modulus of elasticity, E_{eq}, given by

$$E_{eq} = \frac{E_c}{1 + [\frac{(wL_x)^2 A_c E_c}{12T_c^3}]} \tag{B.1}$$

where A_c is area of the cross-section, T_c is the tension in the cable, w is its unit weight, L_x is the projected length in the $X-Z$ plane, and E_c is the modulus of elasticity of the material. The cable stiffness contribution to the global stiffness matrix is only applied when the cable is under tension and is omitted otherwise. The cable elements are modelled as truss elements in Abaqus, and their equivalent elastic module are used in the nonlinear static analysis.

The deck was modelled using the method described in [6] [1] [2], i.e., as a central beam, the spine, which has no mass. Lumped masses are employed to model the mass of the deck, which are connected to the spine using rigid links (see Figure B.6). The masses are included toward a more realistic modelling of the torsional response of the deck to lateral loads.

The deck is made of two main steel girders along each longitudinal edge of the deck supporting the concrete slab (see Figure B.2). Thus, the deck is treated as a C-shaped section as shown in Figure B.7 [6][1] [2]. Here the steel beams represents the flanges of the section, and the concrete slab represents the web of the C-shaped section. The axial stiffness of the deck is calculated by converting the area of the concrete slab into an equivalent area of steel using the ratio of the two elastic module. The area of the equivalent section is 1.844 m^2. The moments of inertia about the vertical and transverse axes are also obtained converting the concrete slab to an equivalent steel structure. The barriers and railings were not taken into consideration because they are not structural elements. The inertia of the typical deck section has values I_{yy}=160.67 m^4, I_{zz}=0.6077m^4. The neutral axis is located at 1.77 m above the bottom of the steel beams.

The calculation of the torsional stiffness of the deck section takes into con-

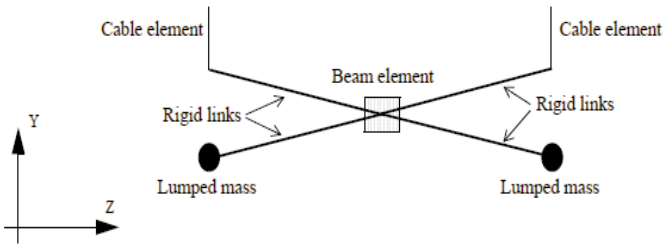

Figure B.6: Cross section of the deck in the f.e.m. model

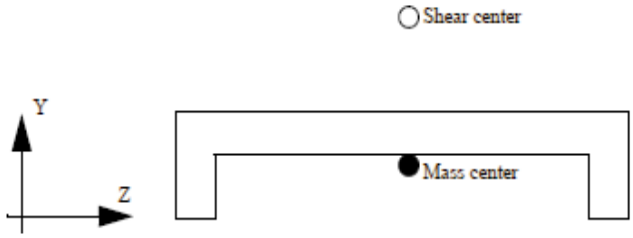

Figure B.7: C-Shape section modelling of the deck

sideration both pure and warping torsional constants. The pure torsion constant is determined by [6]

$$J_t = \sum_{i=1}^{n} \frac{b_i t_i^3}{3} \tag{B.2}$$

where b_i and t_i are the length and thickness of the rectangles forming the deck cross-section. The warping constant is calculated as [7]

$$\Gamma_w = \frac{d^2}{4}\{I_{zz} + e^2 A(1 - \frac{d^2 A}{4I_{yy}})\} \tag{B.3}$$

where d is the distance between the webs of the two steel beams located along the edges of the deck, e is the distance between the neutral axis and the middle of the concrete slab, and A is the equivalent cross sectional area. I_{yy} and I_{zz} are the moments of inertia of the deck about the Y and Z axes,

as determined previously. The torsional stiffness of the deck was obtained using the formula [6]

$$G_s J_{eq} = G_s[J + \frac{E_s \Gamma_w \pi^2}{G_s L^2}] \tag{B.4}$$

where G_s is the steel shear modulus of elasticity, J_{eq} is the equivalent torsional constant, J is the pure torsion constant, E_s is the modulus of elasticity of steel, and L is the length of the main span. So J_{eq} results 0.0677 m^4.
The calculation of the mass of the deck accounts for the steel beams, the rigid concrete slab, the barriers and the railings. The total mass of the deck per unit length was determined to be 2,645.7 kg/m. To preserve the behaviour of the C-shaped section, the deck is represented as two lumped masses, each having a mass equal to half of the total mass of the deck. The masses are joined to the beam element by a rigid link as shown in Figure B.6. The vertical distance between the lumped mass and the center of the beam is equal to the distance between the shear center and the mass center of the C-shaped section shown in Figure B.7.
Because the mass moment of inertia of the main deck is different from the one induced by the lumped masses, it is necessary to connect those quantities. In the calculation, the correction consists in finding the difference between the moment of inertia of the lumped masses and that of the actual deck section. This difference in the mass moment of inertia is added to the node at the center of the deck to achieve the correct value of mass moment of inertia in the section model. The mass moment of inertia of the lumped masses with respect to the j-th axis (either the X, Y, or Z axis), I_j, is calculated using the formula

$$I_j = 2M_l r^2 \tag{B.5}$$

where M_l is the mass of each lumped mass, and r is the perpendicular distance from the mass to each axis. The actual mass moment of inertia of the deck with respect to the j-th axis, I_{mj}, is calculated using the equation

$$I_{mj} = \sum_{i=1}^{n} (I_{mi} + m_i r_i^2) \tag{B.6}$$

where I_{mi} is the mass moment of inertia of each of the component of the deck with respect to its own centroidal axis, m_i is the mass of each component, and r_i is the perpendicular distance between the centroid of each component and the jth axis. Thus, the corrected mass moment of inertia of the section becomes

$$\Delta_j = I_{mj} - I_j \tag{B.7}$$

The value of this parameter about each axis for a typical section of the deck are Δ_X=-4.43 10^6 kgm^2, Δ_Y=-4.45 10^6 kgm^2, Δ_Z=18.3 10^3 kgm^2. Negative values indicate that the contribution of the lumped masses to the mass moment of inertia of the section is larger than the mass moment of inertia of the actual section. Thus, to achieve the correct mass moment of inertia for the section, a negative value is assigned to the spine to balance the larger value included by the lumped masses when the rigid links are condensed out [1] [2].

B.3 Control and monitoring properties

The control devices and the sensors can be placed in the bridge model. For example dissipation devices can be placed between the deck and the piers connecting two nodes. Everywhere devices can be placed connecting different couples of nodes. The effect of these connections is to introduce forces

directly on the nodes.

The sensors can measure different physical parameters (displacement, velocities, accelerations,.. see also Appendix C) and they too can be placed everywhere on the bridge model, for example on the towers or along the deck. This model scheme allows to the user to implement a large variety of control schemes [1] [2].

To evaluate the proposed control strategies, appropriate evaluation criteria and control design constraints are specified within the problem statement. The Benchmark user must define sensors, devices and algorithms to be used in the control strategy. In Figure B.8 the flow scheme is reproduced.

The sensors must be defined to measure the output of the evaluation

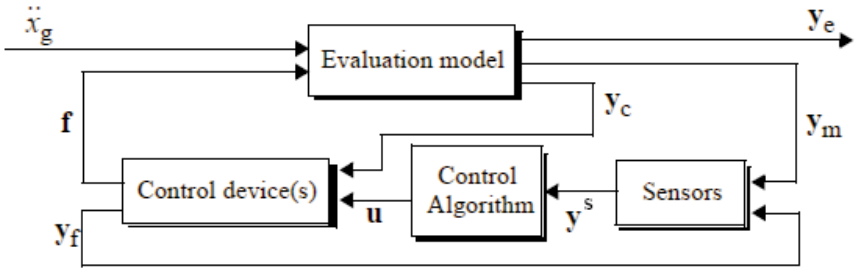

Figure B.8: Flow scheme representation of the model

model y_m. Bridge Benchmark users must develop models for the sensors which take the following form

$$\dot{x}^s = g_1(x^s, y_m, y_f, t) \tag{B.8}$$

$$y^s = g_2(x^s, y_m, y_f, t) \tag{B.9}$$

where x^s is the continuous-time state vector of the sensors and y_s is the continuous-time output of the sensors in volts [V]. y_f is the continuous-

time output vector from the control device model, which may include forces produced by individual control devices, device stroke or device acceleration. It is used for the evaluation of the control strategy and is available for feedback in the control algorithm.

Passive, active, and semi-active control devices (or combinations of them) may be used in designing control systems. For active/semi-active control systems, the associated discrete-time control algorithm must take the form

$$x_{k+1}^c = g_3(x_k^c, y_k^s, k) \tag{B.10}$$

$$u^k = g_4(x_k^c, y_k^s, k) \tag{B.11}$$

where x_k^c is the discrete-time state vector of the control algorithm at each sampling time $t = k\Delta t$, y_k^s is the discrete-time input to the control algorithm from the sensors (which should be discretized in time and quantized to represent an A/D converter), and u_k is the discrete-time control command from the control algorithm.

Dynamic models of the control devices selected by the user are not required for this benchmark study. Ideal control devices may be assumed. Note that the program allows the user to place control devices at constrained nodes although errors will result in the simulated responses. To interface with the benchmark bridge model the control device models must take the form

$$f = g_5(y_c, u_k, t) \tag{B.12}$$

$$y_f = g_6(y_c, u_k, t) \tag{B.13}$$

where y_c contains the continuous-time responses from the evaluation model that influence the control forces, and f is the continuous-time force output

[kN] of the control devices applied to the structure. Researchers/designers who choose to employ dynamic models of their control devices should use the form

$$\dot{x}^d = g_7(x^d, y_c, u_k, t) \tag{B.14}$$

$$f = g_8(x^d, y_c, u_k, t) \tag{B.15}$$

$$y_f = g_9(x^d, y_c, u_k, t) \tag{B.16}$$

where x^d is the continuous-time state vector of the control device.

B.4 Evaluation criteria

For cable-stayed bridges subjected to external dynamic loading, critical responses are related to the structural integrity of the bridge. Thus, in evaluating the performance of each control strategy developed, the shear forces and moments in the towers at key locations must be considered. Additionally, the tension in the cables should never approach zero, and should remain close to the nominal pretension.

A set of eighteen criteria have been developed to evaluate the capabilities of each control strategy. Because the earthquake is assumed to have two horizontal components at a specified incidence angle, several of these criteria are evaluated in both the x (longitudinal) and z (transverse) directions. The first six evaluation criteria consider the ability of the controller to reduce peak responses, the second five criteria consider normed responses over the entire time record, and the last seven criteria consider the requirements of the control system itself.

The first two evaluation criteria are non-dimensionalized measures of the

shear force at key locations in the towers. The elevation of these key locations correspond to the tower base and the deck level. The latter criterion was selected because this elevation corresponds to a drastic reduction in the cross-sectional area of the towers. Evaluation criteria one and two are given by

$$J_1 = max[\frac{max_{i,t}|F_{bi}(t)|}{F_{0b}^{max}}] \tag{B.17}$$

$$J_2 = max[\frac{max_{i,t}|F_{di}(t)|}{F_{0d}^{max}}] \tag{B.18}$$

where $F_{bi}(t)$ is the base shear at the ith tower, $F_{0b}^{max} = max_{i,t}|F_{0bi}(t)|$ is the maximum uncontrolled base shear (of the values at the two towers), $F_{di}(t)$ is the shear at the deck level in the ith tower, $F_{0d}^{max} = max_{i,t}|F_{0di}(t)|$ is the maximum uncontrolled shear at the deck level, and $|.|$ indicates absolute value. The values of F_{0b}^{max}, F_{0d}^{max}, and all other values used to normalize the evaluation criteria, are provided in [1].

The second set of evaluation criterion are non-dimensionalized measures of the moments in the towers at the same key locations, given by

$$J_3 = max[\frac{max_{i,t}|M_{bi}(t)|}{M_{0b}^{max}}] \tag{B.19}$$

$$J_4 = max[\frac{max_{i,t}|M_{di}(t)|}{M_{0d}^{max}}] \tag{B.20}$$

where $M_{bi}(t)$ is the moment at the base of the ith tower, the maximum uncontrolled moment at the base of the two towers is $M_{0b}^{max} = max_{i,t}|M_{0bi}(t)|$, $M_{di}(t)$ is the moment at the deck level in the ith tower, and $M_{0d}^{max} = max_{i,t}|M_{0di}(t)|$ is the maximum uncontrolled moment at the deck level in the two towers.

The fifth evaluation criterion is a non-dimensionalized measure of the deviation of the tension in the stay cables from the nominal pretension, given

by

$$J_5 = max[max_{i,t}\frac{|T_{ai}(t) - T_{0i}|/T_{0i}}{T_{0c}^{max}}] \tag{B.21}$$

where T_{0i} is the nominal pretension in the ith cable, $T_{ai}(t)$ is the actual tension in the cable as a function of time, and $T_{0c}^{max} = max_{i,t}(|T_{a0i}(t) - T_{0i}|/T_{0i})$ is the normalized actual cable tension of the uncontrolled system. This criterion is selected to reduce the likelihood of failure or unseating of the cables.

The sixth evaluation criterion is a measure of the peak deck displacement at piers 1 and 4.

$$J_6 = max[max_{i,t}|\frac{x_{bi}(t)}{x_{0b}}|] \tag{B.22}$$

where x_{bi} is the displacement of the bridge deck at the ith location and x_{0b} is the maximum of the uncontrolled deck response at these locations. This criterion is included to consider the likelihood of impact of the deck at these locations.

The seventh and eighth evaluation criteria are non-dimensionalized measures of the normed values of the base shear and shear at the deck level in each of the towers, respectively, given by

$$J_7 = max[\frac{max_i||F_{bi}(t)||}{||F_{0b}(t)||}] \tag{B.23}$$

$$J_8 = max[\frac{max_i||F_{di}(t)||}{||F_{0d}(t)||}] \tag{B.24}$$

where $||F_{0b}(t)||$ is the maximum of the normed value of the uncontrolled base shear of the two towers, and $||F_{0d}(t)||$ is the maximum of the normed value of the uncontrolled shear at the deck level of the tower. The normed value of the response, denoted $||.||$, is defined as

$$||.|| = \sqrt{\frac{1}{t}\int_0^{t_f}(.)^2 dt} \tag{B.25}$$

where t_f is defined as the time required for the response to attenuate.

The ninth and tenth evaluation criteria are non-dimensionalized measures of the normed values of the overturning moment and moment at the deck level in each of the towers, respectively, given by

$$J_9 = max[\frac{max_i||M_{bi}(t)||}{||M_{0b}(t)||}] \tag{B.26}$$

$$J_{10} = max[\frac{max_i||M_{di}(t)||}{||M_{0d}(t)||}] \tag{B.27}$$

where $||M_{0b}(t)||$ is the maximum of the normed value of the uncontrolled moment at the base of the two towers, and $||M_{0d}(t)||$ is the maximum of the normed value of the uncontrolled moment at the deck level of the two towers.

The eleventh evaluation criterion is a non-dimensionalized measure of the normed value of the deviation of the tension in the stay cables from the nominal pretension, given by

$$J_{11} = max[max_{i,t}\frac{||T_{ai}(t) - T_{0i}||/T_{0i}}{||T_{0c}||}] \tag{B.28}$$

where T_{0i} is the existing pretension in the ith cable, $T_{ai}(t)$ is the actual tension in the ith cable as a function of time, and $||T_{0c}|| = max_{i,t}(||T_{a0i}(t) - T_{0i}||/T_{0i})$ is the maximum of the normed value of the actual cable tension for the uncontrolled system.

The twelfth evaluation criterion deals with the maximum force generated by the control device(s) and is described as

$$J_{12} = max[max_{i,t}(\frac{f_i(t)}{W})] \tag{B.29}$$

where $f_i(t)$ is the force generated by the ith control device over the time history of each earthquake, and $W = 510000KN$ is the seismic weight of

bridge based on the mass of the superstructure (not including the foundation).

The thirteenth criterion is based on the maximum stroke of the control device(s). This performance measure is given as

$$J_{13} = max[max_{i,t}(\frac{|y_i^d(t)|}{x_0^{max}})] \tag{B.30}$$

where $y_i^d(t)$ is the stroke of the ith control device over the time history of each earthquake, and x_0^{max} is the maximum uncontrolled displacement at the top of the towers relative to the ground. When devices are used that do not have an associated stroke (for ex. tuned liquid dampers), this evaluation constraint is zero.

The fourteenth evaluation criterion is a non-dimensionalized measure of the maximum instantaneous power required to control the bridge, and is defined as

$$J_{14} = max[\frac{[\sum_i P_i(t)]}{\dot{x}_0^{max} W}] \tag{B.31}$$

where P_i is a measure of the instantaneous power required by the ith control device, and $\dot{x}_0^{max}$ is the peak uncontrolled velocity at the top of the towers relative to the ground. Values for $\dot{x}_0^{max}$ are provided in [1] each of the earthquakes specified. For active control devices, $P_i(t) = |\dot{y}_i^d(t) f_i(t)|$, where $\dot{y}_i^d(t)$ is the velocity of the ith control device. When semi-active devices are employed, $P_i(t)$ is the actual power required to operate the device. For passive control devices, this criterion is zero.

The fifteenth evaluation criterion is a non-dimensionalized measure of the total power required to control the bridge, and is defined as

$$J_{15} = max[\frac{[\int_0^{t_f} P_i(t)dt]}{x_0^{max} W}] \tag{B.32}$$

This criterion is zero when passive device(s) are used.
The sixteenth evaluation criterion is a measure of the total number of control devices required in the control system to control the bridge.

$$J_{16} = number of control devices \tag{B.33}$$

The seventeenth evaluation criterion is a measure of the total number of sensors required for the proposed control strategy.

$$J_{17} = number of sensors \tag{B.34}$$

The final evaluation criterion provides a measure of the resources required to implement the control algorithm and is given by

$$J_{18} = dim(\mathbf{x_k^c}) \tag{B.35}$$

where $\mathbf{x_k^c}$ is the discrete-time state vector of the control algorithm.

Bibliography

[1] Caicedo J.M., Dyke S.J., Moon S.J., Bergman L., Turan G., Hague S., 2003
Phase II Benchmark Control Problem for Seismic Response of Cable Stayed Bridges
http://wusceel.cive.wustl.edu/quake/.

[2] Caicedo J.M., Dyke S.J., Moon S.J., Bergman L., Turan G., Hague S., 2003
Phase II Benchmark Control Problem for Seismic Response of Cable Stayed Bridges,
Journal of Structural Control, 10:137-168.

[3] Chopra A.K., 2001
Dynamics of Structures: Theory and Applications to Earthquake Engineering,
Prentice Hall, Upper Saddle River, New Jersey.

[4] *Matlab and Simulink*, 1997
The Mathworks Inc., Natick, MA.

[5] *ABAQUS* 1998,
Hibbitt, Karlsson and Sorensen Inc., Pawtucket, RI.

[6] Wilson J., Gravelle W., 1991
Modelling of a Cable-Stayed Bridge for Dynamic Analysis,
Earthquake Engineering and Structural Dynamics, 20:707-721.

[7] Bleich F., 1952
Buckling Strenght of Metal Structures,
Mc Graw-Hill, New York.

Appendix C

Sensors, compensators and amplifier

C.1 Introduction

Sensors, compensators and amplifier play an important role in the control system design, they are the background for an effective structural monitoring in order to perform the more powerful control strategy. Some literature [1] [2] [3] refers about the main contructive details, modelling and use of the monitoring elements commonly met in engineering applications.

C.2 Sensors

C.2.1 Measurements of relative displacements

Any electric displacement gauge, potentiometer, strain-gauge, either inductive or capacitive etc., can be used for measuring displacement of a particular point of the object relative to the base or any other point. Relative displacement results in a change in a certain parameter of the electric circuit, e.g. resistance, inductance or capacitance, which in turn changes the

output variable, say, voltage or current.

Displacement gauges are commonly used in vibration protection systems for measuring processes with relatively low frequencies. In this case, elastic deformations of the gauge component are usually negligible which allows the gauge to be viewed as a massless element with the following characteristic

$$\sigma = f(y) \tag{C.1}$$

where y is the displacement to be measured and σ is the output variable. As a rule, function $f(y)$ is linear for small y such that

$$\sigma = k_y y \tag{C.2}$$

The nonlinearity of the characteristic equation (eq. C.1) must be taken into account for significant relative displacements which are typical for resonant regimes. The dependence $\sigma(y)$ often is bounded and can not exceed fixed saturation maximum and minimum values.

C.2.2 Measurements of absolute displacements

Absolute displacements and absolute accelerations are measured by means of transducers of the seismic type. Design solutions are very different however in all cases the output electric signal depends on displacement of the "seismic mass" relative to the transducer housing, see Figure C.1, this dependence being linear for small displacements. It is easy to show that the relative displacement of the mass m_s is related to the absolute displacement of the housing as follows

$$\Delta(t) = \frac{m_s s^2}{m_s s^2 + b_s s + c_s} x(t) = \frac{T_s^2 s^2}{T_s^2 s^2 + 2\zeta_s T_s s + 1} x(t) \tag{C.3}$$

where c_s and b_s are the rigidity and the resistance factor, respectively, while T_s and ζ_s are the time constant and the damping factor, respectively,

$$T_s = \sqrt{\frac{m_s}{c_s}}, \zeta_s = \frac{b_s}{2\sqrt{c_s m_s}}, k_s = k_\sigma \frac{m_s}{c_s} \tag{C.4}$$

Therefore, the transfer function of the transducer measuring absolute displacement is given by

$$w_{sx}(s) = \frac{k_\sigma T_s^2 s^2}{T_s^2 s^2 + 2\zeta_s T_s s + 1} = \frac{k_s s^2}{T_s^2 s^2 + 2\zeta_s T_s s + 1} \tag{C.5}$$

Here k_σ denotes the proportionality coefficient between the output signal σ and the seismic mass displacement $\Delta(t)$.

For the accelerometer which measures absolute acceleration $\ddot{x}(t)$ one obtains

$$w_{s\ddot{x}}(s) = \frac{k_s}{T_s^2 s^2 + 2\zeta_s T_s s + 1} \tag{C.6}$$

Due to the properties of the resonance characteristics $|w_{sx}(i\omega)|$ and $|w_{s\ddot{x}}(i\omega)|$, a transducer measuring absolute displacement can only be used for measuring high frequency processes ($\omega > 6\pi T_s^{-1}$) while an accelerometer is used at relatively low frequencies ($\omega < 2\pi T_s^{-1}$). For this reason, accelerometers are generally used in active systems.

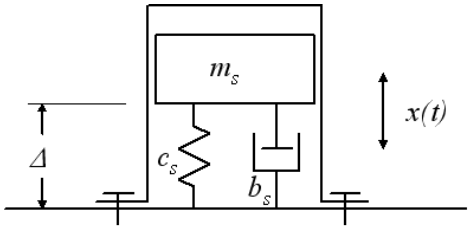

Figure C.1: Device scheme for absolute displacements measurement

C.2.3 Measurements of rotation angles

In some cases, there is the need of measuring the rotation of objects regardes as a rigid bodies.

Relative rotations can be measured indirectly, for this purpose, the relative displacements at several points of the object are measured and then divided by the distance between these points. Devices for measuring the relative displacements can be deemed as massless. For small rotation angles, one gets

$$\sigma = k_\varphi \varphi \tag{C.7}$$

For measuring absolute angles of rotation and accelerations, torsional vibration gauges are used. Their transfer functions are similar to those given by eqs. C.5 and C.6. Gyroscopic transducers, which are single-degree-of- freedom gyros with an elastic element for compensating the gyroscopic moment and a damper, are used for measuring low-frequency angles of rotation. The transfer function of these transducers may be represented in the following form

$$w_{g\theta} = \frac{k_g s}{T_g^2 s^2 + 2\zeta_g T_g s + 1} \tag{C.8}$$

where Here T_g^2 and ζ_g are the system time constant and damping factor.

$$\sigma = w_{g\theta}(s)\theta \tag{C.9}$$

with θ denoting the absolute angle of rotation. The sensitivity of the transducer is dependent on the gain k_g which is proportional to the angular velocity of the gyrowheel.

C.2.4 Measurements of forces

In order to measure the forces acting on the objects or the forces in vibrating components of the object, diverse load gauges are used. They are usually strain-gauge transducers and may be considered as being massless linear elements for which

$$w_{lF}(s) = k_F = const. \tag{C.10}$$

C.3 Compensators and amplifiers

C.3.1 Integrators and differentiators

Signals are frequently integrated and differentiated in control systems. Integration of signal proportional to relative displacement is performed for example for creating astatic systems, while differentiating is utilised for introducing damping into the system [4] [5].

Resistance and capacity (RC) circuits are used as integrators and differen-

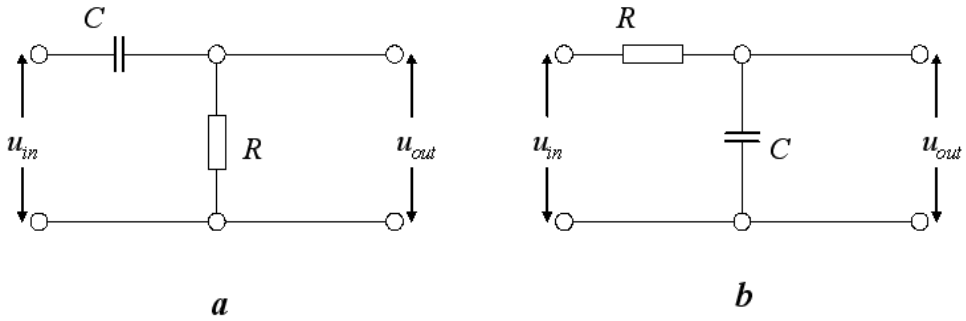

Figure C.2: Simple RC-circuits as integrator and differentiator

tiators. Figure C.2a shows a simple RC-circuit where $u_{out} = w_c(s)u_{in}$ with

the following transfer function

$$w_c(s) = \frac{R}{R + (Cs)^{-1}} = \frac{RCs}{1 + RCs} = \frac{T_c s}{1 + T_c s} \tag{C.11}$$

where $T_c = RC$ is the time constant. If the signal frequency ω satisfies the condition $T_c\omega \ll 1$, this circuit is close to being ideally integrating. Thus, RC-circuits differentiate low frequency signals.

The transfer function of the circuit in Figure C.2b is given by

$$w_c(s) = \frac{(Cs)^{-1}}{R + (Cs)^{-1}} = \frac{1}{1 + CRs} = \frac{1}{1 + T_c s} \tag{C.12}$$

If $T_c\omega \gg 1$ this circuit becomes an integrating one. It is clear that the time constant T_c of the integrator must increase with decreasing signal frequency. For this reason, when integrating very low frequency signals which is often the case in vibration protection systems, it is expedient to use electronic DC amplifiers with capacitive feedback. For large gains, this amplifier is an ideal integrator with the following transfer function

$$w_c(s) = -(T_c s)^{-1} \tag{C.13}$$

Notice that in the case of harmonic input, the phase of a differentiator output leads the input phase by $\pi/2$ whereas the phase of an integrator output lags behind the input phase by $\pi/2$. This is the reason for referring to integrators and differentiators as lead and delay circuits, respectively.

Active vibration protection systems can also utilise some mechanical devices which combine the functions of sensors and compensators. Such a mechanical facility consisting of a spring c and a linear damper b is shown in Figure C.3. Values of σ and σ_1 are related to $y(t)$ by the following expressions

$$\sigma = \frac{bs}{c + bs} y = \frac{T_c s}{1 + T_c s} y \tag{C.14}$$

$$\sigma_1 = \frac{c}{c+bs} y = \frac{1}{1+T_c s} y \tag{C.15}$$

where $T_c = b/c$. Therefore, this system can be used as a differentiator and as an integrator.

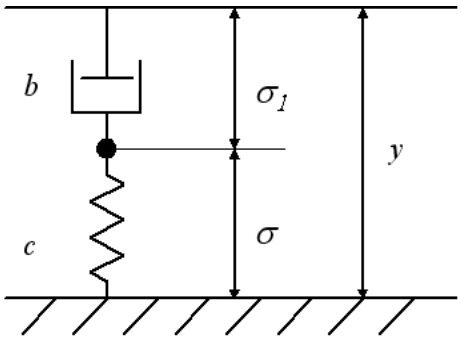

Figure C.3: Mechanical device scheme combining functions of sensor and compensator

C.3.2 Frequency filters

In active systems there is often a need to avoid feedback signals whose frequencies lie in a certain frequency band. In this case, frequency filters are used. Figure C.4a shows a RC-circuit which is a high frequency filter.

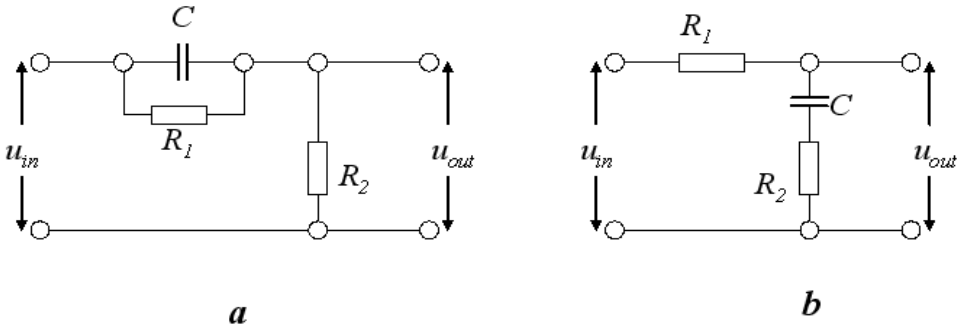

Figure C.4: RC circuits as frequency filters

The output voltage u_{out} is related to the input voltage u_{in} as follows

$$u_{out} = \frac{R_2}{R_2 + (R_1^{-1} + Cs)^{-1}} u_{in} = \frac{R_2}{R_1 + R_2} \frac{1 + T_1 s}{1 + T_2 s} u_{in} = w_c(s) u_{in} \quad \text{(C.16)}$$

where $T_1 = CR_1$ and $T_2 = CR_1R_2/(R_1+R_2)$. If $R_1 \gg R_2$, then, the system does not pass signals with frequencies smaller than T_1^{-1}. If the frequency of the signal is sufficiently high, then

$$|w_c(i\omega)| \simeq \frac{R_2}{R_1} \frac{T_1 \omega}{T_2 \omega} \simeq 1 \quad \text{(C.17)}$$

Figure C.4b shows a circuit which is a low frequency filter. Here

$$u_{out} = \frac{R_2 + (Cs)^{-1}}{R_1 + R_2 + (Cs)^{-1}} u_{in} = \frac{1 + T_1 s}{1 + T_2 s} u_{in} = w_c(s) u_{in} \quad \text{(C.18)}$$

where $T_1 = CR_2$ and $T_2 = C(R_1 + R_2)$. If $R_1 \gg R_2$, the system does not pass the signals with frequencies considerably higher than T_2^{-1}. Mechanical filters may be designed as well. For example, one obtains for the system depicted in Figure C.5 that

$$\sigma = \frac{b_1 s + c}{(b + b_1)s + c} z = \frac{1 + T_2 s}{1 + T_1 s} z \quad \text{(C.19)}$$

where $T_1 = (b + b_1)/c$ and $T_2 = b_1/c$. If $b \gg b_1$, then $T_1 \gg T_2$ and filter C.19 does not pass high frequencies.

C.3.3 Amplifiers

DC and AC amplifiers are used to amplify electric signals. At the frequencies relevant to active vibration protection systems the amplifiers may be considered as being non-inertial with the following transfer function

$$w_c(s) = k \quad \text{(C.20)}$$

Mechanic, pneumatic, hydraulic and pneumomechanic amplifiers can be involved in active systems as well [1][2][3].

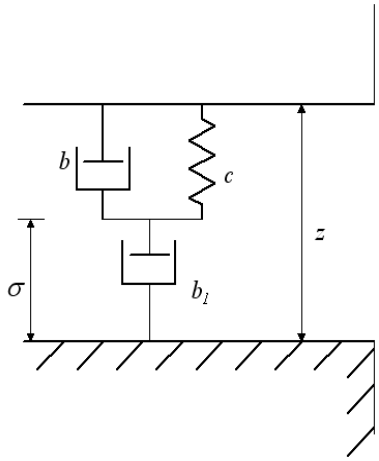

Figure C.5: Scheme of a mechanical filter

Bibliography

[1] Kolovsky M.Z., 1999
Nonlinear Dynamics of Active and Passive Systems of Vibration Protection,
Foundations of Engineering Mechanics, Springer-Verlag, ISBN 3-540-65661-8.

[2] Battaini M., 1998
Sistemi strutturali controllati: progettazione ed affidabilitá,
Ph.D. Thesis (in Italian), Structural Mechanics Dept., University of Pavia.

[3] Marazzi F., 2002
Semi-active control of civil structures: implementation aspects,
Ph.D. Thesis, Structural Mechanics Dept., University of Pavia.

[4] SAMCO (Structural Assesment Monitoring and COntrol), 2003
Proc. of the SAMCO Summary Academy, July 14-18, 2003, Robinson College Cambridge University, Cambridge, UK.

[5] Casciati S., 2004
Damage Detection and Localization in the Space of the Observed Vari-

ables,

Ph.D. Thesis, Structural Mechanics Dept., University of Pavia.

General bibliography

ABAQUS, 1998
Hibbitt, Karlsson and Sorensen Inc., Pawtucket, RI.

Alga S.p.A., Milan, 2005
Products description manuals.

Amini F., 2002
Predictive Active Control Using Pole Assignment Method for Seismic Structures
Proc. of Third World Conference on Structural Control, Vol. 3, John Wiley & sons, 2002, pp. 101-106.

ANSYS and CivilFEM 9.0 User Manual, 2005
ANSYS Inc, USA. CivilFEM Ingeciber s.a., Madrid, Spain.

Augusti G., Baratta A., Casciati F., 1984
Probabilistic Methods in Structural Engineering,
Chapman and Hall Ltd, ISBN 0-412-22230-2.

Bakule L., Paulet-Crainiceau F., Rodellar J., 2004
Decentralized control design for a cable-stayed bridge benchmark
Proc. of the 2002 American Control Conference, IEEE, Piscataway, NJ, 2002, pp.3046-3051.

Bakule L., Paulet-Crainiceau F., Rodellar J., 2004
Reliable control design for a cable-stayed bridge benchmark
Proc. of the 2002 American Control Conference, IEEE, Piscataway, NJ, 2002, pp.5040-5045.

Bakule L., Paulet-Crainiceau F., Rodellar F., Rossel J.M., 2005
Overlapping Reliable Control for a Cable-Stayed Bridge Benchmark
IEEE Transactions on Control Systems Technology, Vol. 13, No. 4.

Battaini M., 1998
Sistemi strutturali controllati: progettazione ed affidabilitá,
Ph.D. Thesis (in Italian), Structural Mechanics Dept., University of Pavia.

Battaini M., Casciati F., Domaneschi M., 2003
Electro-inductive passive and semi-active control devices,
System-based Vision for Strategic and Creative Design (ISEC02), Bontempi (eds.), 23-26, September 2003 Rome, Italy, Kluwer, pp.2085-2090.

Bergmann D., Starossek U., 2004
Numerical-experimental simulation of active flutter control for bridges,
Structural Control and Health Monitoring, Vol. 11, pp. 141-156.

Bleich F., 1952
Buckling Strenght of Metal Structures,
Mc Graw-Hill, New York.

Bontempi F., 2000
Metodi computazionali per l'analisi non lineare di strutture in CA e CAP,
Lectures notes (in Italian), April-July, 2000, Structural Mechanics Dept., University of Pavia.

Bontempi F., 2004
Approccio sistemico alla manutenzione strutturale (in Italian),
Bridge and Viaduct: control, analysis, maintenance, rehabilitation. Politecnico di Milano, Milan, June, 22-25, 2004.

Bontempi F., Casciati F., Giudici M., 2003
Seismic response of a cable-stayed bridge: active and passive control systems (Benchmark Problem),
Journal of Structural Control, 10:169-185.

Bryson A.E., 1981
Applied Optimal Control,
Hemisphere Pub. Corp., ISBN 0891162283.

Caicedo J.M., Dyke S.J., Moon S.J., Bergman L., Turan G., Hague S., 2003

Phase II Benchmark Control Problem for Seismic Response of Cable Stayed Bridges,
Journal of Structural Control, 10:137-168.

Caicedo J.M., Dyke S.J., Moon S.J., Bergman L., Turan G., Hague S., 2003
Phase II Benchmark Control Problem for Seismic Response of Cable Stayed Bridges
http://wusceel.cive.wustl.edu/quake/.

Cimellaro G.P., Casciati F., Domaneschi M., 2005
Fragility of a benchmark problem,
Proc. of The Tenth International Conference on Civil, Structural and Environmental Engineering Computing, B.H.V. Topping, (Ed.), Civil-Comp press, Stirling, United Kingdom, paper 241, 2005.

Casciati F., Domaneschi M., 2004
Confinement of Vibration Applied to a Benchmark Problem
Proc. Of Second European Workshop on Structural Health Monitoring, Monaco (D), July 7-9, 2004, pp 811-818.

Casciati F., Domaneschi M., Faravelli L., 1998
Some Remarks on the Drift of Elasto-Plastic Oscillators Under Stochastic Excititon,
Stochastic Structural Dynamics, Spencer B.F. Jr and Johnson E.A. Eds., Notre Dame, Indiana, USA, 6-8 August 1998, pp. 545-550.

Casciati F., Domaneschi M., Faravelli L., 2004
Active Control Schemes for Managing Nonlinear Passive Devices,
Proc. of the Third European Conference on Structural Control, R. Flesch, H. Irschik, M. Kommer (eds.), Vienna, Austria, July 2004, Vol. II, pp. from S1-23 to S1-26, ISBN-3-901167-90-0.

Casciati F. and Faravelli L., 1991
Fragility Analysis of Complex Structural Sysytems,
Research Study Press Ltd, Taunton, Somerset, England.

Casciati F., Faravelli L., Battaini M., 2000
Ultimate vs. Serviceability Limit State in Designing Bridge Energy Dissipation Devices,
Earthquake Engineering Frontiers in the New Millenium, Spencer B.F. Jr and Hu Y.X. Eds., Beijing, China, 8-11 November 2000, pp. 293-297.

Casciati S., 2004
Damage Detection and Localization in the Space of the Observed Variables,
Ph.D. Thesis, Structural Mechanics Dept., University of Pavia.

Chopra A.K., 2001
Dynamics of Structures: Theory and Applications to Earthquake Engineering,
Prentice Hall, Upper Saddle River, New Jersey.

Close C.M., Frederick D.K., 1995
Modeling and Analysis of Dynamic Systems, second edition
John Wiley and Sons, Inc.

Control System Toolbox, 2002
The Mathworks Inc., Natick, MA.

CNR - 10012, 1985
Instructions for the evaluation of the external actions on structures (in Italian),
Italian Research National Council.

Eurocode No. 2, 1992
Design of Concrete Structures,
ENV 1992-1-1.

Faravelli L., 2001
Modelling the Response of an Elastomeric Base Isolator,
Journal of Structural Control, Vol. 8, Nr. 1.

Giudici M., 2003
Progettazione in regime non lineare di strutture in CAP a cavi aderenti e non aderenti,
Ph.D. Thesis (in Italian), Structural Mechanics Dept., University of Pavia.

http://www.hsba.go.jp/bridge/e-simotu.htm, 2005.

Irwin J.D., Graf E.R., 1979
Industrial Noise and Vibration Control",
Prentice Hall Pubblishers.

Kolovsky M.Z., 1999
Nonlinear Dynamics of Active and Passive Systems of Vibration Protection,
Foundations of Engineering Mechanics, Springer-Verlag, ISBN 3-540-65661-8.

Kovaleva A., 2005
Control Theory with Application to Engineering Systems,
Lectures, January 17-21, 2005, Structural Mechanics Dept., University of Pavia.

Jiménez R., Álvarez-Icaza L., 2005
LuGre friction model for a magnetorheological damper,
Structural Control and Health Monitoring, Vol. 12, Issue 1, pp. 25-45.

Kitagawa M., 2004
Technology of the Akashi Kaikyo Bridge,
Structural Control and Health Monitoring, Vol. 11, pp. 75-90.

Kovaleva A., 1999
Optimal Control of Mechanical Oscillations ,
Foundations of Engineering Mechanics, Springer-Verlag, ISBN 3540654429.

Kwakernaak H., Sivan R., 1972
Linear Optimal Control Systems,
John Wiley and Sons, ISBN 0471511102.

Luo N., Rodellar J., de la Sen M., Veí J., 2002
Decentralized active control of a class of uncertain cable-stayed flexible structures
International Journal of Control, vol. 75 (4), pp. 285-296.

Luo N., Rodellar J., Villarmizar R., Veí J., 2004
Robust control law for a friction-based semi-active controller of a two-span bridge
Proc. of SPIE's 10th Int. Symposium SMART Structures and Materials, 2-6 March 2003, San Diego, California, USA.

Magana M.E., Rodellar J., Casas J.R., Mas J., 1999
Active control of cable-stayed bridges
J. Holnicki-Szulc and J. Rodellar eds., Smart Structures, Kluwer, pp. 193-202.

Marazzi F., 2002
Semi-active control of civil structures: implementation aspects,
Ph.D. Thesis, Structural Mechanics Dept., University of Pavia.

Marioni A., 2004

Dispositivi per la Mitigazione dell'Azione Sismica (in Italian),
Bridge and Viaduct: control, analysis, maintenance, rehabilitation. Politecnico di Milano, Milan, June, 22-25, 2004.

Matlab and Simulink, 1997
The Mathworks Inc., Natick, MA.

Matlab and Simulink, 2002
The Mathworks Inc., Natick, MA.

Meirovitch L., 1990
Dynamics and Control of Structures,
John Wiley and Sons, ISBN 0-471-62858-1.

Monroy C., Rodellar J., Magana M.E., 2000
Performance analysis of a robust local active control scheme of cable-stayed bridges
Proc. of 2nd European Conference on Structural Control, Paris, July 2000.

Ostenfeld K. H., 2004
The Storebelt East Bridge,
Structural Control and Health Monitoring, Vol. 11, pp. 125-139.

Proc. of the Third World Conference on Structural Control, F. Casciati ed., April 7-11, 2002, Como, Italy, Vol. 1-2-3, ISBN 0-471-48980-8.

Proc. of the US-Europe Workshop on Sensors and Smart Structures Technology, L. Faravelli and Billie F. Spencer Jr. eds., April 12-13, 2002, Como and Somma Lombardo, Italy, ISBN 0-471-48980-8.

Proc. of the Third European Conference on Structural Control, R. Flesch, H. Irschik and M. Krommer eds., July 12-15, 2004, Vienna, Austria, ISBN 3-901167-90-0.

Rodellar J., Manosa V., Monroy C., 2002
An active tendon control scheme for cable-stayed bridges with model uncertainties and seismic excitation
Journal of Structural Control, Vol. 9, 75-94.

SAMCO (Structural Assesment Monitoring and COntrol), 2003
Proc. of the SAMCO Summary Academy, July 14-18, 2003, Robinson College Cambridge University, Cambridge, UK.

Spencer Jr. B.F. , Dyke S.J. , Sain M.K. , Carlson J.D., 1997
Phenomenological Model for Magnetorheological Dampers,
Journal of Engineering Mechanics, 123(3), pp. 230-238.

Wilson J., Gravelle W., 1991
Modelling of a Cable-Stayed Bridge for Dynamic Analysis,
Earthquake Engineering and Structural Dynamics, 20:707-721.

Wong K.Y., 2004

Instrumentation and health monitoring of cable-supported bridges, Structural Control and Health Monitoring, Vol. 11, pp. 91-124.